Peroxisome biogenesis and dynamics in Hansenula polymorpha

Krygowska, Malgorzata

Peroxisome biogenesis and dynamics in *Hansenula polymorpha*

The studies presented in this thesis were performed in the research unit Molecular Cell Biology of the Groningen Biomolecular Sciences and Biotechnology Institute (GBB) of the University of Groningen, The Netherlands.

rijksuniversiteit groningen

Peroxisome biogenesis and dynamics in *Hansenula polymorpha*

Proefschrift

ter verkrijging van de graad van doctor aan de
Rijksuniversiteit Groningen
op gezag van de
rector magnificus prof. dr. E. Sterken
en volgens besluit van het College voor Promoties.

De openbare verdedigen zal plaatsvinden op

maandag 14 april 2014 om 11:00 uur

door

Małgorzata Natalia Cepińska

geboren op 3 oktober 1985
te Ostrów Wielkopolski, Poland

Promotor
Prof. dr. I.J. van der Klei

Beoordelingscommisie
Prof. dr. J.M. van Dijl
Prof. dr. K.N. Faber
Prof. dr. H.A.B. Wösten

Foreword

I would like to first thank Prof. dr. I. J. van der Klei for accepting me as a master student and, after 5 months of work, for giving me the opportunity to start my PhD studies in the Molecular Cell Biology group. I am very grateful for all your guidance and encouragement you gave me during the whole 4.5 years. It was thanks to your scientific view, constructive criticism and suggestions that I was able to complete this thesis.

I would like to take this opportunity to thank the Reading Committee members: Prof dr J.M. van Dijl, Prof dr K.N. Faber and Prof. Dr. H.A.B. Wösten for evaluating my thesis.

My sincere thanks to Arjen, Rinse and Anita for the help in fluorescence and electron microscopy. Without you I would be lost!

Special thanks for Adam and Kèvin for being my paranymphs and additional thanks for Kèvin who translated the summary of my thesis.

I would also like to thank Shirisha for being an excellent supervisor and a great colleague. “Thank you, my Master!”

Also, I would like to thank Sophie and Christian for all the Wednesday Magic Nights we had together. They have made my after-lab life much more colorful!

To all the former and current members of the Molecular Cell Biology group: thank you for being such great colleagues! Thank you for all your help and support during my time in the lab and for being so kind and not complain about the music I was playing in the lab.

I express my thanks to our secretary: Jannet and for her kindness and the technical services provided by her.

Being in a foreign country is not easy. Therefore I would like to thank my Polish and Dutch friends: Magda, Łukasz, Gosia, Adam, Kasia, Michiel, Ilona and Marcin for being such great friends and for making me feel more at home in the Netherlands.

Finally, I would like to thank my beloved husband, Filip. Without him, it would be impossible for me to finish this thesis. Thank you for all your daily support, kindness and love, for all the rides to the lab in the middle of the night and during weekends. I would also like to give my sincere thanks to my entire family who was always there for me.

Thank you all again,

Małgosia Cepińska

Table of Contents

Aim and outline

Peroxisomes are ubiquitous, single membrane bound organelles which perform a wide variety of metabolic functions that are tightly regulated to adapt to metabolic needs of the cell. Generalized functions include detoxification of hydrogen peroxide and beta-oxidation of fatty acids. Hence, peroxisomes are highly flexible organelles, of which the number, size and content can easily adapt to changes in environmental conditions.

Peroxisomes may form in two ways namely by division of pre-existing organelles and *de novo* from the ER. Recent studies uncovered a great amount of information supporting existence of both pathways in different organisms. It is still unclear if and which one is the dominant mechanism in wild-type cells. However, rapid adaptation in number most likely requires fission processes rather than *de novo* synthesis, as the kinetics of the latter process is slow relative to fission.

In yeasts peroxisomes are believed to be mainly formed by division, whereas only in cells devoid of these organelles new organelles are formed using the ER as membrane template. The aim of this Thesis was to further understand the principles of peroxisome biogenesis and dynamics in the yeast *Hansenula polymorpha*.

Chapter 1 describes recent advances in peroxisome biogenesis, proliferation and inheritance.

Chapter 2 presents data which demonstrates the ability of certain peroxisome membrane proteins (PMPs) to re-distribute during organelle multiplication. We analyzed *H. polymorpha dnm1* cells, which are unable to perform normal peroxisome fission and fail to carry out the final scission step. Hence, upon fission these organelles produce extensions which are not separated from the mother organelle. Hence, these organelles provide ideal

models to study the fate of PMPs during fisssion. We found that some PMPs (Pex14, Pex8, Pex10 and Pex25), localized mainly to the organelle extension. Others, like Pmp47 remained evenly distributed over the entire organelle. A similar pattern of PMP distribution was also observed in wild-type cells. Interestingly, we show that this uneven PMP distribution is dependent on Pex11. Additionally, we identified a specific region of Pex11 responsible for this phenomenon. The N-terminus of Pex11, which has previously been shown to be involved in membrane bending, also mediates differences in distribution patterns of certain PMPs.

Chapter 3 Until now it was believed that *pex3* cells are devoid of peroxisome structures. Here we describe that *pex3* cells do contain remnants which are unstable and subject to rapid degradation and therefore most likely have been overlooked thus far. However, using an *atg1 pex3* double mutant strain in which autophagy is blocked the organelles were readily detectable and were localized adjacent to the ER and mitochondria. These structures contained components of the matrix protein docking site namely Pex8, Pex13 and Pex14 but not the RING finger complex protein Pex10. Pex10 as well as Pmp47 were unstable and present at very low levels in the cytosol. This indicates that the docking site proteins are inserted in their target membrane independent of Pex3. After re-introduction of Pex3, the membrane vesicles, but not the ER, were the target for Pex3. Upon incorporation of Pex3 these structures rapidly developed in normal peroxisomes. Moreover, we also observed that Pex25 and Pex19, two other peroxins proposed to be involved in the *de novo* peroxisome formation, are not involved in the formation of the vesicles in *pex3* cells. This new insight into peroxisome formation fundamentally differs from the generally accepted models.

Chapter 4 describes new findings on Pex23 family proteins in *H. polymorpha*. We demonstrate that both proteins of the Pex23 family termed Pex23 and Pex32 are localized to peroxisomes. Moreover, Pex23 was also found on the ER. We show that deletion of *PEX23* influences peroxisome and ER shape in conjunction with a minor reduction in growth on methanol. *pex32* cells

however show a severe growth defect on methanol and are peroxisome deficient. Interestingly, upon deletion of *PEX23* in *pex32* cells peroxisomes reappeared. We speculate thatin the absence of Pex23 *de novo* peroxisome formation is stimulated.

Chapter 5 presents data showing that Inp2, a protein required for peroxisome inheritance to the bud, is conserved in other yeast species. The *in silico* analysis identified weakly conserved Inp2 proteins in other budding yeast species, including *H. polymorpha*. We demonstrated that this homologue localizes to peroxisomes, can interact with Myo2 (a motor protein responsible for transporting organelles to the bud along the actin skeleton) and influences peroxisome inheritance.

Chapter 2

Peroxisome fission is associated with reorganization of specific membrane proteins

Małgorzata N. Cepińska, Marten Veenhuis, Ida J. van der Klei and Shirisha Nagotu

Published in Traffic, 12 (2011) 925–937

Abstract

Membrane remodeling is an important aspect in organelle biogenesis. We show that different peroxisome membrane proteins that play a role in organelle biogenesis and proliferation (Pex8, Pex10, Pex14, Pex25 and Pex11) are subject to spatiotemporal behavior during organelle development. Using fluorescence microscopy analysis of *Hansenula polymorpha dnm1* cells that are blocked in the normal fission process, we show that green fluorescent protein (GFP) fusions of Pex8, Pex10, Pex14 and Pex25 show enhanced fluorescence at the organelle extensions that are formed in budding cells. In contrast, Pex11 fluorescence is enriched at the base of this extension on the mother organelle. A fusion protein of GFP with the transporter Pmp47, used as a control, did not show enhanced fluorescence at any specific region of the organelle. The concentration of specific peroxins at the peroxisome surface was lost upon deletion of *PEX11* or the N-terminal domain of Pex11 that is involved in membrane remodeling. Comparable distribution patterns as in *dnm1* cells were observed in wild-type cells where Pex8, Pex10, Pex14 and Pex25, but not Pex11, were especially present at newly formed organelles that migrated to the bud. We speculate that peroxin reorganization events result in enhanced levels of peroxins involved in peroxisome biogenesis in nascent organelles.

Introduction

Understanding the principles of organelle biogenesis is an important aspect of contemporary cell biology. Membrane remodeling is a key feature required for this process. The initial point of view of the random movement of components (proteins and lipids) in biological membranes gradually changed to the view that biological membranes may contain specific subdomains with various protein–protein and protein–lipid interactions (1). The organization of the components of the respiratory chain in the cell membrane of prokaryotes (2) and protein scaffolds like clathrin-coated pits represent some examples of this. The knowledge of subdomains at cell organelles is still in its infancy. However, recent data show that mitochondrial fission proteins are organized into raft-like domains during apoptosis (3). Previously, Boukh-Viner et al. (4) reported that preperoxisomal vesicles of the yeast *Yarrowia lipolytica* contain dynamic ergosterol- and ceramide-rich domains which are involved in the fusion of these vesicles. Also, in mammalian peroxisomes subdomains in which specific peroxisomal membrane proteins (PMPs) concentrate have been observed (5, 6).

Peroxisomes are single membrane-bound structures. These organelles display an unprecedented range of functions that vary with the cell type in which they occur and environmental conditions. A unique feature of this organelle is the posttranslational import of folded oligomeric proteins into its matrix (7). Different machineries exist for the sorting of matrix and membrane proteins (for a recent review see Ref. (8)). Peroxisomes may arise from the endoplasmic reticulum or multiply by fission (9-13). The latter is especially observed during vegetative reproduction of yeast cells when grown at peroxisome-inducing conditions and during organelle inheritance in budding cells (11, 12).

Fission of peroxisomes also includes membrane remodeling, as it involves membrane elongation, constriction and fission. Pex11, a conserved PMP, has been proposed to be involved in this process (14). Initial experiments (12) suggested that Pex11 indeed reorganizes at the peroxisomal membrane during peroxisome fission in *Hansenula polymorpha dnm1* cells and accumulates at

the base of the peroxisome extensions. Recently, we showed that the *N*-terminal α-helix of Pex11 is responsible for membrane curvature (15).

This study aims to elaborate on this observation and addresses the formation of – eventually temporary – protein subdomains on yeast peroxisomes. The advantage of using *H. polymorpha dnm1* mutant cells in this study is that in these cells peroxisomes are arrested in a late step of fission. As a result, these cells invariably contain a single peroxisome. However, early steps of the fission process, except for the final scission step, are still functional. In budding cells, these organelles therefore form two distinct regions: a single large organelle present in the mother cell and a long tubular extension that protrudes into the developing bud, which is connected until it is cleaved off during cytokinesis (12).

In this study, we focus on the suborganellar localization of PMPs involved in a range of processes related to peroxisome biogenesis and function. These include three peroxins involved in matrix protein import: Pex14, a component of the receptor-docking complex; Pex10, an integral membrane protein of the receptor-recycling complex (16) and Pex8, a peripheral membrane protein that has been implicated in the association of both complexes (17) and release of the cargo from the receptor in the peroxisomal matrix (18). In addition, we analyzed two proteins of the Pex11 protein family, namely Pex11 and Pex25 (19), together with Inp1 and Inp2, which are involved in peroxisome inheritance (12, 20-22) as well as Pmp47, an ATP–AMP transporter important for the function of peroxisomes.

The data revealed that in *dnm1* cells heterogeneity exists for specific, but not all PMPs, with respect to their distribution over the organelles that may be related to the organelle developmental stage. This heterogeneity was lost upon deletion of full-length *PEX11* (i.e. in a *dnm1.pex11* double mutant or a *pex11* single mutant) or only the *N*-terminus of Pex11 which is required for membrane curvature (14). These putative PMP reorganizations during peroxisome fission were also observed in wild-type (WT) cells, where peroxins concentrated in the developing organelles. We speculate that this mode of

organelle fission has the advantage that it results in the concentration of peroxins involved in peroxisome biogenesis in nascent organelles, whereas mature organelles contain lower levels of these proteins. Moreover, this process results in the inheritance of nascent organelles with high protein import capacity to the developing bud.

Materials and Methods

Microorganisms and cultivation conditions

Hansenula polymorpha cells were grown at 37◦C on selective YND media containing 0.67% yeast nitrogen base without amino acids or mineral media. Media were supplemented with 0.5% glucose or 0.5% methanol as carbon source and 0.25% ammonium sulfate or 0.25% methylamine as nitrogen source. When required, amino acids or uracil were added to a final concentration of 30 μg/ml. For growth on agar plates, the media were supplemented with 2% agar. For selection of resistant transformants, YPD plates containing 100 μg/ml zeocin or 100 μg/ml nourseothricin (Invitrogen) were used.

For cloning purposes, *Escherichia coli* DH5α was used. Cells were grown at 37◦C in LB supplemented with 100 μg/ml ampicillin or 50 μg/ml kanamycin when required.

Molecular techniques

Yeast strains, plasmids and primers used in this study are listed in **Tables S1–S3**, respectively. Standard recombinant DNA techniques were carried out essentially as described (23). Transformation of *H. polymorpha* cells and site-specific integration in the *H. polymorpha* genome were performed as described (24). DNA-modifying enzymes were used as recommended by the suppliers (Roche and Fermentas). *Pwo* polymerase was used for preparative polymerase chain reactions (PCRs). Oligonucleotides were synthesized by

Biolegio. DNA sequencing reactions were performed at Service XS. For DNA sequence analysis, the CLONE MANAGER 5 PROGRAM (Scientific and Educational Software) was used. BLAST algorithms were used to screen databases at the National Center for Biotechnology Information.

Plasmid and strain constructions

Plasmid pSNA12 (pHIPZ-Pex14-mGFP) was made as follows – primers Pex14GFP-fw and Pex14GFP-rev and the genomic DNA as a template were used to get a PCR product of 563 bp. The obtained PCR product and the pHIPZ-mGFP plasmid were digested with *HindIII* and *BglII*. Subsequently, the 5077 bp fragment of the vector was ligated to 554 bp digested PCR fragment. This resulted in the plasmid pSNA12 which was linearized with *PstI* to integrate into the genome of *dnm1*.DsRed-SKL and *dnm1.pex11*.N4-DsRed-SKL cells.

Plasmid pEXP-PEX25-GFP was constructed using Gateway® Technology. pENTR-221-PEX25 was recombined with vectors pDONR-P4-P1r-PAMO, pDONR-P2r-P3-eGFP-TAMO and pDEST-R4-R3–NAT. The resulting expression vector, pEXP-PEX25-GFP, was then linearized by *DraIII* to enable integration into the *H. polymorpha* genome.

Plasmid pHIPN4 was made by replacing zeocin in pHIPZ4 with nourseothricin from pAG25. For this, the pHIPZ4 vector was linearized with *Asp7181* and this fragment was modified with klenow filling and subsequently digested with *NcoI*. This was ligated with a fragment obtained from *NcoI* (partial digestion)–*EcoRV* digestion of plasmid pAG25 to obtain pHIPN4.

Plasmid pSNA13 (pHIPN4-DsRed-SKL) was obtained by replacing the zeocin marker in the plasmid pHIPZ4-DsRed-SKL with the dominant marker nourseothricin. For this purpose, plasmids pHIPZ4-DsRed-SKL and pHIPN4 were digested with the restriction enzymes *HindIII* and *SalI*. Subsequently, the 6045 bp fragment of the plasmid pHIPZ4-DsRed-SKL was ligated to the 726 bp fragment of the plasmid pHIPN4 to obtain the plasmid pHIPN4-DsRed-SKL.

The resulting plasmid was linearized with *NsiI* to integrate into the *AOX* region of the genome of *H. polymorpha dnm1.pex11* cells.

Plasmid pMCE5 (pHIPZ-Pex10-mGFP) was made as follows: primers Pex10fw, Pex10rev_new and genomic DNA as a template was used to get a 686 bp PCR product. The pHIPZ-mGFP fusinator plasmid and the obtained PCR product were digested using *HindIII* and *BglII*. Ligation of the 5077 bp vector fragment and digested PCR fragment of 674 bp resulted in the plasmid pMCE5 of 5751 bp. The plasmid was linearized using *NheI* for integrating into the genome of *dnm1*.DsRed-SKL, *dnm1.pex11*.N4-DsRed-SKL and DsRed-SKL cells.

A PCR fragment of 730 bp was obtained using primers Pex8fw and Pex8rev1 on the genomic DNA as a template. The PCR fragment and the pHIPZ-mGFP fusinator plasmid were digested using *HindIII* and *BglII*. The vector fragment of 5077 bp and the digested PCR product of 718 bp were ligated. This resulted in the pMCE4 (pHIPZ-Pex8-mGFP) plasmid, which was linearized with *MunI* for integration into the genome of *dnm1*.DsRed-SKL, *dnm1.pex11*.N4-DsRed-SKL and DsRed-SKL cells.

Plasmid pMCE2 was made by replacing the zeocin marker in the pRSA01 plasmid with nourseothricin from pHIPN4. For this, a PCR fragment obtained using Natfw and Natrev1 on a pHIPN4 as a template, and pSNA10 were digested with *SalI* and *SacII* to obtain 1330 and 1352 bp fragments. Fragments were ligated to obtain plasmid pMCE2.

Plasmid pMCE1 (pHIPZ-Pex25-mGFP) was made as follows: primers Pex25mGFPfw, Pex25GFPrev and genomic DNA as a template were used to get a PCR product of 689 bp. The obtained PCR product and the pHIPZ-mGFP fusinator plasmid were digested with *HindIII* and *BglII*. Subsequently, the 5077 bp fragment of the vector was ligated to the 680 bp digested PCR fragment. This resulted in the plasmid pMCE1 which was linearized with *PstI* to integrate into the genome of *dnm1*.DsRed-SKL and *dnm1.pex11*.N4- DsRed-SKL cells.

A PCR fragment of 784 bp was obtained using primers Pex11mCherryfw and Pex11mCherryrev on the genomic DNA as a template. The PCR fragment and the pMCE2 plasmid were digested using *HindIII* and *BglII*. The vector fragment of 4931 bp and the digested PCR product of 772 bp were ligated. This resulted in pMCE3 (pHIPN-Pex11-mCherry) plasmid which was linearized with *XhoI* to integrate into the genome of *dnm1*.DsRed-SKL, *dnm1.pex11*.N4-DsRed-SKL and DsRed-SKL cells.

Plasmid pMCE7 (pHIPZ-PMP47-mGFP) was made as follows: primers PMP47 fw, PMP47 rev and the genomic DNA as a template was used to get a 876 bp PCR product. The obtained PCR product and pHIPZ-mGFP fusinator plasmid were digested using *BsmBI* and *BamHI*. Ligation of the 5081 bp vector fragment and digested PCR fragment of 861 bp resulted in the plasmid pMCE7. The plasmid was linearized using *MunI* for integrating into the genome of *dnm1*.DsRed-SKL, *dnm1.pex11*.N4-DsRed-SKL and DsRed-SKL cells.

Plasmid pMCE6 was constructed as described – a 784 bp fragment comprising the C-terminal part of Pex14 was obtained by PCR using primers Pex14mCherryfw and Pex14mCherryrev on the genomic DNA of *H. polymorpha*. The 5088 bp fragment obtained by digesting pMCE2 with the enzymes *BglII* and *HindIII* was ligated to the *BglII–HindIII*, digested PCR product to obtain plasmid pHIPN-Pex14-mCherry (pMCE6). The plasmid was linearized using *XhoI* for integrating into the genome of WT cells.

Plasmid pMCE8 (pHIPN-Pex10-mCherry) was made as follows: plasmid pMCE5 and pRSA1 were digested using *BglII* and *HindIII*. Subsequently, fragments of 674 and 4931 bp were ligated. The resulting plasmid of 5605 bp was then linearized with *NheI* and integrated into the genome of *pex11* cells.

Plasmid pENTR21-dNPex11 was made as follows: primers dNPex11_fw, dNPex11_rev and pENTR21–Pex11 plasmid as a template were used to obtain a 550 bp PCR product. The PCR fragment and pDONOR221 plasmid were

recombined using Gateway® Technology and resulted in the plasmid ENTR21-dNPex11 of 3012 bp.

A PCR fragment of 1556 bp was obtained using primers Ppex11_fw and Ppex11_rev on the genomic DNA as a template. The PCR fragment and the pDONR_L4R1 plasmid were recombined using Gateway® Technology and resulted in the pENTR-P4-P1r-PPEX11 plasmid of 4147 bp.

Plasmid pENTR-P2r-P3-mGFP-TAMO was made as follows: primes mGFP_G_fw, mGFP_G_rev and plasmid pDONR-P2r-P3-eGFP-TAMO, were used in a site-directed mutagenesis reaction (kit from Stratagene® was used). This gave a pENTR-P2r-P3-mGFP-TAMO of 3759 bp.

Plasmid pMCE9 (pEXP-Pex11-GFP) was constructed using Gateway® Technology. pENTR-221-PEX11 was recombined with vectors pENTR-P4-P1r-PPEX11, pENTR-P2r-P3-mGFP-TAMO and vector pDEST-R4-R3–ZEO. The resulting expression vector, pEXP-PEX11-GFP, was then linearized by *NheI* to enable integration into the *H. polymorpha* genome.

Plasmid pMCE10 (pEXP-dNPex11-GFP) was constructed using Gateway® Technology. pENTR21-dNPex11 was recombined with vectors pENTR-P4- P1r-PPEX11, pENTR-P2r-P3-mGFP-TAMO and vector pDEST-R4-R3–ZEO. The resulting expression vector, pEXP-dNPex11-GFP, was then linearized by *NheI* to enable integration into the *H. polymorpha* genome.

Plasmid pAMK6 was linearized with *NruI* to integrate into the genome of *dnm1*.DsRed-SKL and *dnm1.pex11*.N4-DsRed-SKL cells.

Microscopy

Wide-field fluorescence imaging was performed on a Zeiss Axioskop50 fluorescence microscope (Ziess). Images were taken with a Princeton Instruments 1300Y digital camera.

GFP signal was visualized with a 470/40 nm bandpass excitation filter, a 495 nm dichromatic mirror and a 525/50 nm bandpass emission filter. DsRed

and mCherry fluorescence were visualized with a 546/12 nm bandpass excitation filter, a 560 nm dichromatic mirror and a 575–640 nm bandpass emission filter.

Wide-field fluorescence microscopy was performed with a Zeiss Axio Observer Z1 fluorescence microscope (Zeiss). Images were taken with a Coolsnap HQ2 Camera (Roper Scientific Inc.). GFP signal was visualized with a 470/40 nm bandpass excitation filter, a 495 nm dichromatic mirror and a 525/50 nm bandpass emission filter. DsRed-SKL and mCherry fluorescence were analyzed with a 545/25 nm bandpass excitation filter, a 570 nm dichromatic mirror and a 605/70 nm bandpass emission filter. Z-stack images were made with an interval of 0.3 μm. Image analysis was carried out using IMAGEJ (http://rsb.info.nih.gov/nih-image/) and ADOBE PHOTOSHOP CS3.

Electron microscopy

Cells were fixed in either 1.5%KMnO4 or 3% glutaraldehyde and prepared for electron microscopy and immunocytochemistry, as detailed before (25). Immunocytochemistry was performed on ultrathin sections of Unicryl-embedded samples using polyclonal antibodies against catalase or alcohol oxidase, respectively. 3D structures were constructed on the basis of series of serial sections through 1.5%KMnO4 or 3% glutaraldehyde fixed cells. For preparation of the 3D images, AMIRA 3.1 (TGS) software was used. The peroxisome structures were traced using the isosurface function of AMIRA.

Quantification

Z-stack images were made using a Zeiss Observer Z1 microscope of cells growing mid-exponentially on methanol. The exposure time was set so that no overexposed regions were observed. Of each Z-stack, a maximum intensity projection was made using IMAGEJ. Using elliptical and freehand selection tools, peroxisomes were selected based on the DsRed-SKL images. Of each strain, 100 cells were measured for the mean fluorescence intensity of peroxisomes in the mother cell and in the bud. For each cell, the mean

fluorescence of the peroxisome cluster in the mother cell was divided by the mean fluorescence of the peroxisome in the daughter cell. Finally, those ratios were averaged. To compare the results, we used the student's t -test by which the confidence interval was set to 98%.

Results

Various PMPs are enriched at the peroxisome extensions in H. polymorpha dnm1 cells

Peroxisome fission in WT cells is a highly dynamic process. In order to stabilize the possible spatiotemporal behavior in localizations of PMPs during peroxisome fission, we took advantage of the fact that in *H. polymorpha dnm1* cells organelle fission is blocked at a late stage (12). We analyzed the localization and distribution of Pex8, Pex10, Pex14, Inp1, Inp2, Pex11, Pex25 and Pmp47, tagged with green fluorescent protein (GFP) at the *C*-terminus. DsRed-SKL was introduced in the strains to fluorescently mark the peroxisomal matrix.

Analysis of the localization of Pex14, Pex8, Pex10, Pex25 and Pex11 in non-budding cells revealed that for all proteins the fluorescence was randomly distributed over the organelle surface (**Figure 1(I)**) or organized in a spot with enhanced fluorescence (**Figure 1(II)**). Also, the fluorescence of Inp1-GFP and Inp2-GFP, two proteins involved in peroxisome inheritance, was distributed over the entire organelle surface or concentrated in a spot (**Figure 2(I,II)**) in non-budding cells. Notably, in many non-budding cells Inp2-related fluorescence was below the limit of detection (data not shown).

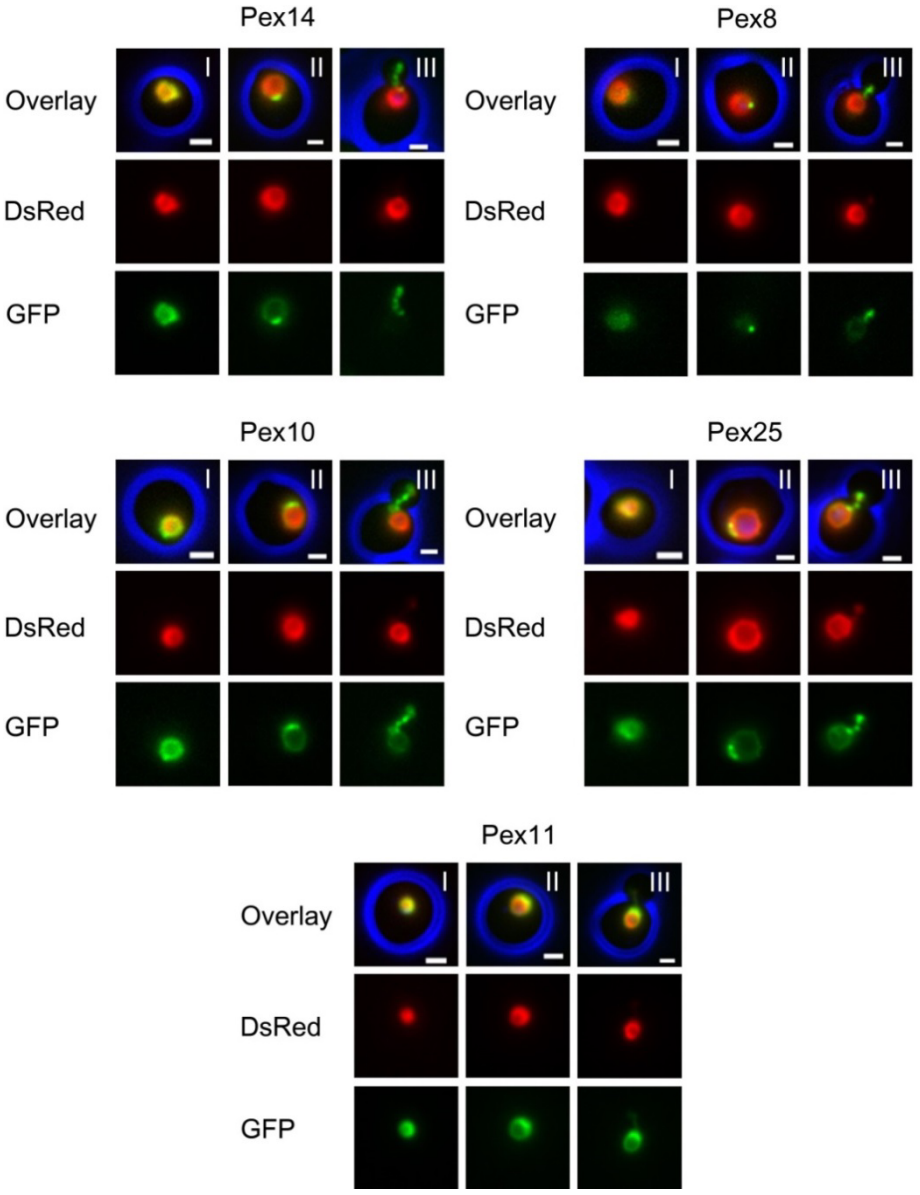

Figure 1: Certain PMPs are localized in subdomains in *dnm1* cells.
dnm1 cells exponentially grown on methanol generally contain one peroxisome per cell which forms a long extension into the bud in dividing cells. The localization of the various PMPs was analyzed by using *C*-terminal GFP fusions and DsRed-SKL to mark peroxisomes. Panels I and II represent non-budding cells and panel III represents budding cells. In non-budding cells Pex14-mGFP, Pex8-mGFP, Pex10-mGFP and Pex25-eGFP were evenly distributed over the organelle surface (I) or, in addition concentrated in spot (II). In budding cells, these peroxins were predominantly localized to the peroxisome extension (III). In nonbudding cells Pex11-eGFP was present on the entire organelle (I) or also enhanced in a patch (II), whereas in budding cells Pex11-eGFP was concentrated at the base of the extension (III). The scale bar represents 1 µm.

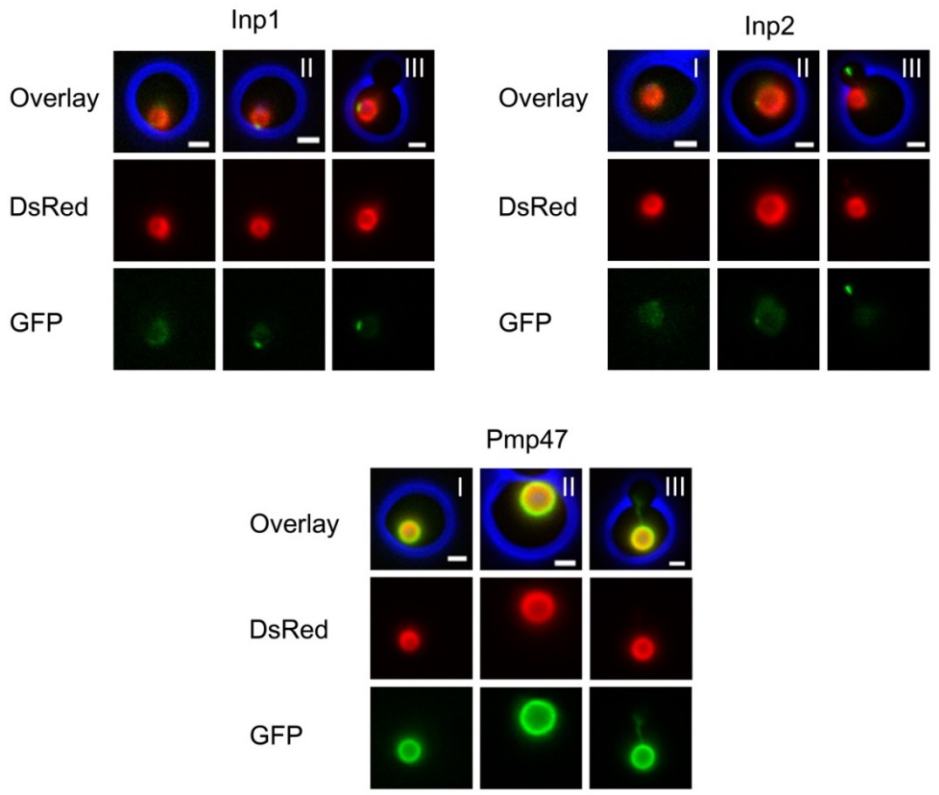

Figure 2: Localization of Inp1, Inp2 and Pmp47 in *dnm1* cells.
dnm1 cells producing DsRed-SKL were grown on methanol. Inp1-eGFP and Inp2-mGFP were present over the entire organellar surface (I) or also partially concentrated in a spot (II) in non-budding cells. In budding cells (III) Inp1-eGFP was localized in a spot at the organelle in the mother cell, whereas Inp2-mGFP was present in a spot at the tip of the peroxisome elongation (III). Pmp47-mGFP never concentrated in spots (I and II) and was present both at the organelle in the mother cell and at its extension in budding cells (III). The scale bar represents 1 μm.

In budding *dnm1* cells, the Pex14-, Pex8-, Pex10- and Pex25-related GFP fluorescence was enriched at the peroxisome extensions (**Figure 1(III)**). In contrast, Pex11 was predominantly localized at the base of the organelle extension on the mother organelle (**Figure 1(III)**). These data suggest that the bulk of the Pex8, Pex10, Pex14 and Pex25 proteins upon cell budding become predominantly localized to the formed extension. In budding cells, the bulk of the Inp1 fluorescence was observed to be concentrated at the organelle in the mother cell, whereas Inp2 fluorescence was most strong at the tip of the

organelle extension in the bud (**Figure 2(III)**). Pmp47-GFP fluorescence was never observed to be concentrated in a spot, but localized both at the extension and relatively evenly distributed on the organelle in the mother cell (**Figure 2(I–III)**).

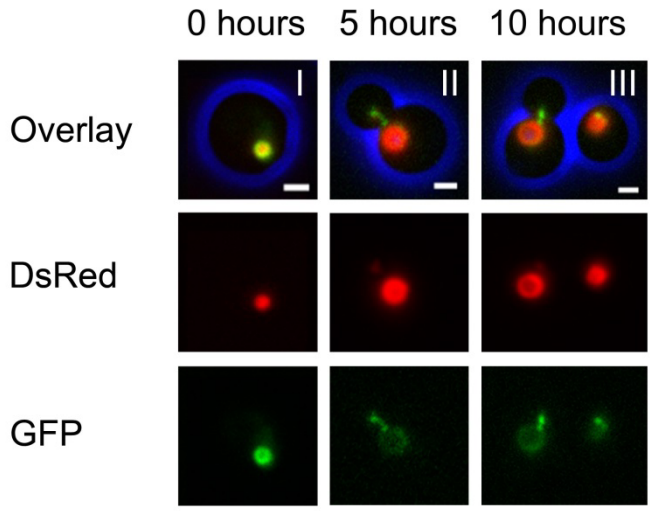

Figure 3: Pex25 moves to peroxisome extensions in budding *dnm1* cells.
dnm1 cells producing Pex25-eGFP under control of the PAMO were precultivated on methanol medium supplemented with methylamine to induce synthesis of Pex25-eGFP and DsRed- SKL. After 5 h of induction, the cells were shifted to methanol medium with ammonium sulfate to repress the PAMO ensuring that no more Pex25-eGFP was produced (I). Pictures were taken at the indicated time points after the shift. In budding cells, Pex25-eGFP is still present at the organelle elongation after 5 (II) or 10 (III) h of incubation. The scale bar represents 1 µm.

We subsequently sought further evidence if specific proteins indeed redistribute during organelle division. To this end, we constructed a strain in which Pex25-GFP was produced under control of the methyl amine-inducible amine oxidase promoter (P_{AMO}). This strain, which also produced DsRed-SKL to mark peroxisomes, was first grown on methanol/methylamine to induce peroxisome biogenesis and Pex25-GFP synthesis. After 5 h of cultivation, cells of these cultures contained peroxisomes with Pex25-GFP fluorescence randomly distributed over the organelle surface. The culture was subsequently shifted to fresh methanol/ammonium sulfate medium, conditions that fully repress

Pex25-GFP synthesis (**Figure 3(I)**). After 5 h of further cultivation, at which time the culture density had doubled, Pex25-GFP fluorescence was observed on organelles and specifically had concentrated on the peroxisome extensions (**Figure 3(II)**). After a further doubling of the culture (**Figure 3(III)**), a similar distribution pattern of Pex25 fluorescence was observed. Because this fluorescence was independent of Pex25-GFP synthesis, as this was blocked in this 10-h time interval, these data strongly suggests that the protein is reallocated to the newly formed organelles/organelle extensions. The decrease in Pex25-GFP fluorescence intensities at the organelles, at which the extensions are formed, strengthens this view.

Pex11 is required to form PMP subdomains

Pex11 plays a crucial role in organelle fission. To analyze if Pex11 is important for the redistribution of PMPs, we determined PMP localizations in *dnm1.pex11* double mutant cells, which are hampered to form extensions because of the deletion of Pex11 (12). In both budding and non-budding cells, Pex14, Pex8, Pex10 and Pex25 fluorescence invariably was observed to be relatively evenly distributed over the organelle surface, comparable to Pmp47. These proteins were never observed concentrating as observed in *dnm1* cells (**Figure 4**). These data suggest that Pex11 is important for specific PMPs to concentrate on the organelle surface.

Interestingly, the localization of Inp1 and Inp2 was unchanged upon deletion of PEX11 in dnm1 cells. Inp1-GFP was still observed as a fluorescent spot both in non-budding and budding cells (**Figure 4**). A faint Inp2 signal could be detected at peroxisomes in non-budding cells. In budding cells, Inp2-GFP was infrequently observed in the fluorescent spot associated with the peroxisome

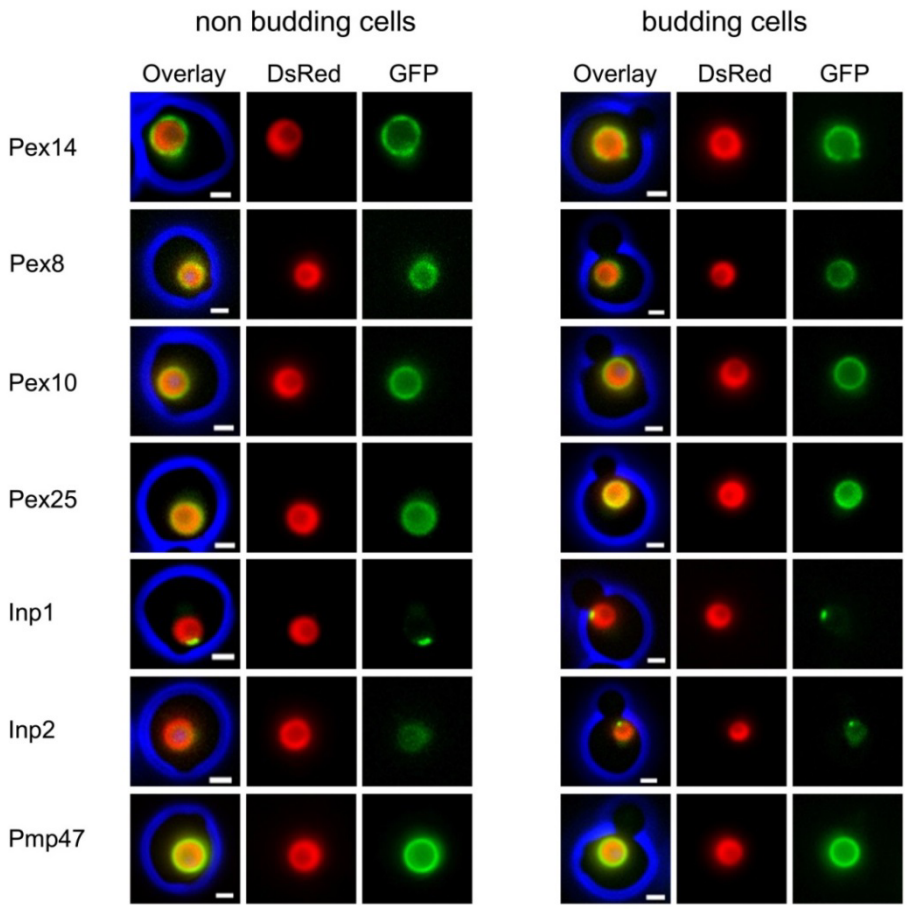

Figure 4: Pex11 is required for reorganization of certain PMPs on the peroxisomal membrane.
dnm1.pex11 cells exponentially grown on methanol generally contain one peroxisome per cell, both in budding and non-budding cells. Localizations of the various PMPs were analyzed using *C*-terminal GFP fusions of the respective proteins and DsRed-SKL to mark the peroxisomal matrix. Pex14- mGFP, Pex8-mGFP, Pex10-mGFP and Pex25-eGFP were never observed in spots, but were distributed evenly on the peroxisome membrane, like Pmp47-mGFP. The localization of Inp1- eGFP and Inp2-mGFP was similar as observed in *dnm1* cells, except that Inp2-mGFP was in a spot on the organelle in the mother cell. The scale bar represents 1 µm.

In WT cells, PMPs also show variable distribution patterns

In control experiments, WT strains that produce GFP-tagged Pex14, Pex8, Pex10, Inp1, Inp2 and Pmp47 as well as DsRed-SKL were used. DsRed-SKL was expressed under control of the methanol-inducible alcohol oxidase

promoter. Cells were precultured on glucose, conditions that repress peroxisome formation as well as DsRed-SKL synthesis and then shifted to media supplemented with methanol as the sole carbon source to induce peroxisome proliferation and DsRed-SKL synthesis. The development of peroxisomes and the distribution patterns of the PMPs under study were followed in time.

In the initial hours of cultivation, when the cells still contain a single peroxisome (as in glucose-grown cells), Pex14-, Pex8-, Pex10 (**Figure 5**)- and Pmp47 (**Figure 6B**)- related fluorescence was observed to be relatively evenly distributed over the organelle surface 5(I). For Pex14, Pex8 and Pex10, but not Pmp47, this fluorescence pattern changed when the organelles entered their first stage of multiplication by fission, generally after 8 h of cultivation. At this time point, most of the fluorescence concentrated in a spot of enhanced fluorescence at the peroxisome (**Figure 5(II)**).

As shown in **Figure 5A(I)**, Pex14-GFP fluorescence was relatively evenly distributed over young developing organelles. After growth/maturation (generally after 8 h of cultivation), the Pex14-GFP fluorescence became concentrated at one spot with lower fluorescence at the remaining part of the organelle surface. This spot probably represented the initiation site of organelle fission and, after scission, resulted in a small organelle with high Pex14-GFP fluorescence together with a mature organelle with lower fluorescence **5A(III)**. In **Figure 5A**, an example is shown after a second fission step **5A(III)**. This cell contains three peroxisomes, of which the small one contains the bulk of the GFP fluorescence but hardly any detectable DsRed-SKL fluorescence yet. Similar phenomena were observed for peroxisome fission events related to budding of the cell (**Figure 5A(IV)**). Essentially, the same observations were made for Pex8 and Pex10 (**Figure 5B,C**). Also, for these proteins the matrix marker DsRed-SKL remained below the limit of detection in the small organelles shortly after fission, and also for the organelles that migrated to the newly developing yeast buds. A characteristic feature of these GFP fusion proteins was their relatively uneven intensity at the larger, mature (low fluorescence) and small, nascent organelles (higher fluorescence). Together, these data lend support to

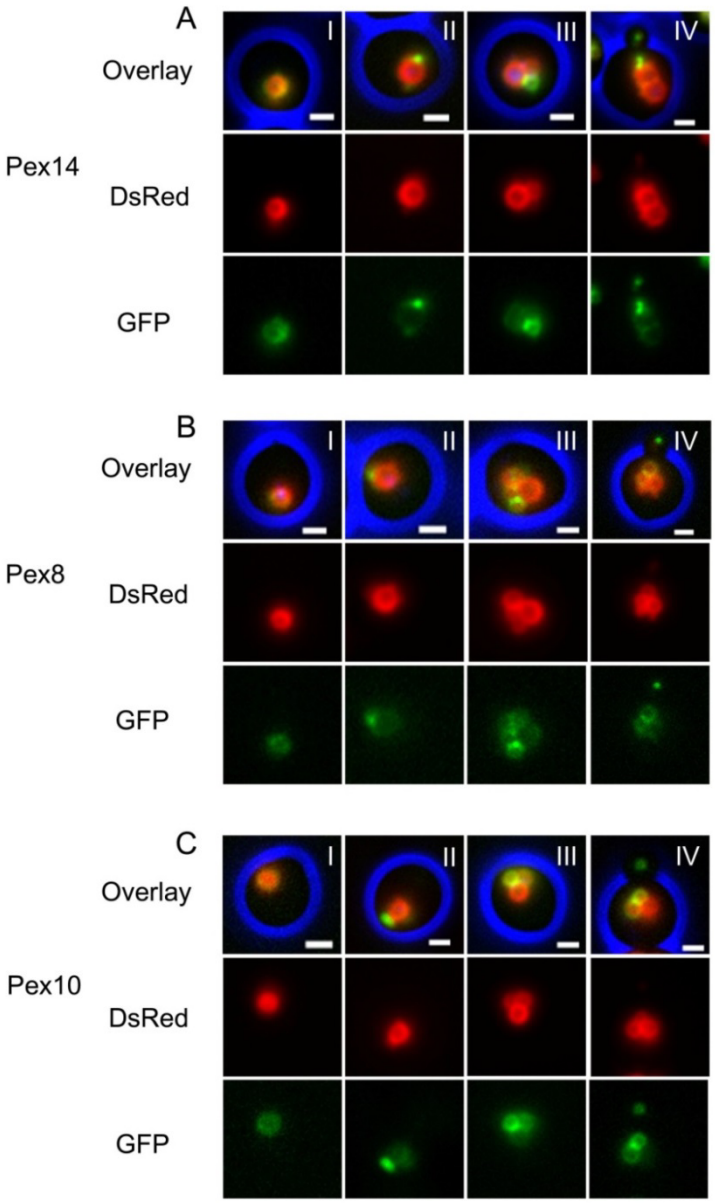

Figure 5: Localization of different PMPs in WT *H. polymorpha* cells.
A) The distribution of Pex14-eGFP. In young cells, on relatively small peroxisomes, Pex14-eGFP is evenly distributed over the organellar surface (I). At a later stage (II), part of the fluorescence concentrates in a spot which develops into a new, small peroxisome. (A) III shows a cell after two peroxisome divisions, where the smallest organelle has the highest Pex14 level and very low amounts of DsRed-SKL. During budding, the small organelle moves into the bud (IV). Similar patterns are observed for Pex8-mGFP (B) and Pex10-mGFP (C). The scale bar represents 1 μm.

the notion that the distribution of specific PMPs over the organelles varies with the organelle developmental stage.

The localization of Pex11 and Pex25 was analyzed in a single strain in which Pex25 was genomically tagged with mGFP and Pex11 with mCherry. In methanolgrown cells, Pex11-mCherry fluorescence was relatively evenly distributed over the peroxisomal surface of all organelles, similar to Pmp47 (**Figure 6A,B**). Fluorescence of Pex11-mCherry, but not of Pex25-mGFP, was invariably very weak on the organelle in the bud (**Figure 6A(IV)**). Pex25-mGFP fluorescence showed a distribution pattern similar to the proteins of the importomer. Also for Pex25 and Pex11, spots of enhanced fluorescence were observed prior to fission of the organelle.

The distribution of Inp1 and Inp2 was essentially similar as in *dnm1* cells (**Figure 6B**). In case of Inp1 one (**Figure 6B**) or multiple (data not shown) spots of enhanced fluorescence are present per cell, which are localized to the peroxisomes in the mother cell. Inp2-GFP fluorescence invariably colocalized with an organelle in the daughter cell (**Figure 6B**). In non-budding cells, the fluorescence of both proteins was very faint or below the limit of detection. This faint fluorescence colocalized with DsRed-SKL (**Figure 6B**).

Quantitative analysis

Strikingly, in case of Pex8, Pex10, Pex14 and Pex25 the fluorescence intensity was relatively high at the organelles in the buds in contrast to the relative low intensity of Pex11 and Pmp47 fluorescence. To quantify this, we determined the average fluorescence intensities on peroxisomes in the mother cells and buds and calculated the ratios of both the intensities. As shown in **Figure 6C**, Pex25, Pex8, Pex10 and Pex14 showed a ratio less than 1 implying that the average fluorescence intensity on peroxisomes was enhanced in the daughter cells relative to those in mother cells. However, the ratio obtained for Pex11 and Pmp47 exceeded 1, indicating that the fluorescence intensities of these proteins were higher on the organelles in the mother cell.

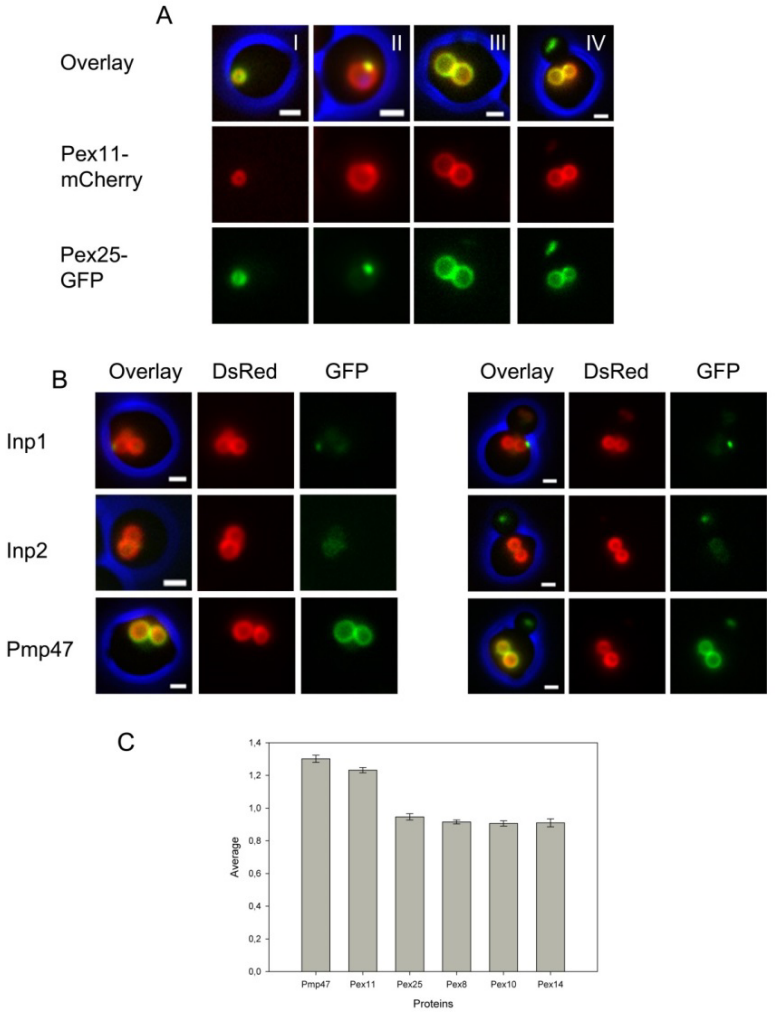

Figure 6: Localization of Pex11, Pex25, Inp1, Inp2 and Pmp47.
A) The localization of Pex11-mCherry and Pex25-mGFP in WT cells. In a young cell, the two proteins are evenly distributed over the organelle surface (I). Subsequently, Pex25-mGFP, and to a much lesser extent Pex11-mCherry, concentrate in a spot (II). When two big organelles are present, as seen in (III), both Pex11-mCherry- and Pex25- mGFP-related fluorescence is present uniformly on the entire peroxisome membrane. In budding cells, Pex25 fluorescence is enhanced at the organelle in the bud when compared to Pex11 (IV). B) The localization of Inp1-eGFP and Inp2-mGFP in non-budding cells (left panels) and budding cells (right panel). Inp1 is invariably present as a spot in addition to weak fluorescence on the entire organellar surface. In budding cells, this spot is present on an organelle in the mother cell. Inp2 fluorescence is very low in non-budding cells, but localizes to peroxisomes. It is present as a spot in the bud in budding cells. The scale bar represents 1 μm. C) Quantification data obtained by calculating the ratio between the mean fluorescence intensity of peroxisomes in the bud and the mean fluorescence intensity of peroxisomes in the mother cell using WT cells (Figures 5 and 6 A,B). For each sample, 100 budding cells were measured. The error bar represents the standard error of mean.

Statistical analysis of the quantitative data revealed no significant difference in the average ratios between Pex25, Pex8, Pex10 and Pex14 ($p < 0.02$). All four proteins, however, showed a significant difference from the ratios of Pex11 and Pmp47. This suggests that we have identified two classes of proteins which show different spatiotemporal behavior related to the organelle fission.

Inp2 is not required for concentration of Pex10-GFP fluorescence in spots

The redistribution of specific PMPs is most striking in budding *dnm1* cells (**Figure 1**). In these cells, a peroxisome elongation containing Pex14, Pex8, Pex10 and Pex25 protrudes into the developing bud, a process that shows parallels with inheritance of small peroxisomes containing these peroxins in WT cells (**Figures 5 and 6**).

To test whether the organelle inheritance process, which involves Inp2, influences the distribution of PMP fluorescence, we constructed a *dnm1.inp2* double deletion strain. As shown in **Figure** 7A, these cells do not contain organelle extensions. This observation indicates that Inp2 plays a role in the formation of the extensions toward the bud in *dnm1* cells. Also, in *dnm1.inp2* cells Pex10-GFPrelated fluorescence still concentrates in a spot on the large organelle in the mother cell, indicating that Inp2 is not involved in the formation of this spot.

Pex11 is required for the redistribution of specific PMPs

In *dnm1* cells, the peroxins Pex14-, Pex8-, Pex10- and Pex25-related GFP fluorescence was enhanced in spots at peroxisomes that were not observed when, in addition, *PEX11* was deleted (i.e. in *dnm1.pex11* cells; **Figure 4**). To analyze whether this effect is due to the combination of deleting *DNM1* and *PEX11*, we also localized Pex10 in a *pex11* single deletion strain. As shown in **Figure 7B**, Pex10-GFP never concentrated, and was observed to be relatively uniformly distributed over the entire organelle, similar to what was observed in

dnm1.pex11. This finding suggests that Pex11 functions in the formation of the fluorescence concentrations.

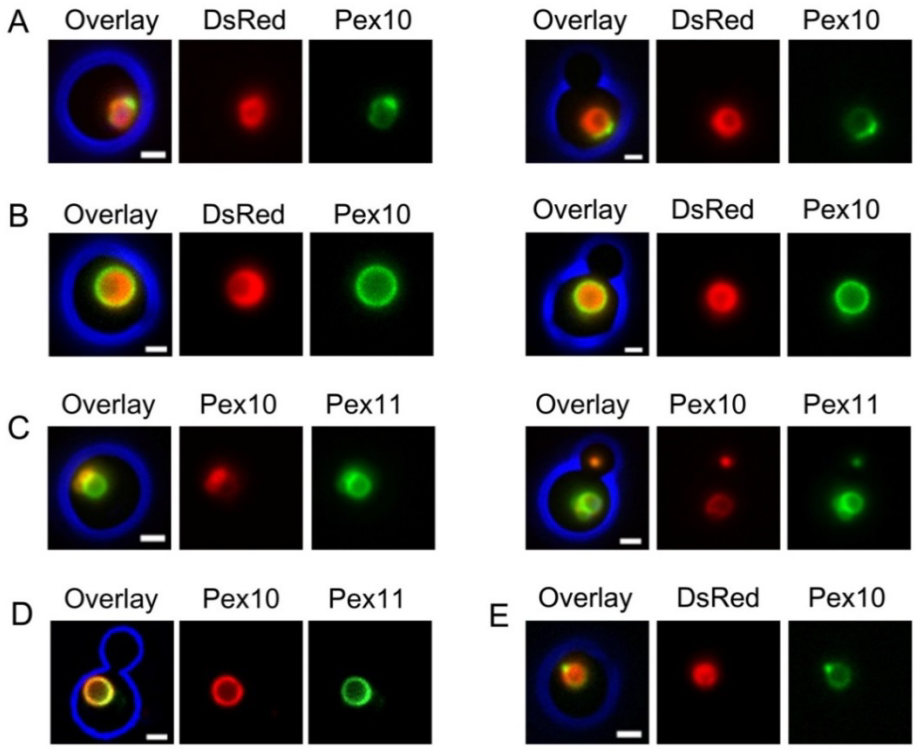

Figure 7: Pex11 is directly involved in the formation of PMP concentrations.
A) The localization of Pex10-mGFP in cells lacking *DNM1* and *INP2*. In both budding and non-budding cells, Pex10 concentrates in a spot on the peroxisome membrane. The peroxisome is marked with DsRed-SKL. B) The localization of Pex10-mGFP in *pex11* cells. These cells contain one peroxisome in the mother cell and no extensions to the bud. Pex10-mGFP was evenly distributed over the organelle membrane and no concentrations were observed. C) The localization of Pex11-mGFP (full-length control; left panel) in *pex11* cells expressing Pex10-mCherry. In these cells, multiple peroxisomes can be observed and Pex10 concentrates on small organelles, like in WT cells. D) The localization of dNPex11-mGFP, which lacks the Pex11 N-terminus in *pex11* cells expressing Pex10-mCherry. In dNPex11-mGFP cells, Pex10 is observed to be localized uniformly over the entire organelle. E) The localization of Pex10-mGFP in *emp24.erp3* cells producing DsRed-SKL to mark peroxisomes. Pex10 concentrates in a spot. The scale bar represents 1 μm.

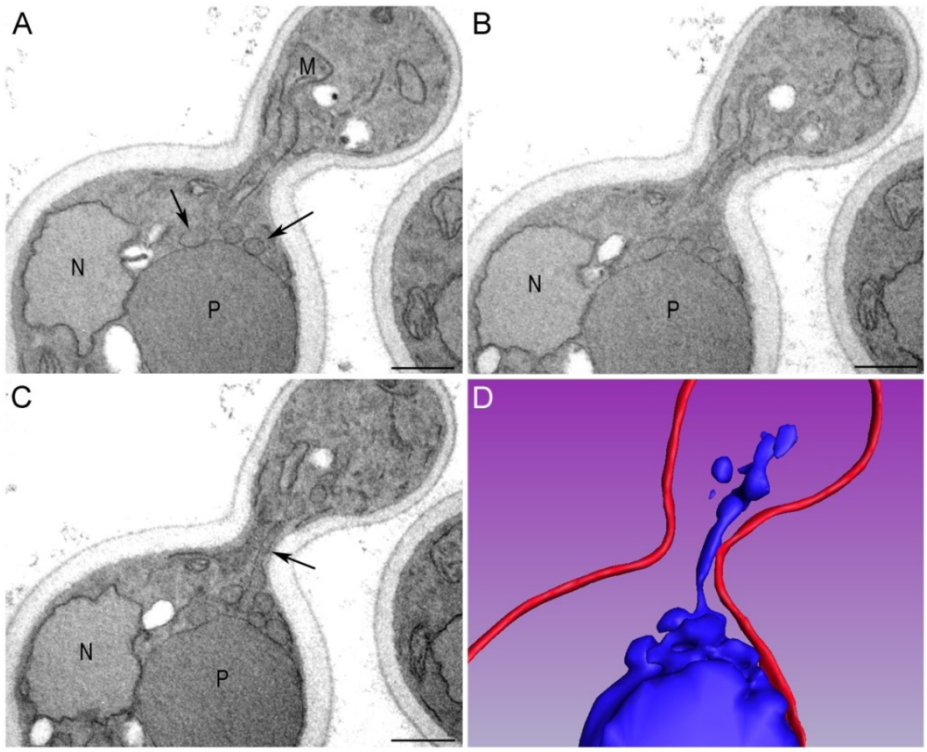

Figure 8: Peroxisomes in *dnm1* cells contain vesicular structures at the base of the extension.
A–C) Three consecutive sections from a series of 25 serial sections through a methanol-grown *dnm1* cell to show the formation of various peroxisome vesicles (arrow) at the site of the formation of the peroxisome extension). A 3D reconstruction of these sections is shown in (D). Arrow in (C) indicates details of the relatively very small diameter of the extension. The scale bar represents 500 nm. Fixation, $KMnO_4$; N, nucleus; P, large mother peroxisome.

We recently showed that the extreme *N*-terminus of Pex11 contains a hydrophobic α-helix which is involved in membrane bending, a process essential prior to the actual fission process (15). To test whether this specific function of Pex11 was required for the formation of PMP-related fluorescent spots, we deleted the region from the Pex11 *N*-terminus that contains this α-helix and introduced it in *pex11* cells. Growth analysis and quantification of peroxisome numbers revealed that this strain has the same phenotype as *pex11* cells, indicating that the membrane bending activity of Pex11 was indeed inactivated (data not shown). As observed in *pex11* cells and also in cells containing the *N*-

terminal truncation of Pex11, Pex10 fluorescence was uniformly distributed over the entire organelle. Concentration of Pex10-mCherry was never observed, suggesting that the activity in the *N*-terminus is important for the distribution of PMPs (**Figure 7D**). In the control strain where *pex11* cells were complemented with full-length Pex11, Pex10-mCherry was observed to be concentrated, like in the WT control (**Figure 7C**).

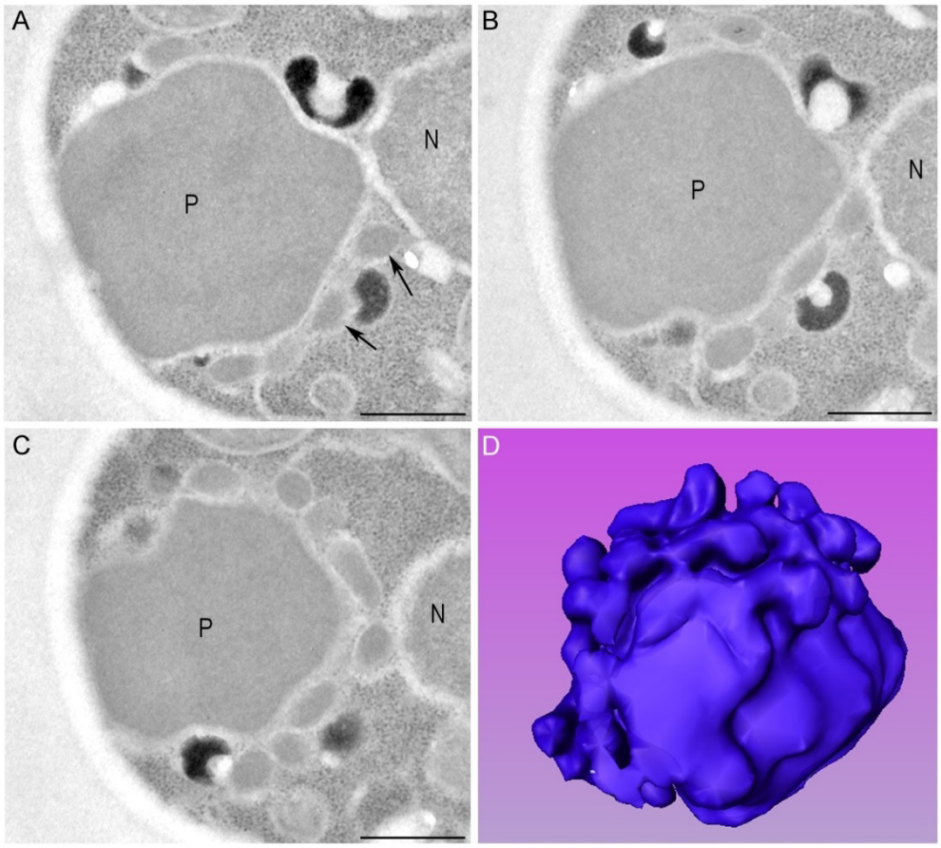

Figure 9: Vesicular structures are still formed in *dnm1.inp2* cells.
A–C) Three consecutive sections from a series of serial sections through a methanol-grown *dnm1.inp2* double mutant cell to show the formation of various peroxisome vesicles (arrow) randomly over the peroxisome surface. An extension is not formed as is also evident from the 3D reconstruction in (D). The scale bar represents 500 nm. fixation, glutaraldehyde; N, nucleus; P, large mother peroxisome.

The above data suggest that Pex11 plays a role in the concentration of specific peroxins at peroxisomes. Alternatively, however, the disappearance of these concentrations in *pex11* or *dnm1.pex11* cells may be indirectly related to the function of PEX11 in fission. To test this, we analyzed the localization of Pex10-GFP in *H. polymorpha* cells that have a defect in peroxisome division because of deletion of *EMP24* and *ERP3* (26). As shown in **Figure 7E**, Pex10-GFP still concentrated a spot that colocalized with peroxisomes in *emp24.erp3* cells, indicating that a defect in peroxisome fission does not invariably result in the disappearance of fluorescence concentrations.

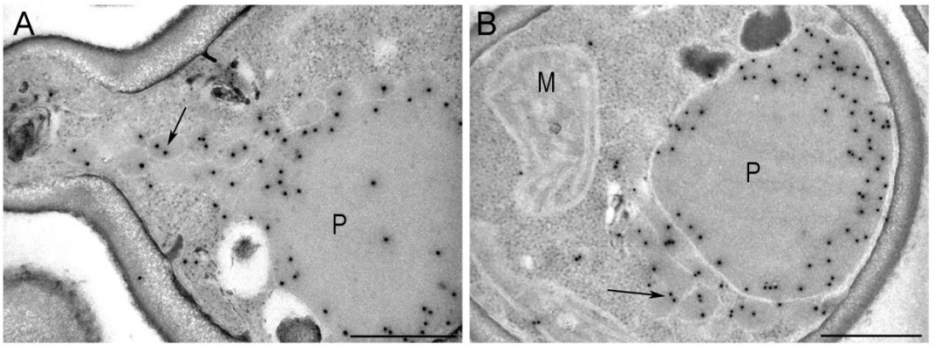

Figure 10: The vesicular structures in *dnm1* and *dnm1.inp2* cells are peroxisomal.
Immunolabeling using anticatalase antibodies. The vesicular structures (arrow) associated with peroxisomes in *dnm1* cells (A) and *dnm1.inp2* cells (B) are peroxisomal in nature as they contain the peroxisomal marker protein catalase. In the large peroxisomal structure, labeling is confined to the periphery of the organelle. This is due to the fact that a crystalloid consisting of alcohol oxidase protein is present in the central part of the organelle (26). The scale bar represents 500 nm. M, mitochondrion; P, peroxisome.

To further understand the mechanistic details of subdomain formation, electron microscopy was performed. These analyses showed that the sites of enhanced Pex11-GFP fluorescence at the base of the extension in *dnm1* cells in fact represented a region of enhanced membrane vesiculation. Numerous vesicles, which measured up to 150–200 nm, were observed still adhering to the mother organelle (**Figure 8A–C**). A representative three-dimensional (3D) reconstruction on the basis of a series of serial sections is presented in **Figure 8D**. This figure also shows that only one extension is formed toward the bud in conjunction with many small vesicles present at the base of the extension.

Similar experiments using the *dnm1.inp2* double mutant again revealed the formation of numerous membrane vesicles (**Figure 9**). However, these cells failed to form an extension, suggesting that the pulling force generated by Myo2 bound to Inp2 is essential for the formation of the extension. Immunocytochemical experiments revealed that the vesicular structures contain catalase (**Figure 10**) and alcohol oxidase (not shown) protein, indicating that they are peroxisomal of nature.

Discussion

We have analyzed the distribution of several different PMPs in WT and mutant strains of the yeast *H. polymorpha*. Differences in distribution were most evident at peroxisomes in cells of an *H. polymorpha DNM1* deletion strain (*dnm1*). In peroxisomes of these cells two subcompartments can be distinguished, namely an enlarged organelle in themother cell from which an extension is formed that protrudes into the newly forming bud. Using fluorescence microscopy and GFP fusion proteins, we showed that Pex14, Pex8 and Pex10, three peroxins involved in peroxisomal protein import, predominantly colocalize with the extension. Pex25, a protein of the Pex11 protein family, showed a similar distribution. Conversely, Pex11 fluorescence was enhanced at the base of the peroxisome extension, suggesting that the protein is involved in the formation of this structure (12). The peroxisomal transporter protein Pmp47 did not appear to concentrate at either the extension or the mother organelle.

So far, only concentrated protein localizations at peroxisomes were reported for Inp1 and Inp2, two proteins involved in peroxisome inheritance (27). In *H. polymorpha dnm1* cells, Inp1-GFP could also be detected as a fluorescent spot colocalizing with the large peroxisome in the mother cell. In contrast, Inp2-GFP fluorescence colocalized with the tip of the extension in the bud.

Summarizing, we observed five different PMP distribution patterns at peroxisomes in budding *dnm1* cells, namely (i) as a spot on the tip of the extension (Inp2), (ii) as a spot on the mother organelle (Inp1), (iii) enhanced at the extension (Pex14, Pex8, Pex10 and Pex25), (iv) enhanced at the base of the extension (Pex11) or (iv) relatively evenly distributed over the entire organelle (Pmp47). The different distribution patterns of these proteins are most probably not related to their topology. This view is based on the findings that Pex14, an integral membrane protein (28), and Pex8, a protein associated with the inner surface of the peroxisomal membrane (Pex8) (29), behave similarly in our experiments. On the other hand, Pmp47, an integral membrane protein (30), displays a different distribution pattern from Pex14 or Pex10 (16, 28). The comparable distribution patterns of Pex14, Pex8 and Pex10 were not unexpected as these proteins have been shown to be in the same protein complex (17, 31). Unexpectedly, Pex25 behaved in a similar manner as the importomer proteins.

These four peroxins accumulate at the peroxisome extensions in *dnm1* cells and are also enhanced at the nascent peroxisomes and organelles in the buds in WT cells. These observations strongly suggest that in fact the peroxisome extension in *dnm1* cells represents a newly formed peroxisome that is not yet separated from the mother organelle. This extension is not an artificial structure as it is also occasionally observed in WT cells by confocal laser scanning microscopy (data not shown). Most probably, pinching off of the newly formed organelle is a rapid process in WT cells, making the visualization of this process very rare.

In WT cells, Pex11 fluorescence was not enhanced at nascent organelles or at the organelles that segregated to the bud, as observed for Pex14, Pex8, Pex10 and Pex25. Quantitative analysis of fluorescence intensities in budding cells strengthened our observation of the exceptional distribution pattern of Pex11.

In WT cells, Pmp47 was the only membrane protein observed that never concentrated in a spot, although the Pmp47-related fluorescence was slightly decreased in nascent organelles relative to the mother organelles. This may be

related to the observation that the nascent organelles, shortly after fission, show a reduced matrix content and therefore may not yet be fully physiologically active at this stage. This strengthens the need for a maximal protein import capacity, as suggested by the enhanced levels of importomer proteins on these organelles.

Recent data by Delille et al. (6) revealed two distinct regions on peroxisomal membranes in mammalian cells overproducing a Pex11β-yellow fluorescent protein (YFP)/GFP fusion protein. Overproduction of this protein was proposed to have a dominant negative effect on peroxisome fission, but the stage and mechanism of this block remained unknown (6). In these cells, globular peroxisomes had long membrane extensions which contained Pex11β-YFP/GFP and Fis1, but no other peroxins or transporter proteins which invariably accumulated only on the extension. Some peroxins were localized to both the globular region and the membrane extensions and others exclusively to the globular domain. In these cells, fission is most probably blocked at a very early stage, because the phenotype did not resemble that of *DLP1* silencing in mammalian cells. This most probably explains the differences in the results obtained in these studies compared with our findings in *dnm1* and WT yeast cells.

The distribution of all peroxins, except for Inp1 and Inp2, became much more homogeneous over the organelle surface upon deletion of *PEX11* in either *H. polymorpha* WT or *dnm1* cells. This suggests that the presence of Pex11 is important for the distribution of peroxins.

We show that not just the presence of Pex11 protein but Pex11 containing its membrane-bending activity in the *N*-terminus is required for PMP distribution. We also show that the formation of fluorescent spots of peroxins is not indirectly related to the fission activity of Pex11, as these spots are still formed in cells of an *emp24.erp3* mutant that are defective in peroxisome fission, like *pex11* cells (32). Also, these spots are still formed upon deletion of *INP2* in *dnm1* cells, which results in the disappearance of the extension toward the bud.

Our detailed electron microscopy studies on *dnm1* cells revealed extensive vesiculation of the peroxisomal membrane at the base of the extension, where Pex11-GFP fluorescence was enhanced. This is fully in line with our recent finding that Pex11 displays peroxisome membrane deforming activities as a first step in organelle fission (15). Indeed, peroxisomal membrane vesiculation was not observed by electron microscopy of thin sections prepared from *H. polymorpha pex11* cells (33).

Despite the numerous vesicles in *dnm1* cells, only a single extension is formed. The fact that Inp2 locates to only a single organelle in budding WT cells is in line with previous observations (21, 22). Our current data also suggest that the pulling force of the Myo2–Inp2 complex is essential for the formation of the extension in *dnm1* cells, because in *dnm1.inp2* cell vesiculation, but no extension was observed. Immunocytochemistry confirmed the peroxisomal nature of the vesicles. Although several vesicles had an open connection to themature peroxisome, it is not yet clear whether this holds true for all these structures. However, after cell division, only one peroxisome per cell is observed in these cells suggesting that these peroxisome vesicles do not develop into separate organelles and hence most probably remain connected to the large organelle.

The differences in protein distribution over the peroxisome membrane may be related to specific subdomains (i.e. lipid rafts) on the membrane or protein–lipid and protein–protein interactions. Alternatively, the curvature of the membranes may affect the localization of the different PMPs. Indeed, the curvature of the membrane may differ in the extension, the region of membrane vesiculation at the base of the extension and in the globular part of the organelle (**Figure 8**).

Similar differences in bending may occur in peroxisomes during fission in the WT cells.

We previously showed that methanol-induced *H. polymorpha* cells harbor a heterogeneous population of peroxisomes with respect to their capacity

to import proteins (34). The small nascent organelles are the preferred sites of import of newly synthesized proteins, whereas the large mature organelles have largely lost the capacity to import matrix proteins. On the basis of these findings, it has been suggested that after reaching the mature size, the organelle divides asymmetrically and possibly donates the bulk of the functional importomer proteins to the nascent organelle.

This mode of PMP movement to nascent organelles may be possible, judged from the results on Pex25 redistribution after inhibition of its synthesis. In this way, the mature organelles may lose the bulk of the importomers and hence the capacity to import matrix proteins. Our current data are fully consistent with this view and suggest that the levels of the proteins of the importomer on a specific organelle determine its protein import competence.

Overall, our data clearly show that PMPs may be organized into multiple subdomains and may redistribute during organelle fission. We propose that this process is required to warrant the formation and eventual inheritance of organelles that are properly equipped for rapid growth by import of membrane and matrix components. We present evidence that Pex11 is involved in this protein reorganization process.

Supporting Information

Supplementary tables:

Table S1: *H. polymorpha* strains used in this study

Strain	**Description**	**Source/Reference**
NCYC 495 leu1.1, ura3	Wild type leu1.1 ura3	(35)
NCYC 495 leu1.1	Wild type leu1.1	(35)
DsRed-SKL	WT cells with integration of pSNA4	(22)
dnm1	Deletion of *DNM1*	(12)
dnm1.DsRed-SKL	*dnm1* with integration of plasmid pSNA03	(12)
dnm1.pex11	Double deletion *DNM1.PEX11*	(35)
dnm1.pex11.DsRed-SKL	*dnm1.pex11* with integration of plasmid pHIPZ4-DsRed-T1-SKL	(35)
*dnm1.pex11.N4*DsRed-SKL	*dnm.1pex11* with integration of plasmid pSNA13	This study
dnm1.inp2	Double deletion *DNM1.INP2*	This study
dnm1.inp2.N4DsRed-SKL	*dnm1.inp2* with integration of plasnid pSNA13	This study
dnm1.inp2.N4DsRed-SKL,Pex10-GFP	*dnm1.inp2*.N4DsRed-SKL with integration of plasmid pMCE5	This study

Pex11-mCherry.Pex25-GFP	Cells with on copy integration of plasmids pMCE1 and pMCE3	This study
dnm1.DsRed-SKL.Pex25-GFP	*dnm1*.DsRed-SKL with one copy integration of plasmid pEXP-Pex25-GFP	This study
dnm1.pex11.DsRed-SKL.Pex25-GFP	*dnm1.pex11*.DsRed-SKL with one copy integration of plasmid pEXP-Pex25-GFP	This study
dnm1.Pex11-GFP.DsRed-SKL	*DNM1* with integration of plasmid pEXP-Pex11.GFP and pHipZ4-DsRed-SKL	(35)
DsRed-SKL.Pex8-GFP	DsRed-SKL with one copy integration of plasmid pMCE4	This study
dnm1.DsRed-SKL.Pex8-GFP	*dnm1*.DsRed-SKL with one copy integration of plasmid pMCE4	This study
*dnm1.pex11.N4*DsRed-SKL.Pex8-GFP	*dnm1.pex11.N4*DsRed-SKL with one copy integration of plasmid pMCE4	This study
DsRed-SKL.Pex10-GFP	DsRed-SKL with one copy integration of plasmid pMCE5	This study
dnm1.DsRed-SKL.Pex10-GFP	*dnm1*.DsRed-SKL with one copy integration of plasmid pMCE5	This study

*dnm1.pex11.N4*DsRed-SKL.Pex10-GFP	*dnm.pex11.N4*DsRed-SKL with one copy integration of plasmid pMCE5	This study
DsRed-SKL.Pex14-GFP	DsRed-SKL with one copy integration of plasmid pSNA12	This study
dnm1.DsRed-SKL.Pex14-GFP	*dnm1*.DsRed-SKL with one copy integration of plasmid pSNA12	This study
*dnm1.pex11.N4*DsRed-SKL.Pex14-GFP	*dnm1.pex11.N4*DsRed-SKL with one copy integration of plasmid pSNA12	This study
DsRed-SKL.Inp1-GFP	Wild type with integration of plasmids pAMK6 and pHIPX7 DsRed–SKL	(22)
dnm1.DsRed-SKL.Inp1-GFP	*dnm1*.DsRed-SKL with one copy integration of plasmid pAMK6	This study
*dnm1.pex11.N4*DsRed-SKL.Inp1-GFP	*dnm1.pex11.N4*DsRed-SKL with one copy integration of plasmid pAMK6	This study
DsRed-SKL.Inp2-GFP	DsRed-SKL with one copy integration of plasmid pSNA11	(12)
dnm1.DsRed-SKL.Inp2-GFP	*dnm1*.DsRed-SKL with one copy integration of plasmid	This study

	pSNA11	
*dnm1.pex11.N4*DsRed-SKL.Inp2-GFP	*dnm1.pex11.N4*DsRed-SKL with one copy integration of plasmid pSNA11	This study
DsRed-SKL.Pmp47-GFP	DsRed-SKL with one copy integration of plasmid pMCE7	This study
dnm1.DsRed-SKL.Pmp47-GFP	*dnm1*.DsRed-SKL with one copy integration of plasmid pMCE7	This study
*dnm1.pex11.N4*DsRed-SKL.Pmp47-GFP	*dnm1.pex11.N4*DsRed-SKL with one copy integration of plasmid pMCE7	This study
pex11	Deletion of *PEX11*	(33)
pex11.Pex10-mCherry	*pex11* with integration of pMCE8	This study
pex11.Pex11-GFP.Pex10-mCherry	*pex11*.Pex10-mCherry with integration of pMCE9	This study
pex11.dNPex11-GFP.Pex10-mCherry	*pex11*.Pex10-mCherry with integration of pMCE10	This study
emp24.erp3	Deletion *of EMP24* and *ERP3*	(32)
emp24.erp3.Pex10-GFP	*emp24.erp3* with integration of plasmid pMCE5	This study
emp24.erp3.N4DsRed-SKL.Pex10-GFP	*emp24.erp3*.Pex10-GFP with integration of plasmid pSNA13	This study

Table S2: Plasmids used in this study

Plasmid	Description	Source/Reference
pCGCN-FAA4	Plasmid containing mGFP	Gift from S. Kohlwein, Graz,Austria
pANL31	Plasmid containing *GFP* without start codon; zeo^R , amp^R	(36)
pHIPZ-mGFP fusinator	Plasmid containing mGFP without start codon; amp^R; zeo^R	(12)
pSNA11	pANL31 containing the 3'-end of the *INP2* gene fused in-frame to GFP; zeo^R, amp^R	(12)
pSNA12	pANL31 containing the 3'-end of the *PEX14* gene fused in-frame to GFP; zeo^R, amp^R	This study
pSNA13	Plasmid containing P_{AOX}*DsRed-SKL*, amp^R, nat^R	This study
pEXP-Pex25-GFP	Plasmid containing C-terminal part of *PEX25* fused to GFP; amp^R; nat^R	This study
pENTR-221-PEX25	Gateway vector containing *PEX25*	Lab collection
pDONR-P4-P1r-P_{AMO}	pDONR P4-1R containing P_{AMO}	(35)
pDONR-P2r-P3-	pDONR P2-P3 containing T_{AMO} and	(35)

eGFP-T_{AMO}	*eGFP*	
pDEST-R4-R3–NAT	pDESTR4-R1 containing nourseothricin marker	(35)
pHIPN4	Plasmid containing amp^R, nat^R	Lab collection
pAG25	Plasmid containing nourseothricin marker	Euroscarf
pRSA01	Plasmid containing mCherry; amp^R; zeo^R	Lab collection
pMCE1	Plasmid containing C-terminal part of *PEX25* fused to GFP; amp^R; zeo^R	This study
pMCE2	Plasmid containing mCherry; amp^R; nat^R	This study
pMCE3	Plasmid containing C-terminal part of *PEX11* fused to mCherry; amp^R; nat^R	This study
pMCE4	Plasmid containing C-terminal part of *PEX8* fused to GFP; amp^R; zeo^R	This study
pMCE5	Plasmid containing C-terminal part of *PEX10* fused to GFP; amp^R; zeo^R	This study
pMCE7	Plasmid containing C-terminal part of *PMP47* fused to GFP; amp^R; zeo^R	This study
pHIPZ4-DsRed-T1-SKL	Plasmid containing P_{AOX}*DsRed-SKL*, amp^R, zeo^R	(37)
pAMK6	pANL31 containing the 3'-end of the *INP1* gene fused in-frame to GFP;	(22)

	zeo^R, amp^R	
pMCE8	Plasmid containing C-terminal part of *PEX10* fused to mCherry; amp^R; nat^R	This study
pMCE9	Expression vector containing Pex11 gene under PEX11 promoter fused without stop codon with mGFP	This study
pMCE10	Expression vector containing Pex11 gene without first 97aa under PEX11 promoter fused without stop codon with mGFP	This study
pENTR21 – Pex11	Gateway vector containing *PEX11*	(35)
pENTR21-dNPex11	Gateway vector containing 98-259 aa of *PEX11*	This study
pENTR-P4-P1r-P_{PEX11}	Gateway vector containing P_{PEX11}	This study
pENTR-P2r-P3-mGFP-TAMO	Gateway vector containing T_{AMO} and m*GFP*	This study
pDEST-R4-R3–ZEO	pDESTR4-R1 containing zeocin marker	Lab collection

Table S3: Primers used in this study

Primer	**Sequence**
mGFP-fw	5' GGAAGATCTGTGAGCAAGGGCGAGGAGCT 3'
mGFP-rev	5'GTCGACGCGTGCATGCATGTTTACTTGTACAGCTCG TCCA 3'
Inp2-GFPforward	5' GTGCGTGCTGCTTGCAATAG 3'
Inp2-GFPreverse	5' CGCGGATCCCAATGCATTCATCAACAGGCC 3'
Pex14-GFPfw	5' CCCAAGCTTCGTTGCAGGAAGTCGACGAA 3'
Pex14-GFPrev	5' AGATCTTCCGGCATTCAGCTGCCACGCCG 3'
EMK1	5' CATTCTGGCACAGTACCTGTCGTC 3'
EMK2	5' GTGCAGATGAACTTCAGGGTCAGCTTG 3'
Pex8fw	5' CCCAAGCTTTACAGAGCGCGGGAAACTGC 3'
Pex8rev1	5' GGAAGATCTTAATTTTGCTTTTTCCTGACTCTCG 3'
Pex10fw	5' CCCAAGCTTAGGAGTACGTGGATCTGGTG 3'
Pex10rev new	5' GGAAGATCTTCGTAGAGGCAACAGCTGCG 3'
Natfw	5' ACGCGTCGACCCCACACACCATAGCTTCAA 3'
Natrev1	5' TCCCCGCGGATCATCGATGAATTCGAGCT 3'
Pex25GFPfw	5' CCCAAGCTTCAACGAAAGTCCTCAAGATG 3'
Pex25GFPrev1	5' GGAAGATCTATTCAGGCAGGGATTTAGCT 3'
Pex11mCherryfw	5' CCCAAGCTTCACGATAACATATCATCCGA 3'

Pex11mCherryrev1	5' GGAAGATCTTAGCACAGAAGACTCGGTCG 3'
Pmp47 fw	5' CGTCTCAAGCTTGGCTTGGAGAGTGCACTGGT 3'
Pmp47 rev	5' CGCGGATCCGATAACGAGATCTTTTGCAG 3'
dNPex11_fw	5'GGGGACAAGTTTGTACAAAAAAGCAGGCTCCATGTTTGAGAGCGTCAAGCAAGC 3'
dNPex11_rev	5'GGGGACCACTTTGTACAAGAAAGCTGGGTCTAGCACAGAAGACTCGGTCG 3'
Ppex11_fw	5'GGGGACAACTTTGTATAGAAAAGTTGCCGACATTCAAAACTGGCAGACAACGC 3'
Ppex11_rev	5'GGGGACTGCTTTTTTGTACAAACTTGCGGATAACTGTCTGTCTGTCCCGAG 3'
mGFP_G_fw	5' GAGCACCCAGTCCAAGCTGAGCAAAG 3'
mGFP_G_rev	5' CTTTGCTCAGCTTGGACTGGGTGCTC 3'

Acknowledgments

We thank Rinse de Boer, Anita Kram and Ramon Sieber for skillful assistance in various parts of this study. This project was carried out within the research program of the Kluyver Centre for Genomics of Industrial Fermentation which is part of the Netherlands Genomics Initiative/Netherlands Organization for Scientific Research.

References

1. Anderson RG, Jacobson K. A role for lipid shells in targeting proteins to caveolae, rafts, and other lipid domains. Science 2002;296(5574):1821-1825.

2. Stroh A, Anderka O, Pfeiffer K, Yagi T, Finel M, Ludwig B, Schagger H. Assembly of respiratory complexes I, III, and IV into NADH oxidase supercomplex stabilizes complex I in *Paracoccus denitrificans*. J Biol Chem 2004;279(6):5000-5007.

3. Ciarlo L, Manganelli V, Garofalo T, Matarrese P, Tinari A, Misasi R, Malorni W, Sorice M. Association of fission proteins with mitochondrial raft-like domains. Cell death and differentiation 2010;17(6):1047-1058.

4. Boukh-Viner T, Guo T, Alexandrian A, Cerracchio A, Gregg C, Haile S, Kyskan R, Milijevic S, Oren D, Solomon J, Wong V, Nicaud JM, Rachubinski RA, English AM, Titorenko VI. Dynamic ergosterol- and ceramide-rich domains in the peroxisomal membrane serve as an organizing platform for peroxisome fusion. J Cell Biol 2005;168(5):761-773.

5. Schrader M, Reuber BE, Morrell JC, Jimenez-Sanchez G, Obie C, Stroh TA, Valle D, Schroer TA, Gould SJ. Expression of *PEX11*β mediates peroxisome proliferation in the absence of extracellular stimuli. J Biol Chem 1998;273(45):29607-29614.

6. Delille HK, Agricola B, Guimaraes SC, Borta H, Luers GH, Fransen M, Schrader M. Pex11pβ-mediated growth and division of mammalian peroxisomes follows a maturation pathway. J Cell Sci 2010.

7. Girzalsky W, Saffian D, Erdmann R. Peroxisomal protein translocation. Biochim Biophys Acta 2010;1803(6):724-731.

8. Rucktaschel R, Girzalsky W, Erdmann R. Protein import machineries of peroxisomes. Biochim Biophys Acta 2010.

9. Nagotu S, Veenhuis M, van der Klei IJ. *Divide et impera*: the dictum of peroxisomes. Traffic 2010;11(2):175-184.

10. Hoepfner D, Schildknegt D, Braakman I, Philippsen P, Tabak HF. Contribution of the endoplasmic reticulum to peroxisome formation. Cell 2005;122(1):85-95.

11. Motley AM, Hettema EH. Yeast peroxisomes multiply by growth and division. J Cell Biol 2007;178(3):399-410.

12. Nagotu S, Saraya R, Otzen M, Veenhuis M, van der Klei IJ. Peroxisome proliferation in *Hansenula polymorpha* requires Dnm1p which mediates fission but not *de novo* formation. Biochim Biophys Acta 2008;1783(5):760-769.

13. Kim PK, Mullen RT, Schumann U, Lippincott-Schwartz J. The origin and maintenance of mammalian peroxisomes involves a de novo PEX16-dependent pathway from the ER. J Cell Biol 2006;173(4):521-532.

14. Thoms S, Erdmann R. Dynamin-related proteins and Pex11 proteins in peroxisome division and proliferation. The FEBS journal 2005;272(20):5169-5181.

15. Opalinski L, Kiel JA, Williams C, Veenhuis M, van der Klei IJ. Membrane curvature during peroxisome fission requires Pex11. Embo J 2011;30(1):5-16.

16. Tan X, Waterham HR, Veenhuis M, Cregg JM. The *Hansenula polymorpha PER8* gene encodes a novel peroxisomal integral membrane protein involved in proliferation. J Cell Biol 1995;128(3):307-319.

17. Agne B, Meindl NM, Niederhoff K, Einwachter H, Rehling P, Sickmann A, Meyer HE, Girzalsky W, Kunau WH. Pex8p: an intraperoxisomal organizer of the peroxisomal import machinery. Molecular cell 2003;11(3):635-646.

18. Wang D, Visser NV, Veenhuis M, van der Klei IJ. Physical interactions of the peroxisomal targeting signal 1 receptor pex5p, studied by fluorescence correlation spectroscopy. J Biol Chem 2003;278(44):43340-43345.

19. Kiel JA, Veenhuis M, van der Klei IJ. *PEX* genes in fungal genomes: common, rare or redundant. Traffic 2006;7(10):1291-1303.

20. Fagarasanu M, Fagarasanu A, Tam YY, Aitchison JD, Rachubinski RA. Inp1p is a peroxisomal membrane protein required for peroxisome inheritance in *Saccharomyces cerevisiae*. J Cell Biol 2005;169(5):765-775.

21. Fagarasanu A, Fagarasanu M, Eitzen GA, Aitchison JD, Rachubinski RA. The peroxisomal membrane protein Inp2p is the peroxisome-specific receptor for the myosin V motor Myo2p of *Saccharomyces cerevisiae*. Developmental cell 2006;10(5):587-600.

22. Saraya R, Cepińska MN, Kiel JA, Veenhuis M, van der Klei IJ. A conserved function for Inp2 in peroxisome inheritance. Biochim Biophys Acta 2010;1803(5):617-622.

23. Sambrook J, Fritsch EF, Maniatis T. Molecular cloning: a laboratory manual 2nd ed. New York: Cold Spring Harbor Laboratory; 1989.

24. Faber KN, Haima P, Harder W, Veenhuis M, Ab G. Highly-efficient electrotransformation of the yeast *Hansenula polymorpha*. Current genetics 1994;25(4):305-310.

25. Waterham HR, Titorenko VI, Swaving GJ, Harder W, Veenhuis M. Peroxisomes in the methylotrophic yeast *Hansenula polymorpha* do not necessarily derive from pre-existing organelles. Embo J 1993;12(12):4785-4794.

26. Keizer I, Roggenkamp R, Harder W, Veenhuis M. Location of catalase in crystalline peroxisomes of methanol-grown *Hansenula polymorpha*. FEMS microbiology letters 1992;72(1):7-11.

27. Fagarasanu A, Mast FD, Knoblach B, Rachubinski RA. Molecular mechanisms of organelle inheritance: lessons from peroxisomes in yeast. Nat Rev Mol Cell Biol 2010;11(9):644-654.

28. Komori M, Rasmussen SW, Kiel JA, Baerends RJ, Cregg JM, van der Klei IJ, Veenhuis M. The *Hansenula polymorpha PEX14* gene encodes a novel peroxisomal membrane protein essential for peroxisome biogenesis. Embo J 1997;16(1):44-53.

29. Waterham HR, Titorenko VI, Haima P, Cregg JM, Harder W, Veenhuis M. The *Hansenula polymorpha PER1* gene is essential for peroxisome biogenesis and encodes a peroxisomal matrix protein with both carboxy- and amino-terminal targeting signals. J Cell Biol 1994;127(3):737-749.

30. Jank B, Habermann B, Schweyen RJ, Link TA. PMP47, a peroxisomal homologue of mitochondrial solute carrier proteins. Trends in biochemical sciences 1993;18(11):427-428.

31. Hazra PP, Suriapranata I, Snyder WB, Subramani S. Peroxisome remnants in *pex3*Δ cells and the requirement of Pex3p for interactions between the peroxisomal docking and translocation subcomplexes. Traffic 2002;3(8):560-574.

32. Kurbatova E, Otzen M, van der Klei IJ. p24 proteins play a role in peroxisome proliferation in yeast. FEBS Lett 2009;583(19):3175-3180.

33. Krikken AM, Veenhuis M, van der Klei IJ. *Hansenula polymorpha pex11* cells are affected in peroxisome retention. The FEBS journal 2009;276(5):1429-1439.

34. Veenhuis M, Sulter G, van der Klei I, Harder W. Evidence for functional heterogeneity among microbodies in yeasts. Arch Microbiol 1989;151(2):105-110.

35. Sudbery PE, Gleeson MA, Veale RA, Ledeboer AM, Zoetmulder MC. *Hansenula polymorpha* as a novel yeast system for the expression of heterologous genes. Biochemical Society transactions 1988;16(6):1081-1083.

36. Leao-Helder AN, Krikken AM, van der Klei IJ, Kiel JA, Veenhuis M. Transcriptional down-regulation of peroxisome numbers affects selective

peroxisome degradation in *Hansenula polymorpha*. J Biol Chem 2003;278(42):40749-40756.

37. Monastyrska I, van der Heide M, Krikken AM, Kiel JA, van der Klei IJ, Veenhuis M. Atg8 is essential for macropexophagy in *Hansenula polymorpha*. Traffic 2005;6(1):66-74.

Chapter 3

Preperoxisomal vesicles can form in the absence of Pex3

Kèvin Knoops[1], Selvambigai Manivannan[1], Małgorzata N. Cepińska, Arjen M. Krikken, Anita M. Kram, Marten Veenhuis and Ida J. van der Klei*

[1]These authors contributed equally to this work.

Published in the Journal of Cell Biology, 204 (2014) 659-668

Abstract

We demonstrate that Pex3 is not required for the formation of preperoxisomal vesicles, as yeast *pex3* cells already contain reticular and vesicular structures, which harbour key proteins of the peroxisomal receptor docking complex, Pex13 and Pex14, as well as the matrix proteins Pex8 and alcohol oxidase. Other peroxisomal membrane proteins in these cells are unstable and transiently localized to the cytosol (Pex10, Pmp47) or endoplasmic reticulum (Pex11). The structures are more abundant in cells of a *pex3 atg1* double deletion strain, as the absence of Pex3 may render them susceptible for autophagic degradation, which is blocked in this double mutant. Our data indicate, contrary to earlier suggestions, that peroxisomes are not formed *de novo* from the ER when the *PEX3* gene is re-introduced in *pex3* cells. Instead, we find that re-introduced Pex3 sorts to the preperoxisomal structures in *pex3* cells, after which they mature into normal peroxisomes.

Introduction

Peroxisomes are ubiquitous cell organelles that are involved in a large variety of metabolic functions (1-3). It is generally accepted that peroxisomes proliferate by fission or form *de novo* from the endoplasmic reticulum (ER). Although it is still debated which mechanism of organelle multiplication prevails in wild-type (WT) cells, data obtained in yeast indicate that peroxisome fission is the most likely mechanism of peroxisome proliferation in normal WT cells (4-6).

In *pex3* mutant cells, which are reported to lack peroxisomal membrane structures, new organelles appear upon reintroduction of the *PEX3* gene. A generally accepted view is that in these cells the reintroduced Pex3 sorts to the endoplasmic reticulum (ER), followed by the formation of pre-peroxisomal structures, which pinch off from the ER and develop into mature peroxisomes. It has been suggested that all peroxisomal membrane proteins (PMPs) accumulate at the ER in *pex3* cells (7) and that upon reintroduction of Pex3, these PMPs are incorporated in two types of pre-peroxisomal vesicles that fuse to form peroxisomes (8). According to this model, Pex3 is important for the exit of PMPs from the ER into pre-peroxisomal vesicles.

To date, relatively little is known about the molecular mechanisms involved in the reintroduction of peroxisomes in *pex3* cells. Here, we re-investigated this process focusing on the ultrastructure of these cells and the subcellular localization of different PMPs prior to and after reintroduction of Pex3 using a *Hansenula polymorpha pex3 atg1* double deletion strain. The rationale for this approach is that we have previously shown that removal of Pex3 from the peroxisomal membrane is an essential early step in selective autophagic degradation of peroxisomes (9, 10). This implies that the presence of Pex3 at the peroxisomal membrane protects the organelles against autophagy. Hence, if peroxisomal membrane structures develop in *pex3* cells, they are likely to be rapidly degraded after their formation. To prevent autophagy, we deleted *ATG1*, a gene essential for this process, in a *H. polymorpha pex3* strain. Our results show that *pex3 atg1* cells contain preperoxisomal membrane structures,

which are the target for reintroduced Pex3 after which they mature into normal peroxisomes.

Materials and Methods

Strains and growth conditions

The *H. polymorpha* strains used in this study are listed in Table S1. Yeast cultures were grown at 37°C, either on (1) YPD media containing 1% yeast extract, 1% peptone and 1% glucose, (2) selective media containing 0.67% yeast nitrogen base without amino acids (YNB; Difco), or (3) mineral media (MM) (11) supplemented with 0.5% glucose (MM-Glu), 0.5% methanol or a mixture of 0.5 % methanol and 0.05 % glycerol (MM-M/G) as carbon sources and 0.25% ammonium sulphate or 0.25% methylamine as nitrogen sources. If required, amino acids, uracil or leucine were added to a final concentration of 30 μg/ml. For growth on agar plates, the medium was supplemented with 2% agar. For the selection of resistant transformants, YPD plates containing 100 μg/ml zeocin (Invitrogen), 300 μg/ml hygromycine B (Invitrogen) or 100 μg/ml nourseothricin (Werner Bioagents) were used.

For cloning purposes, *Escherichia coli* DH5α was used. Cells were grown at 37 °C in LB media supplemented with 100 μg/ml ampicillin or 50 μg/ml kanamycin, when required.

Molecular and biochemical techniques

Standard recombinant DNA techniques and transformation of *H. polymorpha* was performed by electroporation as described previously (12). Cell extracts of TCA treated cells were prepared for SDS-PAGE as detailed previously (13). SDS-PAGE and western blotting (WB) were performed by established methods. Equal amounts of protein were loaded per lane and blots were probed with rabbit polyclonal antisera against Pex11, Pex14 or pyruvate carboxylase-1 (Pyc1). mGFP-fusion proteins of Pex8, Pex10, Pex13 and Pmp47 were detected

using mouse monoclonal antiserum against green fluorescent protein (GFP; Santa Cruz Biotechnology, sc-9996). Secondary antibodies conjugated to horseradish peroxidase were used for detection. Pyc1 was used as a loading control. Blots were scanned by using a densitometer (Biorad GS-710) and quantified using Image J (http://rsbweb.nih.gov/ij/). From two individual blots per sample, the total intensity of the band of interest was measured and corrected for background intensity and Pyc1 loading amount.

Construction of H. polymorpha *strains*

The plasmids and primers used in this study are listed in Table S2 and S3. All integrations were confirmed by PCR. All deletions were confirmed by PCR and Southern blotting.

Construction of the pex3 atg1 *and* pex19 atg1 *double deletion strain, and the* pex3 atg1 pex25 *triple deletion strain*

The *pex3 atg1* double deletion strain was obtained by crossing a *H. polymorpha pex3* strain (14) with an *atg1* strain (15). Diploids were subjected to random spore analysis and prototrophic segregants were subjected to complementation analysis to determine their genotypes (16). The *pex3 atg1 pex25* triple deletion strain was made as follows. A PCR fragment of 2912 bp was obtained by PCR using primers Pex25-F and Pex25-R and plasmid pRSA018 as a template (6). This PCR fragment was transformed to the *pex3 atg1* double deletion strain. For the *pex19 atg1* double deletion strain, a PEX19-deletion cassette plasmid (pHOR30b) was digested with *Bgl*II and *Eco*RI to replace the URA3 gene with the LEU2 gene, which was obtained after digestion of pBS-CaLeu2 with *Bam*HI and *Eco*RI. The final deletion PEX19-deletion plasmid (pSEM188) was digested with *Bam*HI and the resulting 4434 bp fragment was integrated in the genome of *atg1* cells (15).

Construction of other strains

Plasmids pHIPZ-*PEX8*-mGFP (pMCE4), pHIPZ-*PEX10*-mGFP (pMCE5), pHIPZ-*PEX25*-mGFP (pMCE1), pHIPZ-*PMP47*-mGFP (pMCE7) (17),

pHIPZ5-*PEX3*-eGFP and pHIPZ4-BiP$_{N30}$-eGFP-HDEL (pRSA017) (18) were linearized and integrated in the endogenous promoter regions in the *pex3 atg1* strain producing Pex14-mCherry essentially as described previously (17, 18).

For the construction of plasmid pSEM01, a PCR fragment of 563 bp was obtained by using primers Pex14-F and Pex14-R on genomic DNA. After digestion with *Hin*dIII and *Bgl*II, the resulting fragment was inserted between the *Hin*dIII and *Bgl*II sites of pMCE02, resulting in pSEM01 (5488 bp) containing pHIPN-PEX14-mCherry. For stable integration in the *PEX14* promoter region, *Xho*I linearized plasmid was transformed to the *pex3 atg1* double mutant, resulting in a strain producing Pex14-mCherry under control of the endogenous promoter.

Plasmid pSEM02 (pHIPZ-*PEX11*-mGFP) was obtained as follows: Digestion of the pHIPZ-mGFP fusinator plasmid with *Hin*dIII and *Bgl*II yields a fragment of 5077 bp. Similarly, the pHIPN-*PEX11*-mCherry plasmid (pMCE3) was digested with *Hin*dIII and *Bgl*II to obtain a fragment of 772 bp. Ligation of the 772 bp and 5077 bp fragments resulted in pSEM02 of 5849bp. The plasmid was linearized using *Pst*1 and integrated in the genome of *pex3 atg1* producing Pex14-mCherry.

To construct plasmid pSEM03 (pHIPZ-*PEX13*-mGFP), PCR was performed on genomic DNA using the primers Pex13-F and Pex13-R. The PCR product of 1146 bp was digested with *Hin*dIII and *Bgl*II and the resulting fragment was inserted between the *Hin*dIII and *Bgl*II sites of pHIPZ-mGFP fusinator plasmid. The resulting plasmid of 6223 bp, designed pSEM03, was linearized with *ApaI* and transformed to *H. polymorpha pex3 atg1* producing Pex14-mCherry.

For the construction of plasmid pSEM04, a PCR fragment of 2547 bp was obtained using plasmid pHIPZ5-PEX3-eGFP plasmid (Table S2) as a template and primers H5-F and H5-R. The PCR fragment was digested with *Not*I and *Psp*XI and the resulting fragment was ligated in *Not*I and *Sal*I digested pHIPH4, resulting in plasmid pSEM04, which contains pHIPH5-P$_{AMO}$-*PEX3*.

The plasmid was linearized with *Bsi*WI and integrated in strain *pex3 atg1*.Pex14-mCherry producing Pex10-mGFP or Pmp47-mGFP.

Similarly, plasmid pSEM05 was made by PCR amplification of an 885 bp fragment using genomic DNA and primers Pex19-F and Pex19-R (Table S3). After digestion with *Hin*dIII and *Xba*I, the resulting fragment was ligated in *Hin*dIII and *Xba*I digested pHIPH4, resulting in plasmid pSEM05 containing pHIPH4-P_{AOX}-PEX19. For stable integration, *Stu*I linearized plasmid was transformed to *H. polymorpha pex3 atg1*.Pex14-mCherry producing Pex10-mGFP or Pmp47-mGFP.

For the construction of plasmid pAKW27, a vector of 5831 bp was obtained by *Bam*HI and *Sal*I digestion of pHIPZ7, whereas the 736 bp eGFP-SKL insert was obtained by *Bam*HI and *Sal*I digestion of pFEM35 followed by gel extraction. Ligation resulted in the plasmid pAKW27 containing pHIPZ7-P_{TEF1}-GFPSKL. For stable integration, *stu*I linearized plasmid was transformed to *H. polymorpha pex3 atg1*.Pex14-mCherry producing Pex3 under control of the inducible P_{AMO}.

Cell fractionation and membrane flotation

Crude extracts were prepared as described before (19). Briefly, protoplasts were prepared with Zymolyase (Brunschwig Chemie, Amsterdam, the Netherlands) and homogenized using a Potter homogenizer. To remove cell debris, the homogenate was centrifuged 2x at 3,000 x g (10 min, 4 °C). The supernatant (PNS) was then subjected to centrifugation at 30,000 x g (30 min, 4 °C) to separate the soluble fraction (supernatant: S) from the membrane pellet (P).

The 30,000 x g organelle pellet was used for flotation centrifugation as described before (19). Briefly the pellet was dissolved in 50% sucrose and over layered with 40%, 30% and 20% sucrose. Centrifugation was performed at 140,000 x g for 16 h at 4 °C. 10 fractions of 200 µl were collected from the top and analysed by SDS-PAGE and WB.

Fluorescence microscopy

All images were made using a 100x 1.30 NA Plan-Neofluar objective (Carl Zeiss). For wide-field microscopy, the GFP signal was visualized with a 470⁄40 nm band pass excitation filter, a 495 nm dichromatic mirror, and a 525⁄50 nm band-pass emission filter. mCherry fluorescence was visualized with a 587/25 nm band pass excitation filter, a 605 nm dichromatic mirror, and a 647/70 nm band-pass emission filter. DsRed, FM4-64 and Mitotracker Orange fluorescence were visualized with a 546/12 band-pass excitation filter, a 560 nm dichromatic mirror, and a 575–640 nm band-pass emission filter. Images were captured using a Zeiss Axioskop50 fluorescence microscope (Carl Zeiss, Sliedrecht, the Netherlands) using MetaVue software and a Princeton Instruments 1300Y digital camera. The images were captured in the media in which the cells were grown.

Mitochondria were stained by incubation of intact cells for 30 min at 37 °C with 0.5 μg/ml MitoTracker Orange (Invitrogen) followed by extensive washing with medium. For vacuolar staining, 1 ml of cell culture was supplemented with 1 μl FM4-64 (Invitrogen), incubated for 60 min at 37 °C and analysed.

Live cell imaging was performed on a Zeiss Observer Z1 using Axiovision software and a Photometrics Coolsnap HQ2 digital camera. Cells were grown on 1% agar containing growth medium and the temperature of the heating chamber XL was set at 37°C. Three z –axis planes were acquired for each time interval using 0.5 sec exposure times for both GFP and mCherry.

Confocal images were captured with a confocal microscope (LSM510; Carl Zeiss), equipped with photomultiplier tubes (Hamamatsu Photonics) and Zen 2009 software. For live cell imaging, the temperature of the objective and object slide was kept at 37°C and the cells were grown on 1% agar in medium. GFP fluorescence was analysed by excitation of the cell with a 488-nm argon ion laser (Lasos), and emission was detected using a 500–550 nm band-pass emission filter. During simultaneous GFP and FM4-64 detection, both probes

were excited with a 488-nm argon ion laser and GFP was detected using 500–530 nm band-pass emission filter and FM4-64 was detected using a 560 nm long-pass emission filter. Six z-axis planes were acquired for each time interval.

Image analysis was carried out using ImageJ and figures were prepared using Adobe Photoshop CS4. Unless indicated otherwise, the intensity minimum and maximum of the image were set equal for all images represented within a single figure panel, thus facilitate direct fluorescence intensity comparison between different strains.

For quantitative analysis of Pex14-mGFP fluorescent spots, Z-stacks were made of randomly chosen fields. Quantification was done on 4 images per culture, containing at least 65 cells per image. Cells were stained with FM4-64 to allow discrimination between vacuolar mGFP and cytosolic mGFP spots. The average number of spots was calculated from 350 cells per culture. The error bars indicate the standard error of the mean.

For the quantification of cytosolic mGFP intensity, single plane images were acquired on a Zeiss Axioskop50, after which the total intensity of ~100 individual cells was measured and corrected for the background intensity. The error bars indicate the standard deviation between individual cells.

Electron microscopy

H. polymorpha pex3 atg1 were fixed in 1.5% potassium permanganate, stained en block with 0.5% uranylacetate and embedded in Epon 812 (Serva, 21045). For morphological studies, ultrathin sections were viewed in a Philips CM12 TEM. For electron tomography, serial sections of 150 nm thick were cut. The serial images of whole cells were stacked and aligned using MIDAS (20), after which individual cells could be scrutinized for peroxisomal remnants. 10 nm gold beads were layered on top of the serial sections and acted as fiducial markers for electron tomography. Two single-axis tilt series, each containing 141 images with 1° tilt increments, were acquired with a pixel size of 0.7 nm on a FEI Tecnai12 at 120 kV using the SerialEM acquisition software (21) and a cooled

slow-scan charge-coupled device camera (4k Eagle; FEI Company) in 2x2 binned mode. The tilt series were aligned and reconstructed using the IMOD software package and analysed using the AMIRA visualization package (TGS Europe). To generate 3-dimensional surface rendered models in AMIRA, first, masks of organelles were drawn manually and afterwards improved by nonlinear anisotropic diffusion filtering followed by thresholding.

Cryosectioning and immuno-gold labelling

For immuno-gold labelling, cells were fixed in 3% glutaraldehyde in 0.1 M cacodylatebuffer pH 7.2 for 1 h on ice and treated afterwards with 0.4% Na-periodate (15 min) and 1% NH_4Cl (15 min). Upon embedding in 12% gelatine in phosphate buffer pH 7.4, ~0.5 mm^3 cubes were infiltrated overnight in 2.3 M sucrose in the same buffer. Cryosections of 60 nm were cut using a cryo diamond knife (Diatome) at -120 °C in a Reichert Ultracut. Sections were mounted on carbon-coated formvar nickel grids. Gelatine was removed by incubating the grids for 30 minutes on 2% gelatine in phosphate buffer (pH 7.4) at 30 °C. Pex14, Pex5 and alcohol oxidase were localized using polyclonal antibodies raised against Pex14, Pex5 and alcohol oxidase, respectively, and goat-anti-rabbit antibodies conjugated to 10 nm gold (Aurion). Sections were stained with 2% uranyloxalate (pH 7.0) for 10 minutes, briefly washed on three drops of distilled water and embedded in 0.5% methylcellulose and 0.5% uranylacetate on ice for 10 min before viewing them in the CM12 electron microscope (22).

Results and Discussion

H. polymorpha pex3 atg1 cells contain vesicular structures that harbour PMPs

Careful electron microscopy (EM) analysis of *H. polymorpha pex3 atg1* cells, grown at peroxisome inducing conditions (mineral medium containing methanol and glycerol ; MM-M/G), revealed that these cells contain clusters of

Figure-1

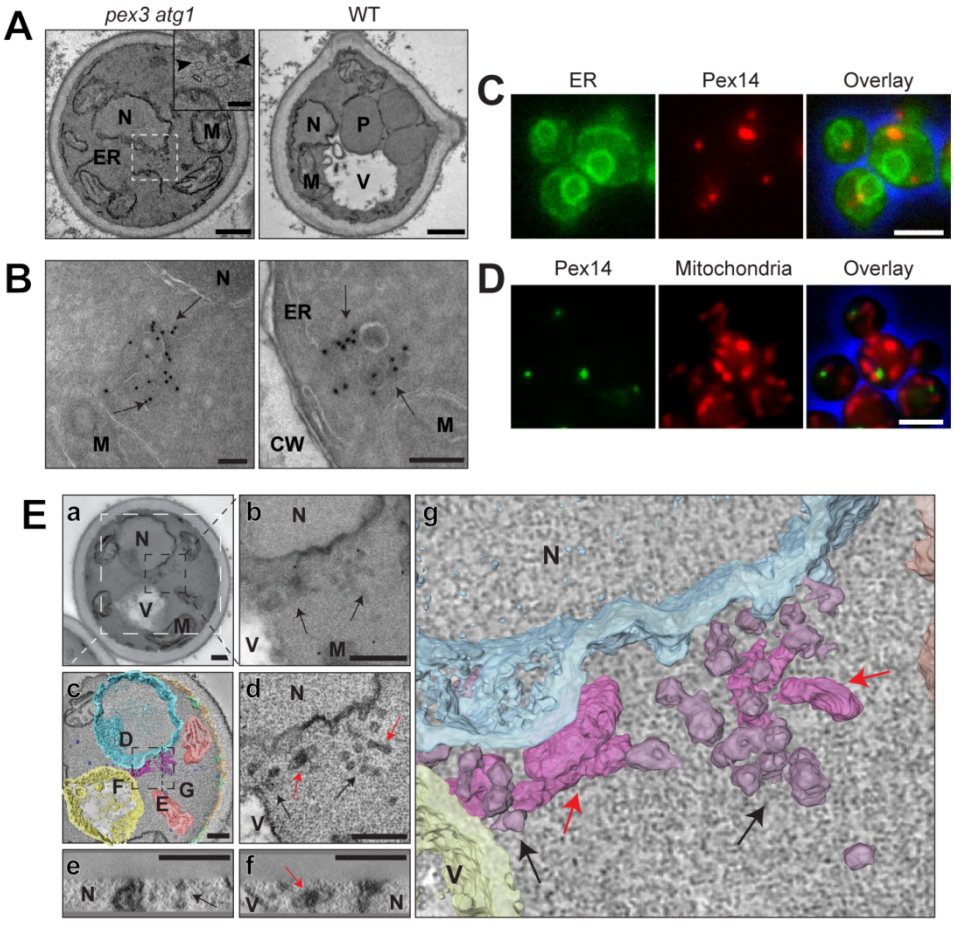

Figure 1. *pex3 atg1* cells harbour Pex14-containing structures.
(A) EM analysis of $KMnO_4$-fixed *pex3 atg1* and WT cells grown for 16 h on MM-M/G. The inset shows a cluster of vesicles. (B) iEM analysis of *pex3 atg1* cells using α-Pex14 antibodies. (C,D) FM images of *pex3 atg1* cells producing (C) Pex14-mCherry and the ER marker BiP_{N30}-eGFP-HDEL, or (D) Pex14-mGFP complemented with Mitotracker orange staining. (E) Electron tomography analysis of (a) a serial-sectioned *pex3 atg1* cell containing (b) a perinuclear membrane cluster (arrows). (d-f) 10 nm thin digital slices through the tomogram reconstruction revealed vesicles (black arrows) and reticular structures (red arrows). The surface-rendered reconstructions in (c) and (g) respectively show the viewing direction of (d-g) and reticulo-vesicular structures in 3-D. Bars: (A) 500 nm, (A_{inset},B) 100 nm, (C,D) 2.5 µm or (E) 250 nm. CW – cell wall; M – mitochondrion; N – nucleus; P – peroxisome; V – vacuole.

vesicular structures, which measure up to 70 nm in diameter and have an electron dense content. These structures were not detected in WT control cells

(Fig. 1A). Immuno-EM (iEM) indicated that these structures contain Pex14, a PMP involved in peroxisomal matrix protein import. The structures were generally observed in the vicinity of the nuclear envelope, lateral ER and mitochondria (Fig. 1B). In support of our EM results, mGFP- or mCherry-tagged Pex14 was observed as fluorescent spots adjacent to the nuclear envelope, ER (Fig. 1C) or mitochondria (Fig. 1D). Electron tomography analysis indicated that the clusters consist of reticular and vesicular structures (Fig. 1E and Video S1). Distinct connections with other cell organelles were not detected.

The PMP containing structures in pex3 cells are susceptible to autophagic degradation

Although previous fluorescence microscopy (FM) studies suggested that, in *H. polymorpha pex3* cells, Pex14-GFP is present in spots associated with mitochondria (23), iEM revealed that these spots also represent clusters of vesicles, located adjacent to the nuclear envelope, ER (not shown) or mitochondria at distances that cannot be resolved by FM (Fig. 2A). The number of Pex14-mGFP spots is strongly reduced in *pex3* cells, as was evident from quantitative analysis of FM images (1.3 +/- 0.04 spots per cell in *atg1 pex3* cells, relative to 0.6 +/- 0.04 in *pex3* cells; Fig. 2B). In *pex3* cells, but not in *pex3 atg1* cells, mGFP fluorescence was also observed in vacuoles (Fig. 2C), indicating autophagic degradation of the structures. This was supported by western blot (WB) analysis, which revealed that the level of Pex14 was strongly reduced in *pex3* cells, compared to WT and *pex3 atg1* cells (Fig. 2D).

Several peroxisomal proteins co-localize with Pex14 in* pex3 atg1 *cells

To examine whether other PMPs are also associated with the structures, we performed co-localization studies using *pex3 atg1* strains producing Pex14-mCherry together with different

Figure-2

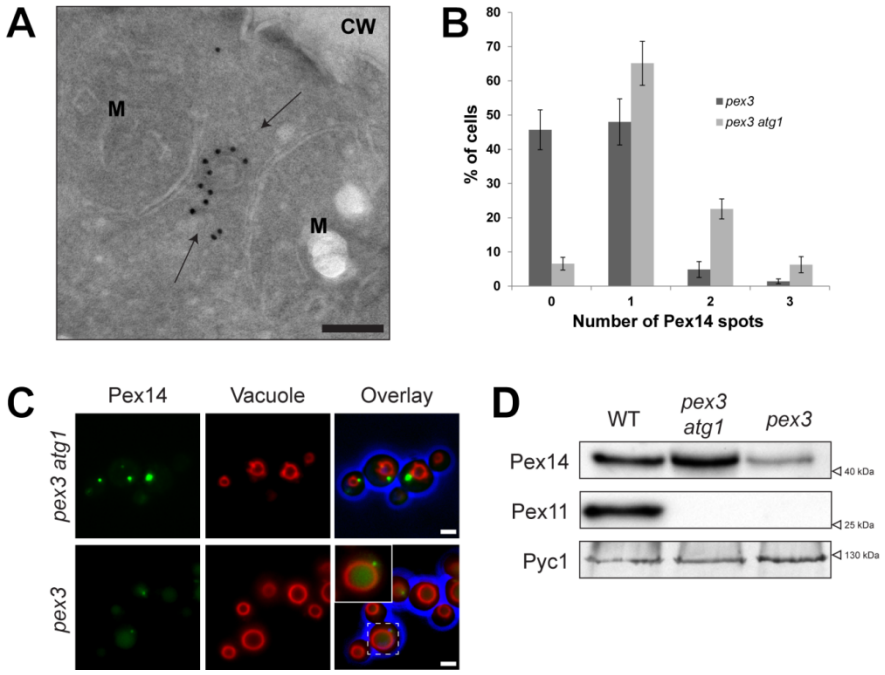

Figure 2. *pex3 atg1* cells contain enhanced numbers of Pex14-containing structures. (A) iEM analysis of *pex3* cells using α-Pex14 antibodies, identifying structures (arrows) in the vicinity of mitochondria. CW – cell wall; M – mitochondrion. (B) Quantification of Pex14-mGFP spots in *pex3* and *pex3 atg1* cells. (C) FM images of *pex3 atg1* or *pex3* cells, producing Pex14-mGFP complemented with FM4-64 vacuolar staining. The inset shows optimized intensities for *pex3* cells, highlighting the Pex14-mGFP spot and vacuolar mGFP. (D) WB analysis of cells grown for 16 h on MM-M/G using α-Pex11 or α-Pex14 antibodies. Pyruvate carboxylase (Pyc1) was used as loading control. Error bars: SEM. Scale bars: (A) 100 nm or (C) 1 µm.

PMP-mGFP fusion proteins, all under control of their endogenous promoter. We analysed Pex8, Pex10 and Pex13, proteins of the importomer (24), as well as Pex11, a PMP involved in peroxisome fission (25), and Pmp47, a peroxisomal carrier protein (26). In WT cells grown for 16 h on MM-M/G, all mGFP fusion proteins were readily detected at peroxisomes ("unpublished data"). In *pex3 atg1* cells, Pex8-mGFP and Pex13-mGFP co-localized with Pex14-mCherry, whereas the levels of Pex10-mGFP, Pex11-mGFP and Pmp47-mGFP were below the limit of detection (Fig. 3A).

Figure-3

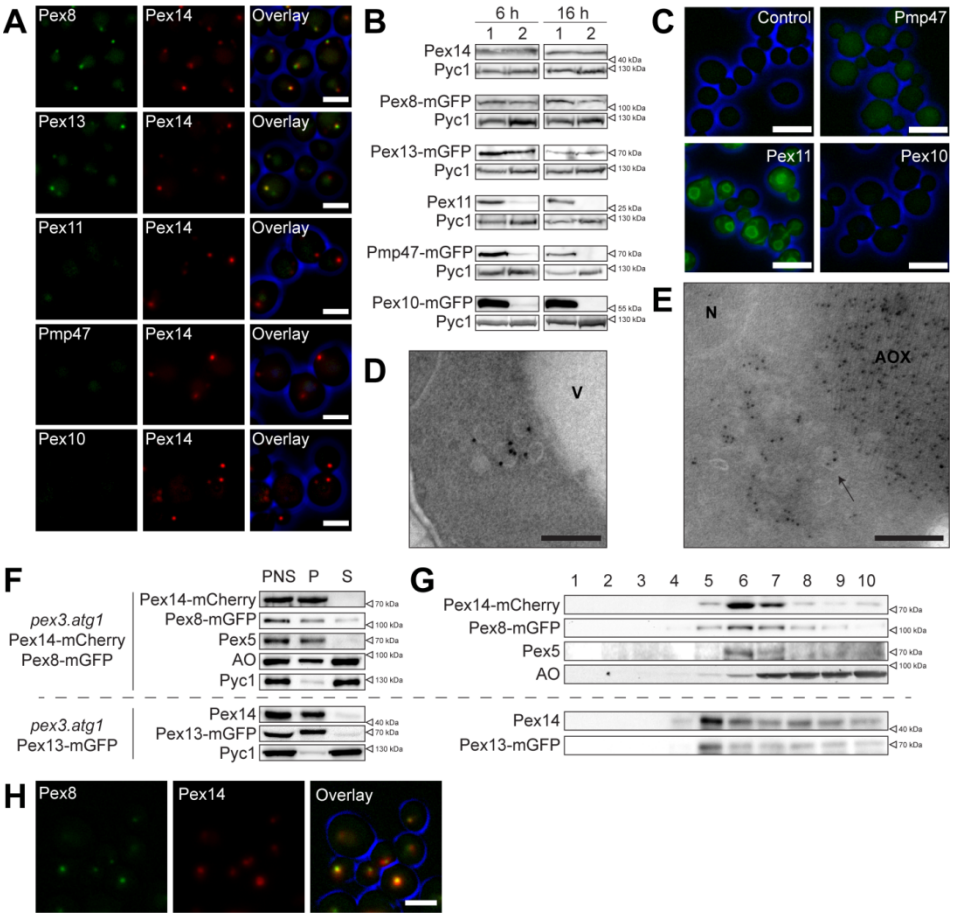

Figure 3. Pex10, Pex11 and Pmp47 do not localize with Pex14.
(A) FM images of *pex3 atg1* cells grown for 16 h on MM-M/G. Besides Pex14-mCherry, cells produced C-terminal mGFP fusions of the indicated proteins. (B) WB analysis of (1) WT and (2) *pex3 atg1* cells, grown for 6 or 16 h on MM-M/G. (C) FM images showing mGFP-fluorescence in *pex3 atg1* cells producing Pex14-mCherry (control) or Pex14-mCherry together with the indicated mGFP fusion protein. Cells were grown for 6h on MM-M/G. (D,E) iEM analysis of *pex3 atg1* cells using (D) α-Pex5 or (E) α-alcohol oxidase antibodies. (F) Cell fractionation analysis of the indicated strains. Post nuclear supernatants (PNS) were subjected to differential centrifugation resulting in a 30,000 x g organelle pellet (P) and supernatant fraction (S). (G) Flotation analysis of the organelle pellet showing the distribution of the indicated proteins in the top (1) to bottom (10) fractions. (H) Co-localisation of Pex8-GFP and Pex14-mCherry in *pex10* cells. Bars: (A) 2.5 µm, (C) 5 µm, or (D,E) 100 nm. AOX – cytosolic alcohol oxidase crystalloid; N – nucleus; V – vacuole. **

To precisely compare the levels of the above proteins, we monitored their induction after shifting cells from peroxisome repressing (glucose; MM-

Glu) to peroxisome inducing conditions (MM-M/G). In *pex3 atg1* cells, Pex8, Pex13 and Pex14 showed similar induction patterns (Fig. S1A-C) and protein levels (Fig. 3B) as WT controls. Conversely, Pex10, Pex11 and Pmp47 were only detected in *pex3 atg1* cells at the initial stages after the shift, with the highest levels after 6 h of induction (Fig. S1D-E) followed by a very strong reduction after prolonged cultivation. However, at 6 h their levels were still strongly reduced compared to the WT controls (Fig. 3B). FM revealed that in these cells Pex11-mGFP is predominantly localized to the nuclear envelope and lateral ER, while Pmp47-mGFP was dispersed over the cytosol and Pex10-mGFP below the limit of detection (Fig. 3C).

The strong reduction in Pex10, Pex11 and Pmp47 levels cannot be (fully) explained by a sudden arrest in the synthesis of these PMPs, since growth was minimal between 6 and 8 h (Fig. S1G), and hence must be caused by proteolytic degradation. Therefore, we conclude that in *H. polymorpha pex3 atg1* cells two classes of PMPs can be discriminated: i.e. those that sort independently of Pex3 to vesicular structures, where they are relatively stable; and PMPs that require Pex3 for sorting and stability.

Pex13 and Pex14 are associated with membranes in* pex3 atg1 *cells

To study whether PMPs are membrane-bound in *atg1 pex3* cells a flotation analysis of an organelle pellet was performed. Pex8, Pex13 and Pex14, were detected in the organelle pellet and migrated to fractions of low density upon flotation centrifugation (Fig. 3F,G). Pex10 and Pmp47 could not be analysed because of strong degradation during the fractionation procedure ("unpublished data"). Interestingly, the PTS1-receptor Pex5, as well as a minor portion of the peroxisomal matrix protein alcohol oxidase, co-fractionated with Pex14 (Fig. 3F,G). Bulk of the pelleted AO represent cytosolic crystalloids, which do not float. Localisation of Pex5 and AO at the vesicles was confirmed by iEM (Fig. 3D,E). The accumulation of Pex5 at these structures can be explained by the presence of a functional receptor docking complex, and the absence of Pex10, which is essential for receptor recycling. Our observation that the structures contain matrix protein is supported by the electron density of their

lumen (Fig. 1A,B). Association of Pex8 with the Pex14-containing structures is in line with observations obtained in *Pichia pastoris*, which revealed that Pex8 import into peroxisomes only depends on PTS receptors and Pex14 (27, 28). Also in *H. polymorpha pex10* cells, Pex8 co-localizes with Pex14 (Fig. 3H).

Pex14-containing structures in* pex3 atg1 *cells develop into peroxisomes upon reintroduction of Pex3

To analyse whether the membrane structures can develop into peroxisomes upon re-introduction of Pex3, we constructed a *pex3 atg1* strain that contained *PEX3-eGFP* under control of the inducible amine oxidase promoter (P_{AMO}). Cells were extensively pre-cultivated on MM-Glu in the presence of ammonium sulphate to fully repress P_{AMO}. Subsequently, cells were shifted to MM-M/G/methylamine to induce P_{AMO} and peroxisome proliferation. Live cell imaging revealed that the first eGFP fluorescence invariably co-localized with the Pex14-mCherry spots (Fig. 4B). The Pex14-mCherry spots present in *pex3* single deletion cells also appeared to be the sole targets for reintroduced Pex3-eGFP (Fig. 4A).

We then examined Pex10-mGFP and Pmp47-mGFP upon reintroduction of Pex3 using strains that also produced Pex14-mCherry and P_{AMO}-driven *PEX3*. In cells pre-cultivated on MM-Glu with ammonium sulphate, these PMPs (with the exception of Pex14-mCherry) were below the limit of detection ("unpublished data"). Upon induction of *PEX3* expression, the first Pex10-mGFP fluorescence signal appeared after 5 h, and invariably co-localized with Pex14-mCherry (Fig. 4C). A similar result was observed for Pmp47-mGFP, except that the first fluorescence was detected after 8 h (Fig. 4D).

Finally, we tested whether the Pex14-containing vesicles are capable of importing the matrix marker GFP-SKL upon *PEX3* induction. As shown in Figure 4E, GFP-SKL was cytosolic prior to Pex3 reintroduction, but found to be concentrated at the Pex14-mCherry spots when Pex3 synthesis was induced.

These results indicate that in *pex3 atg1* cells the Pex14-containing structures, rather than the ER, are the target for re-introduced Pex3.

Subsequently, Pex10 and Pmp47 also sort to these structures, which mature into normal peroxisomes that import GFP-SKL.

Figure-4

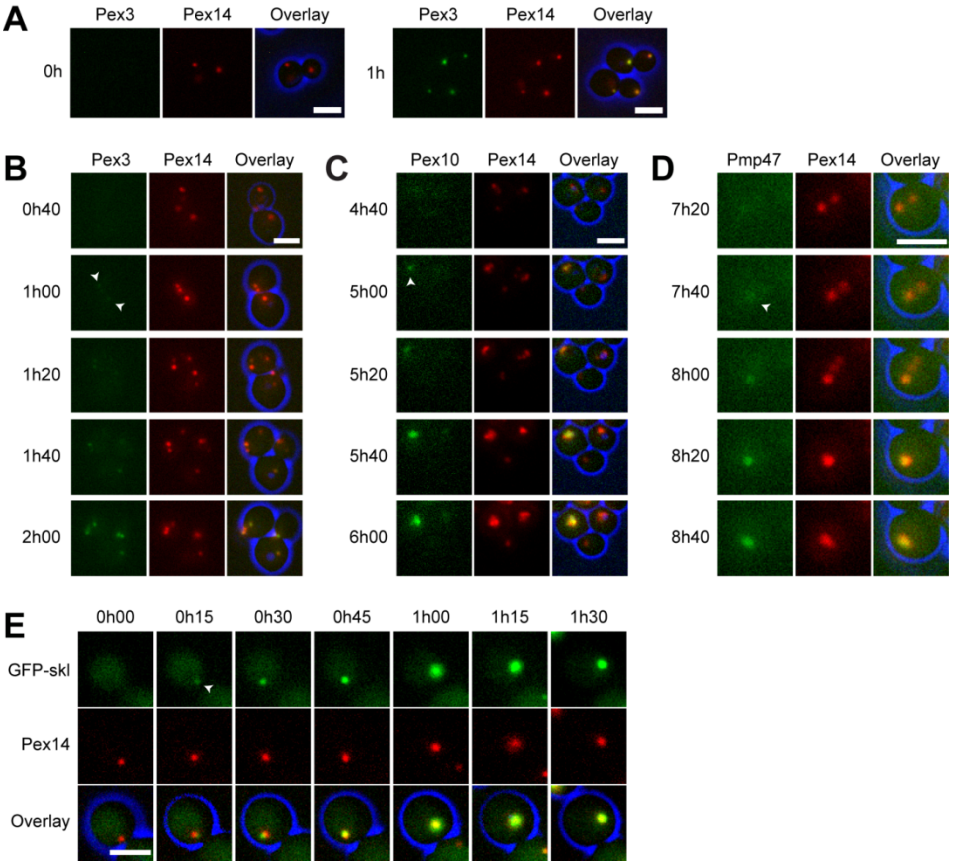

Figure 4. The Pex14-containing vesicular structures mature into peroxisomes upon reintroduction of *PEX3*.
(A) FM images of *pex3* cells with Pex14-mCherry upon Pex3-eGFP reintroduction after shifting cells from MM-Glu with ammonium sulphate to MM-M/G with methylamine. (B-E) Live cell FM images of *pex3 atg1* cells upon Pex3 reintroduction. *pex3 atg1* cells producing Pex14-mCherry and (B) P_{AMO}*PEX3*-eGFP, (C) P_{AMO}*PEX3.PEX10*-GFP, (D) P_{AMO}*PEX3.PMP47*-GFP or (E) P_{AMO}*PEX3*.P_{TEF}GFP-SKL. Cells were grown similar as in (A). Bars: 2.5 µm. The arrows in B-D indicate the first GFP signal that was detected.

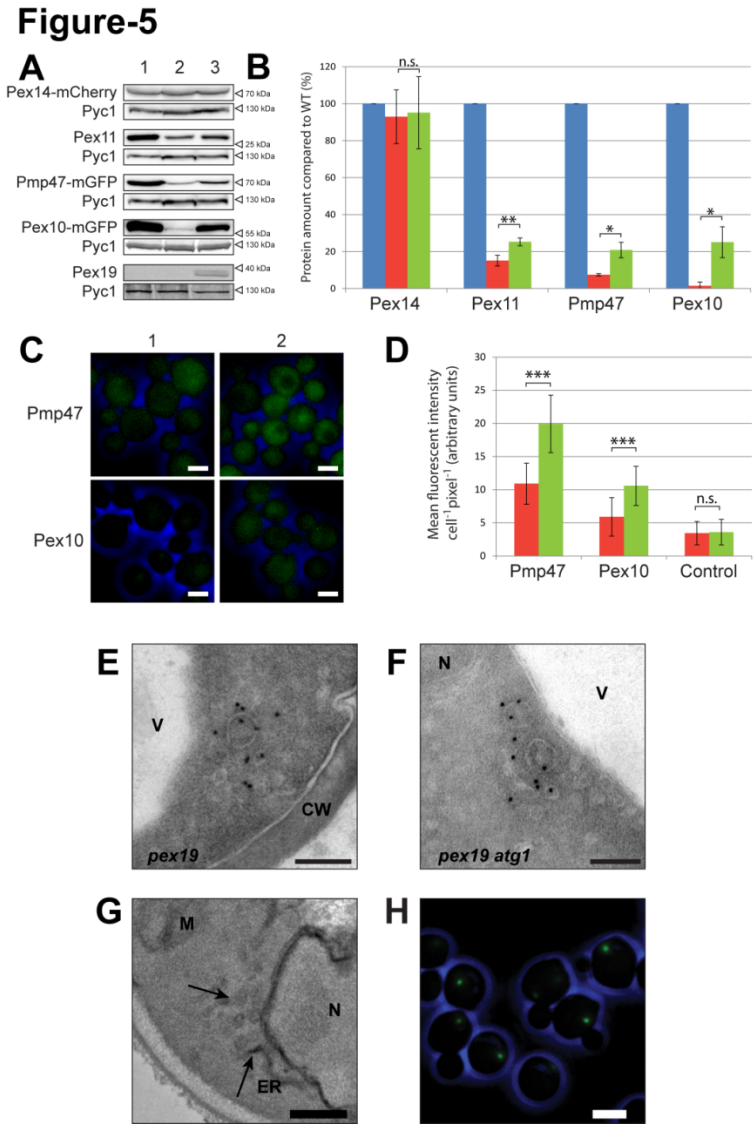

Figure 5. Pex19 overproduction and *PEX19* or *PEX25* deletion.
(A) WB analysis and (B) quantification of the indicated proteins in WT (lane 1; blue), *pex3 atg1* (lane 2; red), and *pex3 atg1*-P$_{AOX}$*PEX19* (lane 3; green) cells grown for 6 h on MM-M/G. In B, the protein levels of WT cells were set to 100 %. (C) FM images and (D) quantification of Pmp47-mGFP and Pex10-mGFP in *pex3 atg1* (1; red) and *pex3 atg1*-P$_{AOX}$Pex19 (2; green) cells grown for 6 h on MM-M/G. Control cells in D did not produce mGFP. Significance indications: *NS=p<0.10,* *=*0.10>p>0.05,* **=*0.05>p>0.01,* ***=*p<0.01*. Error bars: SD. (E-F) iEM analysis of (E) *pex19* and (F) *pex19 atg1* cells using α-Pex14 antibodies. (G) EM analysis of $KMnO_4$-fixed *pex3 atg1 pex25* cells grown for 16 h on MM-M/G showing clusters of membrane structures (arrows). (H) FM image of *pex3 atg1 pex25* cells producing Pex14-mGFP. Scale bars: (C) 2 µm, (E-F) 100 nm, (G) 250 nm, or (H) 2.5 µm. CW – cell wall; ER – endoplasmic reticulum; M – mitochondrion; N – nucleus; V – vacuole.

Pex10, Pex11 and Pmp47 are stabilized upon Pex19 overproduction

One of the models of Pex19 function proposes that cytosolic Pex19 binds newly synthesized PMPs, followed by recruitment of the complex by Pex3, and subsequent insertion of the PMPs into the peroxisomal membrane (29). This led us to speculate that in the absence of Pex3, Pex19 may become saturated with PMPs that are dependent on the Pex3/Pex19 machinery, since cargo release is abolished. As a consequence, additionally synthesized PMPs cannot bind to Pex19 and may become susceptible to degradation. To test this, we analysed the effect of Pex19 overproduction, finding indeed an increase of the levels of Pex10, Pex11 and Pmp47, but not of Pex14 (Fig. 5A,B). The enhanced protein levels allowed visualization of Pex10 and Pmp47 by FM, which revealed that they both are cytosolic (Fig. 5C,D).

These findings are consistent with a model that newly synthesized Pex10, Pex11 and Pmp47 directly insert into the peroxisomal membrane by a process that requires Pex3 and Pex19.

Pex19 and Pex25 are not required for vesicle formation in* pex3 atg1 *cells

Because *in vitro* assays suggested that Pex19, rather than Pex3, is essential to form peroxisomal vesicles from the ER (30, 31), we analyzed whether Pex14-containing structures occur in *H. polymorpha pex19* and *pex19 atg1* cells. As shown in Fig. 5 E-F, structures, similar to those observed in *pex3* cells, are also present in these cells.

It is known that Pex25 is required for the reintroduction of peroxisomes in *H. polymorpha pex3* cells (6). However, as clusters of vesicular structures and Pex14-mGFP spots, similar as those observed in *pex3 atg1* cells, were also observed in cells of a *pex3 atg1 pex25* triple deletion strain (Fig. 5G,H), this suggests that Pex25 is not required for the formation of these vesicles.

Conclusions

Because peroxisomal membranes to which common marker PMPs co-localize were not detected in yeast (14, 32, 33) or mammalian (34) cells lacking a functional *PEX3* gene, it is generally accepted that cells lacking Pex3 are unable to form peroxisomal membranes. Instead, FM analysis suggested that PMPs were localized to the ER, mitochondria or were below the limit of detection, depending on the marker PMP examined (7, 23, 32, 35). Here, we show that in the absence of Pex3, the PMPs Pex13 and Pex14 co-localize at membrane structures that are often located adjacent to other cell organelles at distances that cannot be resolved by FM. Apparently, these PMPs can insert in membranes independent of Pex3 (Fig. S2).

Based on FM, van der Zand et al. (7) concluded that, in *S. cerevisiae pex3* cells Pex13 and Pex14 are present in foci at the ER. We consider it likely that these foci represented similar structures. Indeed, our iEM analyses on *S. cerevisiae pex3 atg1* cells revealed that these cells also harbour Pex14-containing vesicles ("unpublished data"). Our observations are furthermore supported by the presence of PMP containing membrane structures in *P. pastoris pex3* cells (36).

In contrast to Pex13 and Pex14, the Pex10, Pex11 and Pmp47 apparently do require the Pex3/Pex19 machinery for insertion into these membrane structures, given that in cells lacking Pex3 they do not co-localize with Pex14 and are very instable. Instead, they are stabilized and sorted to the structures upon Pex3 reintroduction. In addition, their levels increase in *pex3 atg1* cells upon *PEX19* overexpression, suggesting that Pex19 serves as cytosolic receptor for these PMPs (Fig. S2). Pex10 and Pmp47 were invariably cytosolic in *pex3 atg1* cells, which is consistent with the cytosolic localization of the mammalian Ant1 (a homologue of Pmp47) in *PEX3* mutant cells (37).

Pex11 was the only PMP which we (transiently) observed at the ER, but only in minor amounts, with the protein being very instable. The latter finding is consistent with pulse-chase experiments using *S. cerevisiae pex3* cells, which

showed that Pex11 is normally synthesized, but – unlike in the WT control – rapidly degraded (32). This instability suggests that localization at the ER may not be an intermediate stage of its normal sorting pathway. However, at this stage it cannot be excluded that Pex11 traffics via the ER to peroxisomes and is degraded in *pex3* cells because of its inability to exit the ER. We note, however, that this pathway is not consistent with our observation that Pex11 levels increase upon Pex19 overproduction in *pex3* cells.

The most pressing question is the nature of the vesicles in *pex3* cells. Our data indicate that they have several properties in common with normal peroxisomal membranes as they appear to contain a functional receptor docking site to which Pex5 associates, and are capable of importing matrix proteins (Pex8, alcohol oxidase). This property is shared with peroxisomal membrane ghosts that are present in *H. polymorpha PEX* deletion strains, which are defective in receptor recycling, e.g. *pex4* or *pex10* (38). Thus, they may represent peroxisomal ghosts, an assumption that is reinforced by the finding that they mature into normal peroxisomes upon Pex3 reintroduction.

According to our model (Fig. S2), the vesicles may proliferate from a pre-existing peroxisomal membrane structure. Alternatively, they may form from other membranes. If so, they are most likely formed from the ER (39, 40), possibly by a similar mechanism as the *in vitro* generated vesicles reported by Lam et al. (31) and Agrawal et al. (30). Importantly, our current data demonstrate that, if these structures indeed derive from the ER, their formation does not require Pex3.

Online supplemental material

Fig. S1A-G. Induction of PMP's in WT and *pex3 atg1* cells after a shift from MM-Glu to MM-M/G and the corresponding growth curves. Fig. S2. Model. Video S1. Tilt series, reconstructed tomogram and surface rendering of a *pex3 atg1* cell. Table S1, S2 and S3 contain the *H. polymorpha* strains, plasmids and primers used in this study, respectively.

Abbreviations

CLSM	confocal laser scanning microscopy
FM	fluorescence microscopy
iEM	immuno electron microscopy
MM-Glu	mineral medium containing 0.5% glucose
MM-M/G	mineral medium containing 0.5% methanol and 0.05% glycerol
P_{AMO}	amine oxidase promoter
Pex	peroxin
PMP	peroxisomal membrane protein
Pyc1	pyruvate carboxylase-1
WB	western blot
WT	wild-type

Supplemental data

Supplemental tables:

Table S1. *H. polymorpha* strains used in this study

Strains	**Characteristics**	**Reference**
wild-type (WT)	NCYC 495 *leu1.1*	(41)
atg1	*ATG1* deletion strain, *leu 1.1*	(33)
pex3	*PEX3* deletion strain, *ura3*	(20)
pex19	*PEX19* deletion strain, *ura3*	(42)
pex10	*PEX10* deletion strain	(43)
pex3 atg1	*PEX3 ATG1* double deletion strain	This study
pex19 atg1	*PEX19 ATG1* double deletion strain	This study
pex3 atg1.PEX14-mCherry	*pex3 atg1* with pSEM01	This study
pex3 atg1.PEX14-mCherry.*PEX8*-mGFP	*pex3 atg1* with pSEM01 and pMCE4	This study
pex3 atg1.PEX14-mCherry.*PEX10*-mGFP	*pex3 atg1* with pSEM01and pMCE5	This study
pex3 atg1.PEX14-mCherry.*PEX11*-mGFP	*pex3 atg1* with pSEM01 and pSEM02	This study
pex3 atg1.PEX14-mCherry.*PEX13*-mGFP	*pex3 atg1* with pSEM01 and pSEM03	This study

pex3 atg1.PEX14-mCherry.*PMP47*-mGFP	*pex3 atg1* with pSEM01 and pMCE7	This study
pex3 atg1.PEX13-mGFP	*pex3 atg1* with pSEM03	This study
pex3 atg1.PEX14-mCherry-BiP$_{N30}$-eGFP-HDEL	*pex3 atg1* with pSEM01 and pRSA017	This study
pex3 atg1.PEX14-mCherry.*PEX10*-mGFP – P$_{AOX}$ *PEX19*	*pex3 atg1* with pSEM01, pMCE05 and pSEM05	This study
pex3 atg1.PEX14-mCherry.*PMP47*-mGFP – P$_{AOX}$ *PEX19*	*pex3 atg1* with pSEM01, pMCE07 and pSEM05	This study
pex3 atg1.PEX14-mGFP	*pex3 atg1* with pSNA12	This study
pex3 atg1 pex25	*pex3 atg1* with pRSA018	This study
pex3 atg1 pex25.PEX14-mGFP	*pex3 atg1 pex25* with pSNA12	This study
pex3 atg1.PEX14-mCherry – P$_{AMO}$ *PEX3*-eGFP	*pex3 atg1* with pSEM01 and pHIPZ5-P$_{AMO}$ *PEX3*-eGFP	This study
pex3 atg1.PEX14-mCherry.PEX10-mGFP–P$_{AMO}$ PEX3	*pex3 atg1* with pSEM01, pMCE5 and pSEM04	This study
pex3 atg1.PEX14-mCherry.*PMP47*-mGFP–P$_{AMO}$ PEX3	*pex3 atg1* with pSEM01, pMCE7 and pSEM04	This study
pex3 atg1.PEX14-mCherry – P$_{AMO}$ *PEX3*-eGFP – P$_{TEF1}$	*pex3 atg1* with pSEM01, pSEM04 and pAKW27	This study

eGFP-SKL		
pex10. *PEX8*-mGFP.*PEX14*-mCherry	*pex10* with pSEM01 and pMCE4	This study
WT. *PEX13*-mGFP	WT with pSEM03	This study
WT. DsRed-SKL.*PEX8*-mGFP	WT. DsRed-SKL with pMCE4	(35)
WT. DsRed-SKL.*PEX10*-mGFP	WT. DsRed-SKL with pMCE5	(35)
WT. DsRed-SKL.*PMP47*-mGFP	WT. DsRed-SKL with pMCE7	(35)
WT. PEX10-mGFP.*PEX14*-mCherry	WT with pSEM01 and pMCE7	This study
WT. *PEX11*-mGFP.*PEX14*-mCherry	WT with pSEM01 and pMCE3	This study
WT. DsRed-SKL.*PEX13*-mGFP	WT. DsRed-SKL with pSEM03	This study

Table S2. Plasmids used in this study

Plasmid	**Characteristics**	**Reference**
pSEM01	pHIPN Plasmid containing C-terminal part of *PEX14* fused to mCherry; nat^R; amp^R	This study

pSEM02	Plasmid containing C-terminal part of *PEX11* fused to mGFP; zeo^R; amp^R	This study
pSEM03	Plasmid containing C-terminal part of *PEX13* fused to mGFP; zeo^R; amp^R	This study
pSEM04	pHIPH5 containing *PEX3* under control of P_{AMO}, Hph^R; amp^R	This study
pSEM05	pHIPH4 containing *PEX19* under control of P_{AOX}, Hph^R; amp^R	This study
pSEM188	Plasmid containing *PEX19* deletion cassette; *LEU2*; amp^R	This study
pHIPZ5-PEX3-eGFP	pHIPZ5 containing *PEX3*-eGFP under control of P_{AMO}, zeo^R; amp^R	(5)
pRSA017	pHIPZ4 containing BiP_{N30}-eGFP-HDEL under control of P_{AOX}; zeo^R; amp^R	(6)
pHIPH4	pHIP containing hygromycine B marker, amp^R	(6)
pHIPZ7	pHIP containing TEF1 promoter, zeo^R; amp^R	(37)
pFEM35	pHIPX7 containing eGFP with C-terminal PTS1 under control of P_{AOX}; Leu2; kan^R	(44)
pHIPZ-mGFP fusinator	pHIPZ containing mGFP and *AMO* terminator; zeo^R; amp^R	(36)
pMCE02	pHIPN plasmid containing mCherry; nat^R; amp^R	(35)
pSNA12	Plasmid containing C-terminal part of *PEX14*	(35)

	fused to mGFP; zeo^R; amp^R	
pMCE1	C-terminus of *PEX25* fused to mGFP*;* zeo^R; amp^R	(35)
pMCE3	Plasmid containing C-terminal part of *PEX11* fused to mCherry; nat^R; amp^R	(35)
pMCE4	Plasmid containing C-terminal part of *PEX8* fused to mGFP; zeo^R; amp^R	(35)
pRSA018	pDEST-R4-R3 containing *PEX25* deletion cassette, nat^R; amp^R	(6)
pMCE5	Plasmid containing C-terminal part of *PEX10* fused to GFP; zeo^R; amp^R	(35)
pMCE7	Plasmid containing C-terminal part of *PMP47* fused to GFP; zeo^R; amp^R	(35)
pAKW27	Plasmid containing eGFP-SKL under control of P_{TEF1}; zeo^R; amp^R	This study
pHOR30b	Plasmid containing *PEX19* deletion cassette; *URA3*; amp^R	(45)
pBS-CaLeu2	Plasmid containing *C. albicans LEU2* gene; amp^R	(45)

Table S3. Primers used in this study

Primer	Sequence	Reference
Pex25-F	5′-CTGGATGGAGGCTTCATCTC-3′	(6)
Pex25-R	5′-GGAGCTGCTGTGCTTGTATG-3′	(6)
H5-F	5′-GTGCTGCAAGGCGATTAAGT-3′	This study
H5-R	5′-AGAGCTCGAGGTTAAGCATCGAAATTAGAGTAG AC-3′	This study
Pex13-F	5′-AAAAGCTTATGACTACACCACGTCCAAAGCC-3′	This study
Pex13-R	5′-AAAGATCTGATCAATAGCTTTTGATCTTTCTTGA AC-3′	This study
Pex14-F	5′-CCCAAGCTTCGTTGCAGGAAGTCGACGAA-3′	This study
Pex14-R	5′-AGATCTTCCGGCATTCAGCTGCCACGCCG-3′	This study
Pex19-F	5′-AAAAGCTTATGAGCGAGAAAAAGTCC-3′	This study
Pex19-R	5′-ATCTAGACTATGTTTGTTTGCAAGTGTCTTCC-3′	This study

Supplemental figures:

Figure-S1

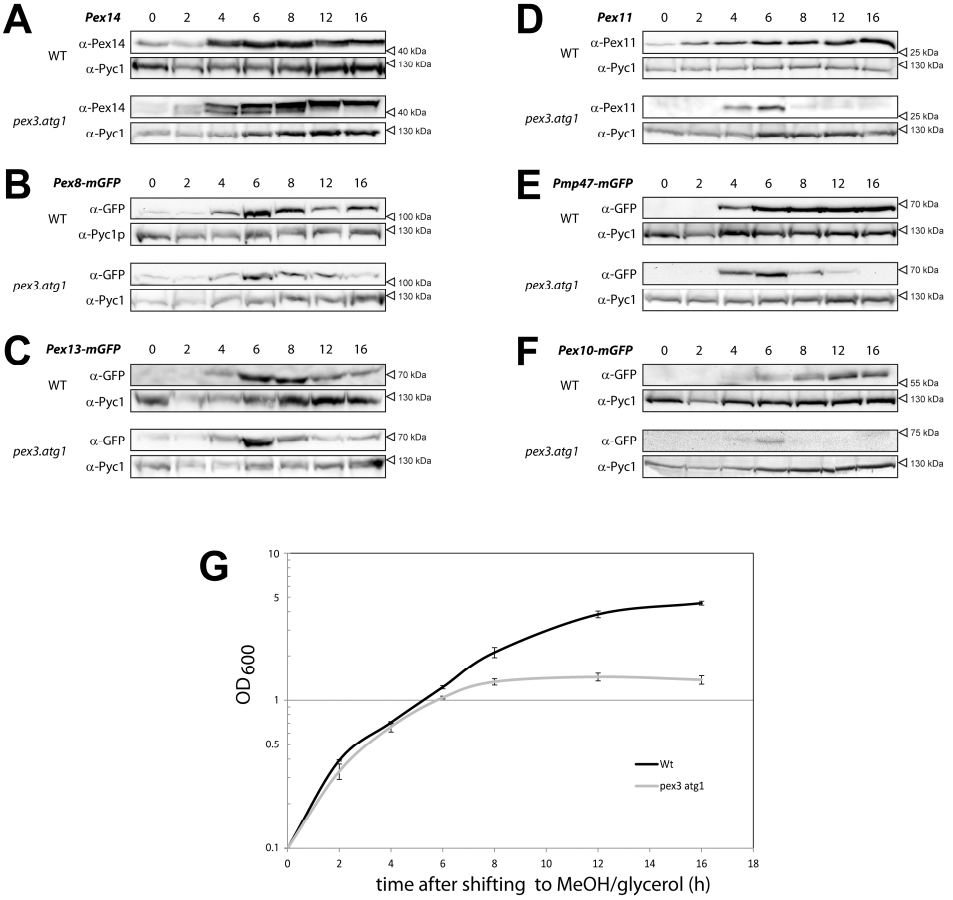

Figure S1. Induction of PMPs in WT and *pex3 atg1* cells. (A-F) Cells, pre-cultivated on MM-Glu (oh), were shifted to MM-M/G. Samples were taken at the indicated time points. (G) Growth curves of the WT and *pex3 atg1* cultures. Error bars: SD of 5 experiments.

Figure-S2

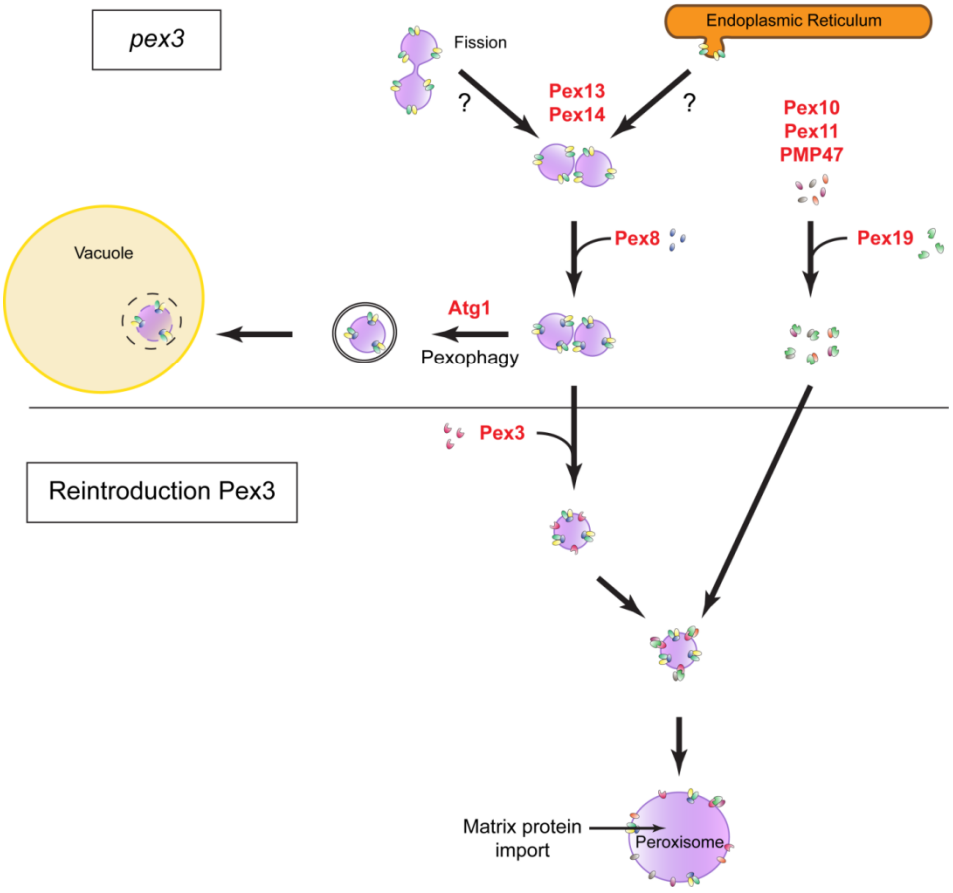

Figure S2. Model. In *pex3* cells Pex13/Pex14-containing structures exist that import Pex8. These structures may arise by proliferation of a pre-existing structure or form from the ER. They are constitutively degraded by autophagy, unless *ATG1* is deleted. Pex10, Pex11 and PMP47 are instable, because they are not inserted into these structures. Re-introduced Pex3 is sorted to the structures, followed by insertion of the other PMPs by the Pex3/Pex19 machinery and import of matrix proteins.

Acknowledgements

We thank Ruchi Saraya, Geerke Maathuis and Chris Williams for their valuable contributions. We thank Abraham Koster (LUMC) for making the electron tomography facilities available. This work was supported by an EU Marie Curie IEF grant to K.K. (FP7-330150).

References

1. Wanders RJ, Waterham HR. Biochemistry of mammalian peroxisomes revisited. Annual review of biochemistry 2006;75:295-332.

2. Hu J, Baker A, Bartel B, Linka N, Mullen RT, Reumann S, Zolman BK. Plant peroxisomes: biogenesis and function. The Plant cell 2012;24(6):2279-2303.

3. Kohlwein SD, Veenhuis M, van der Klei IJ. Lipid Droplets and Peroxisomes: Key Players in Cellular Lipid Homeostasis or A Matter of Fat--Store 'em Up or Burn 'em Down. Genetics 2013;193(1):1-50.

4. Motley AM, Hettema EH. Yeast peroxisomes multiply by growth and division. J Cell Biol 2007;178(3):399-410.

5. Nagotu S, Saraya R, Otzen M, Veenhuis M, van der Klei IJ. Peroxisome proliferation in *Hansenula polymorpha* requires Dnm1p which mediates fission but not *de novo* formation. Biochim Biophys Acta 2008;1783(5):760-769.

6. Saraya R, Krikken AM, Veenhuis M, van der Klei IJ. Peroxisome reintroduction in *Hansenula polymorpha* requires Pex25 and Rho1. J Cell Biol 2011;193(5):885-900.

7. van der Zand A, Braakman I, Tabak HF. Peroxisomal membrane proteins insert into the endoplasmic reticulum. Molecular biology of the cell 2010;21(12):2057-2065.

8. van der Zand A, Gent J, Braakman I, Tabak HF. Biochemically distinct vesicles from the endoplasmic reticulum fuse to form peroxisomes. Cell 2012;149(2):397-409.

9. Bellu AR, Salomons FA, Kiel JA, Veenhuis M, Van Der Klei IJ. Removal of Pex3p is an important initial stage in selective peroxisome degradation in *Hansenula polymorpha*. J Biol Chem 2002;277(45):42875-42880.

10. Williams C, van der Klei IJ. Pexophagy-linked degradation of the peroxisomal membrane protein Pex3p involves the ubiquitin-proteasome system. Biochemical and biophysical research communications 2013;438(2):395-401.

11. van Dijken JP, Otto R, Harder W. Growth of *Hansenula polymorpha* in a methanol-limited chemostat. Physiological responses due to the involvement of methanol oxidase as a key enzyme in methanol metabolism. Arch Microbiol 1976;111(1-2):137-144.

12. Faber KN, Haima P, Harder W, Veenhuis M, Ab G. Highly-efficient electrotransformation of the yeast *Hansenula polymorpha*. Current genetics 1994;25(4):305-310.

13. Baerends RJ, Faber KN, Kram AM, Kiel JA, van der Klei IJ, Veenhuis M. A stretch of positively charged amino acids at the N terminus of *Hansenula polymorpha* Pex3p is involved in incorporation of the protein into the peroxisomal membrane. J Biol Chem 2000;275(14):9986-9995.

14. Baerends RJ, Rasmussen SW, Hilbrands RE, van der Heide M, Faber KN, Reuvekamp PT, Kiel JA, Cregg JM, van der Klei IJ, Veenhuis M. The *Hansenula polymorpha PER9* gene encodes a peroxisomal membrane protein essential for peroxisome assembly and integrity. J Biol Chem 1996;271(15):8887-8894.

15. Komduur JA, Veenhuis M, Kiel JA. The *Hansenula polymorpha PDD7* gene is essential for macropexophagy and microautophagy. FEMS yeast research 2003;3(1):27-34.

16. Sudbery PE, Gleeson MA, Veale RA, Ledeboer AM, Zoetmulder MC. *Hansenula polymorpha* as a novel yeast system for the expression of heterologous genes. Biochemical Society transactions 1988;16(6):1081-1083.

17. Cepińska MN, Veenhuis M, van der Klei IJ, Nagotu S. Peroxisome fission is associated with reorganization of specific membrane proteins. Traffic 2011;12(7):925-937.

18. Saraya R, Cepińska MN, Kiel JA, Veenhuis M, van der Klei IJ. A conserved function for Inp2 in peroxisome inheritance. Biochim Biophys Acta 2010;1803(5):617-622.

19. Baerends RJ, Salomons FA, Kiel JA, van der Klei IJ, Veenhuis M. Deviant Pex3p levels affect normal peroxisome formation in *Hansenula polymorpha*: a sharp increase of the protein level induces the proliferation of numerous, small protein-import competent peroxisomes. Yeast 1997;13(15):1449-1463.

20. Kremer JR, Mastronarde DN, McIntosh JR. Computer visualization of three-dimensional image data using IMOD. Journal of structural biology 1996;116(1):71-76.

21. Mastronarde DN. Automated electron microscope tomography using robust prediction of specimen movements. Journal of structural biology 2005;152(1):36-51.

22. Slot JW, Geuze HJ. Cryosectioning and immunolabeling. Nature protocols 2007;2(10):2480-2491.

23. Haan GJ, Baerends RJ, Krikken AM, Otzen M, Veenhuis M, van der Klei IJ. Reassembly of peroxisomes in *Hansenula polymorpha pex3* cells on reintroduction of Pex3p involves the nuclear envelope. FEMS yeast research 2006;6(2):186-194.

24. Rucktaschel R, Girzalsky W, Erdmann R. Protein import machineries of peroxisomes. Biochim Biophys Acta 2011;1808(3):892-900.

25. Thoms S, Erdmann R. Dynamin-related proteins and Pex11 proteins in peroxisome division and proliferation. The FEBS journal 2005;272(20):5169-5181.

26. Sakai Y, Saiganji A, Yurimoto H, Takabe K, Saiki H, Kato N. The absence of Pmp47, a putative yeast peroxisomal transporter, causes a defect in transport and folding of a specific matrix enzyme. J Cell Biol 1996;134(1):37-51.

27. Ma C, Schumann U, Rayapuram N, Subramani S. The peroxisomal matrix import of Pex8p requires only PTS receptors and Pex14p. Molecular biology of the cell 2009;20(16):3680-3689.

28. Zhang L, Leon S, Subramani S. Two independent pathways traffic the intraperoxisomal peroxin PpPex8p into peroxisomes: mechanism and evolutionary implications. Molecular biology of the cell 2006;17(2):690-699.

29. Schliebs W, Kunau WH. Peroxisome membrane biogenesis: the stage is set. Current biology : CB 2004;14(10):R397-399.

30. Agrawal G, Joshi S, Subramani S. Cell-free sorting of peroxisomal membrane proteins from the endoplasmic reticulum. Proceedings of the National Academy of Sciences of the United States of America 2011;108(22):9113-9118.

31. Lam SK, Yoda N, Schekman R. A vesicle carrier that mediates peroxisome protein traffic from the endoplasmic reticulum. Proceedings of the National Academy of Sciences of the United States of America 2011;108(14):E51-52.

32. Hettema EH, Girzalsky W, van Den Berg M, Erdmann R, Distel B. *Saccharomyces cerevisiae* pex3p and pex19p are required for proper localization and stability of peroxisomal membrane proteins. Embo J 2000;19(2):223-233.

33. Wiemer EA, Luers GH, Faber KN, Wenzel T, Veenhuis M, Subramani S. Isolation and characterization of Pas2p, a peroxisomal membrane protein essential for peroxisome biogenesis in the methylotrophic yeast *Pichia pastoris*. J Biol Chem 1996;271(31):18973-18980.

34. Shimozawa N, Suzuki Y, Zhang Z, Imamura A, Ghaedi K, Fujiki Y, Kondo N. Identification of *PEX3* as the gene mutated in a Zellweger syndrome patient lacking peroxisomal remnant structures. Human molecular genetics 2000;9(13):1995-1999.

35. South ST, Sacksteder KA, Li X, Liu Y, Gould SJ. Inhibitors of COPI and COPII do not block *PEX3*-mediated peroxisome synthesis. J Cell Biol 2000;149(7):1345-1360.

36. Hazra PP, Suriapranata I, Snyder WB, Subramani S. Peroxisome remnants in *pex3*Δ cells and the requirement of Pex3p for interactions between the peroxisomal docking and translocation subcomplexes. Traffic 2002;3(8):560-574.

37. Fang Y, Morrell JC, Jones JM, Gould SJ. PEX3 functions as a PEX19 docking factor in the import of class I peroxisomal membrane proteins. J Cell Biol 2004;164(6):863-875.

38. Koek A, Komori M, Veenhuis M, van der Klei IJ. A comparative study of peroxisomal structures in *Hansenula polymorpha pex* mutants. FEMS yeast research 2007;7(7):1126-1133.

39. Tabak HF, Braakman I, van der Zand A. Peroxisome formation and maintenance are dependent on the endoplasmic reticulum. Annual review of biochemistry 2013;82:723-744.

40. Fakieh MH, Drake PJ, Lacey J, Munck JM, Motley AM, Hettema EH. Intra-ER sorting of the peroxisomal membrane protein Pex3 relies on its luminal domain. Biology open 2013;2(8):829-837.

41. Saraya R, Krikken AM, Kiel JA, Baerends RJ, Veenhuis M, van der Klei IJ. Novel genetic tools for *Hansenula polymorpha*. FEMS yeast research 2012;12(3):271-278.

42. Otzen M, Perband U, Wang D, Baerends RJ, Kunau WH, Veenhuis M, Van der Klei IJ. *Hansenula polymorpha* Pex19p is essential for the formation of functional peroxisomal membranes. J Biol Chem 2004;279(18):19181-19190.

43. Tan X, Waterham HR, Veenhuis M, Cregg JM. The *Hansenula polymorpha PER8* gene encodes a novel peroxisomal integral membrane protein involved in proliferation. J Cell Biol 1995;128(3):307-319.

44. Krikken AM, Veenhuis M, van der Klei IJ. *Hansenula polymorpha pex11* cells are affected in peroxisome retention. The FEBS journal 2009;276(5):1429-1439.

45. Otzen M, Krikken AM, Ozimek PZ, Kurbatova E, Nagotu S, Veenhuis M, van der Klei IJ. In the yeast *Hansenula polymorpha*, peroxisome formation

from the ER is independent of Pex19p, but involves the function of p24 proteins. FEMS yeast research 2006;6(8):1157-1166.

Chapter 5

A conserved function for Inp2 in peroxisome inheritance

Ruchi Saraya, Małgorzata N. Cepińska, Jan A.K.W. Kiel, Marten Veenhuis and Ida J. van der Klei

Published in Biochimica et Biophysica Acta, 1803 (2010) 617–622

Abstract

In budding yeast *Saccharomyces cerevisiae,* the peroxisomal protein Inp2 is required for inheritance of peroxisomes to the bud, by connecting the organelles to the motor protein Myo2 and the actin cytoskeleton. Recent data suggested that the function of Inp2 may not be conserved in other yeast species. Using *in silico* analyses we have identified a weakly conserved Inp2-related protein in 18 species of budding yeast and analysed the role of the identified protein in the methylotrophic yeast *Hansenula polymorpha* in peroxisome inheritance**.** Our data show that *H. polymorpha* Inp2 locates to peroxisomes, interacts with Myo2, and is essential for peroxisome inheritance.

Introduction

Peroxisomes are ubiquitous organelles and component of various eukaryotes. The organelles display a wide range of functions that varies with the cell/organism in which they occur, their developmental stage and environmental conditions (1). Key functions of peroxisomes are hydrogen peroxide metabolism and oxidation of fatty acids (1, 2).

In yeast species, peroxisomes are predominantly involved in the metabolism of various unusual carbon sources, i.e. fatty acids, alkanes, methanol, purines and D-amino acids. Cultivation of these organisms on either one of these compounds is associated with proliferation of peroxisomes that are crucial for growth, as they contain the key enzymes involved in the metabolism of these carbon sources (3). In wild type (WT) *Saccharomyces cerevisiae* and *Hansenula polymorpha* cells, peroxisomes have been shown to predominantly multiply by fission from pre-existing organelles (4, 5). However, the organelles may also form *de novo* from the endoplasmic reticulum (ER) at conditions that the cells lack peroxisomes, e.g. due to a failure in inheritance (6). During normal growth of WT yeast cells at peroxisome-inducing conditions, *de novo* synthesis most likely does not contribute significantly to the total organelle population (4, 5), although exceptions may occur i.e. in *Yarrowia lipolytica* (7). In contrast, in plants and mammals, *de novo* peroxisome formation appears to be a more prominent process (8, 9). As during vegetative reproduction of WT yeast cells new peroxisomes derive by fission, the organelle population must be contained during multiple rounds of budding. Upon division, part of the organelle population is administered to the bud. In the methylotrophic yeast *H. polymorpha*, this is accompanied by asymmetrical peroxisome fission and subsequent migration of the newly formed, small organelle to the developing bud. The number of organelles migrating to the bud is dependent on the cultivation conditions (10).

In *S. cerevisiae*, peroxisome inheritance requires the function of Inp1, Inp2, the class V myosin motor Myo2 and the actin cytoskeleton (11-13). Recently, a function in inheritance was also attributed to Pex3 (14) and in *H.*

polymorpha to Pex19 (6) and Pex11 (15). *H. polymorpha* and *S. cerevisiae* cells lacking Pex3 or Pex19 are devoid of any peroxisomal remnants (16-18). In contrast, overproduction of Pex3 leads to a dramatic increase in peroxisomal structures (19). Of the proteins involved in inheritance, Inp1 is directly involved in organelle retention in the mother cell, whereas the integral membrane protein Inp2 attaches the globular tail of Myo2 to the peroxisome to enable its transport to the bud. In a recent study, Chang and coworkers (20) suggested that Inp2 is unique for *S. cerevisiae* and most likely not present in other organisms. These authors demonstrated that in *Y. lipolytica* a Pex3 paralog, designated Pex3B (21), played a crucial role in organelle inheritance through direct interaction with the Myo2 globular tail. A similar role was suggested for Pex3 in *Y. lipolytica* and *S. cerevisiae*, implying that Pex3 family members may be more relevant in organelle inheritance than Inp2.

This led us to investigate whether in *H. polymorpha* a similar mechanism is responsible for peroxisome inheritance. Our data show that this organism contains a *bona fide* Inp2 homolog that locates to peroxisomes, interacts with Myo2, and is essential for peroxisome inheritance.

Materials and Methods

Strains and growth conditions

Yeast strains used in this study are listed in **Table 1**. Plasmids and primers are listed in **Supplementary Tables 1 and 2,** respectively. Yeast cultures were grown at 37 ºC on (i) YPD media containing 1 % yeast extract, 1 % peptone and 1 % glucose, (ii) selective media containing 0.67 % yeast nitrogen base without amino acids, supplemented with 1 % glucose (YND) or 0.5 % methanol (YNM), or (iii) mineral media (MM) (22) supplemented with 0.5 % glucose or 0.5 % methanol as carbon sources and 0.25 % ammonium sulphate as a nitrogen source. When required, amino acids and nucleotides were added to a final concentration of 20 μg/ml (histidine, adenine) or 30 μg/ml (leucine, lysine,

uracil). For growth on agar plates the medium was solidified with 2 % agar. For the selection of dominant markers, YPD plates containing 100 µg/ml nourseothricin or zeocin (Invitrogen, Breda, the Netherlands) were used. For cloning purposes *Escherichia coli* DH5α was used. *E. coli* cells were grown at 37 ºC in LB media supplemented with 50 µg/ml kanamycin or 100 µg/ml ampicillin, when required.

Molecular techniques

Standard recombinant DNA techniques were carried out according to Sambrook et al (23). Transformation of *H. polymorpha* cells (24) and site specific integration in the *H. polymorpha* genome (24) were performed as described. DNA modifying enzymes were used as recommended by the suppliers (Fermentas, St. Leon-Rot, Germany and Roche Diagnostics, Mannheim, Germany). *Pwo* polymerase was used for polymerase chain reactions (PCR). Oligonucleotides were synthesized by MWG Operon (Ebersberg, Germany). For DNA sequence analysis, the Clone Manager 5 program (Scientific and Educational Software, Durham, USA) was used.

Construction of an H. polymorpha INP2 null mutant

An *inp2* deletion strain was constructed by replacing the genomic region of *INP2* comprising nucleotides +1 to +1914 by the *H. polymorpha URA3* marker as follows: First, a 630 bp 5' flanking fragment and a 690 bp 3'flanking fragment of *INP2* were amplified from *H. polymorpha* WT genomic DNA using the primer combinations INP2-5UTR-FW + INP2-5UTR-RV and INP2-3UTR-FW + INP2-3UTR-RV, respectively. The fragments were digested with *Asp*718I + *Sal*I and *Spe*I + *Not*I, respectively, and cloned into pBluescript II SK+ digested with the same enzyme combinations, yielding pBS-INP2-5UTR and pBS-INP2-3UTR, respectively. Subsequently, the 663 bp *Asp*718I-*Bam*HI fragment of pBS-INP2-5UTR was cloned into *Asp*718I+*Bam*HI-digested pBS-INP2-3UTR, yielding pBS-INP2-5&3UTRs. Finally, a 1573 bp *Sal*I-*Spe*I fragment from plasmid pSK81 containing *H. polymorpha URA3* was inserted

between the *Sal*I and *Spe*I sites of pBS-INP2-5&3UTRs, yielding pBS-INP2-del-ODC1.

Table 1. Yeast strains used in this study

Strain	Description	Source/Reference
H. polymorpha		
NCYC495	Wild type, *ura3 leu1.1*	(25)
HF246	NCYC495 with one copy integration of plasmid pHI-GFP-SKL, *leu1.1*	(26)
inp2	NCYC495 with deletion of *INP2* deletion, *leu1.1*	This study
inp2 GFP•SKL	*inp2* with integration of plasmid pHIPZ4-GFP-SKL, zeo^R	This study
DsRed•SKL	NCYC495 with integration of plasmid pSNA03, *leu1.1*	This study
DsRed•SKL INP2•GFP	DsRed•SKL with integration of plasmid pSNA11, *leu1.1* zeo^R	This study
S. cerevisiae		
L-40	MATa *leu2 his3 trp1 ade2 GAL4 gal80 LYS2::(lexAop)$_4$-HIS3 URA3::(lexAop)$_8$-lacZ*	Clontech
L-40-*Hp*PEX19	*L-40* with integration of plasmid pEXP-Met25-PEX19-Tcyc, nat^R	This study

nat^R, nourseothricin resistant; zeo^R, zeocin resistant

For deletion of *INP2,* the deletion cassette was excised from pBS-INP2-del-ODC1 by *Asp*718I+*Not*I-digestion and transformed into *H. polymorpha* NCYC495 *leu1.1 ura3* cells. Uracil-prototrophic transformants were selected. Correct deletion was confirmed by PCR and Southern blot analysis (data not shown) and the resulting strain was designated *inp2*. For visualization of peroxisomes, *Sph*I-linearized plasmid pHIPZ4-GFP-SKL, allowing production of the peroxisome-located GFP•SKL protein, was integrated at the P_{AOX} region of the *H. polymorpha inp2* genome.

Localization of Inp2 in H. polymorpha

To determine the subcellular location of Inp2 in *H. polymorpha*, a plasmid was constructed carrying an in-frame *INP2•mGFP* fusion gene under the control of the endogenous *INP2* promoter. First, a 746 bp fragment comprising mGFP was obtained by PCR with primers mGFP-fw and mGFP-rev using plasmid pCGCN-FAA4 as template. The PCR product was digested with *Bgl*II and *Sal*I and cloned between the *Bgl*II and *Sal*I sites of plasmid pANL31 resulting in pSNA10. Subsequently, an 805 bp fragment containing the *INP2* gene lacking a stop codon was amplified with primers Inp2-GFPforward and Inp2-GFPreverse using *H. polymorpha* WT genomic DNA as template. The PCR product was digested with *Bam*HI and cloned into plasmid pSNA10, digested with *Hin*dIII (blunted by Klenow treatment) and *Bgl*II. This resulted in plasmid pSNA11.

To simultaneously mark peroxisomes with a red fluorescent marker protein, *Sac*II-linearized plasmid pSNA03, producing peroxisome-located DsRed•SKL protein, was transformed into *H. polymorpha* NCYC495 *leu1.1 ura3* cells. Uracil-prototrophic transformants were selected. Correct integration at the *H. polymorpha AOX* locus was confirmed by PCR and fluorescence (data not shown). This yielded strain *H. polymorpha* DsRed•SKL. Subsequently, plasmid pSNA11 was linearized with *Apa*I and integrated at the *INP2* locus of the genome of *H. polymorpha* DsRed•SKL cells. Zeocin-resistant transformants were selected. Correct integration was confirmed by PCR (data not shown).

Yeast 2-hybrid analysis

The LexA system was used for screening interactions between *H. polymorpha* proteins using derivatives of the reporter strain *S. cerevisiae* L-40.

For *INP2* and *MYO2*, a 1935 bp DNA fragment comprising the entire *INP2* coding sequence (CDS; GenBank accession number GU591963) and a 1379 bp DNA fragment encoding the C-terminal globular domain of *H. polymorpha* Myo2 (aa 1083 to 1535; GenBank accession number GU591964) were amplified with primer combinations RSAinp2fwbamhi + RSAinp2revecori and RSAmyo2fwbamhi + RSAmyo2revecori, respectively, using genomic *H. polymorpha* WT DNA as template. PCR fragments were digested with *Bam*HI and *Eco*RI and inserted between the *Bam*HI and *Eco*RI sites of the vectors pBTM116-C and pVP16-C, respectively. This yielded plasmids pBTM116-INP2, pVP16-INP2, pBTM116-MYO2 and pVP16-MYO2, respectively.

For *PEX19*, a DNA fragment of 887 bp, comprising the entire CDS of the gene, was obtained by PCR with primers RB16 and RB17 using genomic *H. polymorpha* WT DNA as template, digested with *Bam*HI and *Sal*I and inserted between the *Bam*HI and *Sal*I sites of pBTM116-C and pVP16-C to obtain pBTM116-PEX19 and pVP16-PEX19.

For *PEX3,* a 1489 bp *Bam*HI-*Sal*I fragment comprising the entire CDS of the gene was isolated from plasmid pBSKS-PER9 and inserted between the *Bam*HI and *Sal*I sites of pBTM116-C and pVP16-C to obtain pBTM116-PEX3 and pVP16-PEX3.

To enable production of *H. polymorpha* Pex19 in *S. cerevisiae* L-40, a plasmid expressing *HpPEX19* was constructed using Gateway® Technology. First, PCR amplification of the *MET25* promoter region was performed with primers SUM004 and SUM005 using plasmid pRS416-Pmet25 as template. The 433 bp PCR fragment was recombined into the vector pDONR-P4-P1R, resulting in the entry vector pENTR-P4-P1R-P_{MET25}. Subsequently, a 934 bp fragment comprising the entire *HpPEX19* CDS was amplified with the primers RSA-

attB2Pex19revstop and RSA-attB1Pex19fw using genomic *H. polymorpha* WT DNA as template and recombined into the vector pDONR221 resulting in plasmid pENTR221-PEX19. A destination vector carrying the nourseothricin resistance (*nat*) gene was constructed as follows: By PCR with primers DOM1 and DOM2 using plasmid pHIPN4 as template, a 1307 bp DNA fragment comprising the nourseothricin marker with its expression signals was isolated and cloned into vector pDEST-R4-R3 digested by *Ehe*1, resulting in the destination vector pDEST-R4-R3-NAT. Finally, pEXP-Pmet25-PEX19-Tcyc was obtained by recombination of the entry vectors pENTR-P4-P1R-P_{MET25}, pENTR221-PEX19, pSUM91 and the destination vector pDEST-R4-R3-NAT.

For stable integration of the plasmid pEXP-Pmet25-PEX19-Tcyc into the *S. cerevisiae* L-40 genome, the plasmid was linearized with *Mun*I in the P_{MET25} region and transformed into *S. cerevisiae* L-40 cells. Nourseothricin-resistant colonies were selected. Correct integration was confirmed by PCR using primers RSA-Pmet25 and RSA-Pex19rev (data not shown).

S. cerevisiae L-40 and L-40-*Hp*PEX19 cells were co-transformed with the indicated pVP16- and pBTM116-derived fusion constructs. Subsequently, β-galactosidase filter lift assays were performed according to the manufacturer's instructions (Clontech). From each co-transformation three independent transformants were tested. Empty vectors were used to check for reporter self-activation. The well-established *Hp*Pex3-*Hp*Pex19 interaction was used as a positive control. We determined that the LexA-BD•Inp2 fusion protein caused self-activation, precluding its use in further binding studies.

In silico analysis

Inp1- and Inp2-related proteins in budding yeast species were identified using the primary sequences of *S. cerevisiae* Inp1 and Inp2 in Gapped Blast and Position Specific Iterated (PSI) Blast analyses (27) on the budding yeasts dataset (taxid: 4892) of the non-redundant (nr) protein database at the National Center for Biotechnological Information (NCBI; version November 2009). In the PSI-Blast analyses a statistical significance value of 0.001 was used as a threshold for

the inclusion of homologous sequences in each next iteration. The *H. polymorpha* genome sequence (28) was searched by TBlastN with all identified protein sequences as queries for the presence of an Inp2-related protein. Additionally, the *H. polymorpha* protein database was screened with Genome2D (29) using a query based on the Inp2 motif 3: [LIM]-[KR]-[KR]-X-X-[LIV]-C-X-L-L-X-[LIMV] (see **Supplementary Fig. 2**).

Alignments of amino acid sequences were constructed using the Clustal_X program (30) or the SIM algorithm (31) and displayed using GeneDoc (http://www.psc.edu/biomed/genedoc). Graphics showing the distribution and amino acid composition of consensus sequences were generated using Weblogo ((32); http://weblogo.berkeley.edu/). Coiled coils were identified in protein sequences using the COILS program (33). Membrane spanning regions and amphipathic helices were identified in sequence alignments using MemGen (34). PEST motifs as potential proteolytic cleavage sites were found in protein sequences using ePESTfind (http://emboss.bioinformatics.nl/cgi-bin/emboss/epestfind).

Microscopy

Wide-field images were made using a Zeiss Axioskop50 fluorescence microscope (Carl Zeiss, Sliedrecht, The Netherlands). Images were taken using a Princeton Instruments 1300Y digital camera. The GFP signal was visualized with a 470/40 nm band pass excitation filter, a 495 nm dichromatic mirror, and a 525/50 nm band pass emission filter. The DsRed signal was visualized with a 546/12 nm band pass excitation filter, a 560 nm dichromatic mirror, and a 575–640 nm band pass emission filter.

Confocal images were made using a Zeiss LSM510 confocal microscope, using Hamamatsu photomultiplier tubes. GFP fluorescence was analyzed by excitation of the cells with a 488 nm argon ion laser (Lasos), and emission was detected using a 500–550 nm band pass emission filter.

Results

Identification of Inp2-related proteins in budding yeast species

Previously, we identified the *H. polymorpha* Inp1 protein and demonstrated its conserved role in peroxisome inheritance (15). Inp1-related proteins are very weakly conserved, but can nevertheless be identified in all species of budding yeast (**Table 2, Supplementary Fig. 1**). This led us to analyse whether a similar approach was feasible for Inp2.

By Gapped Blast and PSI-Blast analyses we identified a weakly conserved Inp2-related protein encoded by the genomes of 17 budding yeast species (**Table 2,** compare Inp2 sequence conservation with Pex3 data). Despite the weak conservation, all identified proteins had a similar structure (**Fig. 1**), comprising three conserved sequence motifs (**Supplementary Fig. 2**), a putative membrane spanning region (MSR) and a C-terminal coiled-coil (absent in *Candida albicans* and *Candida dubliniensis*). Previously it was demonstrated that in *S. cerevisiae* the region C-terminal from the MSR interacts with Myo2 (12).

Blast analyses combined with Genome2D analysis using the newly identified Inp2 Motif 3 consensus (**Fig. 1**) identified a single protein in the *H. polymorpha* genome database (Hp44g705) that had the same overall structure. Remarkably, this protein showed weak similarity to the protein identified in its close relative *Pichia pastoris* (**Table 2**). Based on its low conservation, it is difficult to determine whether Hp44g705 is a true ortholog of *S. cerevisiae* Inp2. Nevertheless, our functional analysis (*see below*) indicated that the protein is indeed its functional counterpart. Therefore, we have designated the Hp44g705 protein *H. polymorpha* Inp2.

Table 2. Inp1-, Inp2- and Pex3-related proteins in budding yeast species

Species	Inp1-related protein	Identity to closest homolog[1]	Inp2-related protein	Identity to closest homolog[1]	Pex3	Identity to closest homolog[1]	Pex3B
Group 1 *Saccharomyces cerevisiae* related organisms							
Sc	NP_013931	37 % (Vp)	NP_013886	30 % (Zr)	CAA41309	48 % (Zr)	na
Zr	CAR27899	29 % (Kl)	CAR25758	30 % (Sc)	CAR27952	51 % (Lt)	na
Vp	EDO19485	37 % (Sc)	EDO17827	30 % (Sc)	EDO18651	47 % (Zr)	na
Cg	CAG62208	32 % (Sc)	CAG59921	26 % (Sc)	CAG62379	42 % (Zr)	na
Ag	AAS53190	32 % (Cg)	AAS53181	29 % (Lt)	AAS52217	51 % (Lt)	na
Lt	CAR21271	36 % (Cg)	CAR24196	30 % (Kl)	CAR23208	51 % (Ag)	na
Kl	CAG98072	29 % (Zr)	CAG99111	30 % (Lt)	AAD01495	50 % (Lt)	na
Group 2 *Debaryomyces hansenii* related organisms							
Dh	XP_458910	37 % (Ps)	XP_462532	49 % (Pg)	CAG89890	59 % (Pg)	na
Pg	XP_001482722	34 % (Dh)	XP_001486211	49 % (Dh)	XP_001485386	59 % (Dh)	na
Ps	ABN65023	37 % (Dh)	ABN64437	42 % (Dh)	ABN67699	67 % (Cd)	na
Ct	EER32348	47 % (Ca)	EER35790	38 % (Ps)	EER32494	77 % (Cd)	na
Ca	EAL02027	88 % (Cd)	EAK91856	63 % (Cd)	EAK94978	98 % (Cd)	na
Cd	CAX40730	88 % (Ca)	CAX40040	63 % (Ca)	CAX44998	98 % (Ca)	na
Le	EDK46872	30 % (Ps)	EDK45072	29 % (Ps)	EDK42669	66 % (Cd)	na
Cl	EEQ36864	32 % (Pg)	EEQ39047	34 % (Dh)	EEQ41736	53 % (Pg)	na
Group 3 methylotrophic yeast species							
Pp	CAY71639	26 % (Hp)	CAY67780	[2]	CAY71136	54 % (Hp)	na
Hp	ACN62084	26 % (Pp)	GU591963†	[2]	AAC49471	54 % (Pp)	na
Group 4 *Yarrowia lipolytica*							

Yl	CAG78899	[2]	CAG79064	[2,3]	AAO33094	32 % (Hp),[4]	CAG83356 (31 %; Hp)

Key: Ag, *Ashbya gossypii*; Ca, *Candida albicans*; Cd, *Candida dubliniensis*; Cg, *Candida glabrata*; Cl, *Clavispora lusitaniae*; Ct, *Candida tropicalis*; Dh, *Debaryomyces hansenii*; Hp, *Hansenula polymorpha*; Kl, *Kluyveromyces lactis*; Le, *Lodderomyces elongisporus*; Lt, *Lachancea thermotolerans*; Pg, *Pichia guilliermondii*; Pp, *Pichia pastoris*; Ps, *Pichia stipitis*; Sc, *Saccharomyces cerevisiae*;Vp, *Vanderwaltozyma polyspora*; Yl, *Yarrowia lipolytica*; Zr, *Zygosaccharomyces rouxii*. na, not present in these yeast species.
[1], alignments were performed using the SIM algorithm. Pex3 proteins align over the entire length of the sequences. For Inp1- and Inp2-related proteins, in most instances the indicated values represent aligned regions that span only 50-75 % of both sequences.
[2], in these cases the identity to other protein sequences was too low for the SIM algorithm to produce aligned regions spanning more than 50 % of both sequences.
[3], the *Y. lipolitica* Inp2-related protein shows significant similarity to a conserved protein in filamentous fungi (e.g. 25 % identity with accession number EDU50979 from *Pyrenophora tritici-repentis*).
[4], *Y. lipolytica* Pex3 shows highest similarity to Pex3 proteins from filamentous fungi (e.g. 35 % identity with accession number XP_387118 from *Gibberella zeae*).
† All Genbank accession numbers represent protein sequences, except that for *H. polymorpha* Inp2, which represents a DNA sequence.

The Weblogo graphic shows the distribution and amino acid composition of the major conserved region in Inp2-related proteins (Motif 3; for sequences see **Supplementary Fig. 2**). Residues with similar properties are indicated in the same color. Polar amino acids are green (G, S, T, Y, C) or purple (Q, N), basic amino acids blue (K, R, H), acidic amino acids red (D, E) and hydrophobic amino acids are black (A, V, L, I, P, W, F, M).

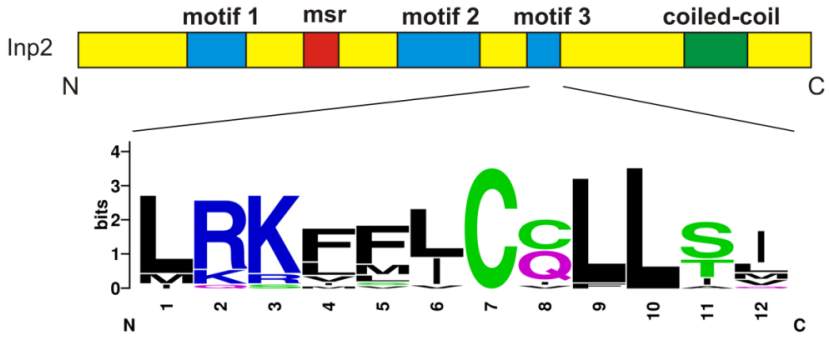

Fig. 1. Schematic representation of Inp2-related proteins in budding yeasts.
Homologous regions (*motifs 1-3*) are indicated in *blue*. A hydrophobic region possibly representing a membrane spanning region (msr) is indicated in *red*. A putative coiled-coil region is indicated in *green*.

Peroxisome inheritance is disturbed in H. polymorpha cells lacking Inp2

To investigate the role of the identified protein in peroxisome inheritance, we cultivated *H. polymorpha inp2* cells producing GFP•SKL as peroxisome marker on methanol to the mid-exponential growth stage and analyzed these by CLSM for possible inheritance defects. Quantification experiments were performed to determine the number of buds that contained peroxisomes relative to those in WT control cells. We only selected budding cells in which the bud had developed to approximately 40-50 % of the size of the mother cell. The data, summarized in **Fig. 2 A**, show that in budding *H. polymorpha* WT cells approximately 95 % of the buds contained at least one small peroxisome, as expected.

However, in budding *inp2* mutant cells most of the buds lacked peroxisomes and only approximately 20 % of the cells contained a single organelle in the bud. Characteristic fluorescence micrographs, demonstrating this mode of organelle distribution, are depicted in **Fig. 2 B & C.**

***H. polymorpha* Inp2 localizes to peroxisomes**

The localization of *H. polymorpha* Inp2 was analyzed in methanol-grown WT cells that expressed an *INP2•mGFP* fusion gene from the endogenous *INP2* promoter. These cells also produced DsRed•SKL to mark peroxisomes. In normal non-budding cells, weak GFP fluorescence was observed on all red fluorescent organelles present in the cells, suggesting that Inp2 was randomly distributed over the peroxisomal membrane (**Fig. 2 D**). In budding cells, the organelles also displayed weak GFP fluorescence over the organelle surface invariably concomitant with the presence of a bright fluorescent spot (**Fig. 2E**). This suggests that Inp2 concentrates at specific locations on organelles tagged for inheritance. After cytokinesis these spots disappeared and GFP fluorescence was again distributed over the entire organelle.

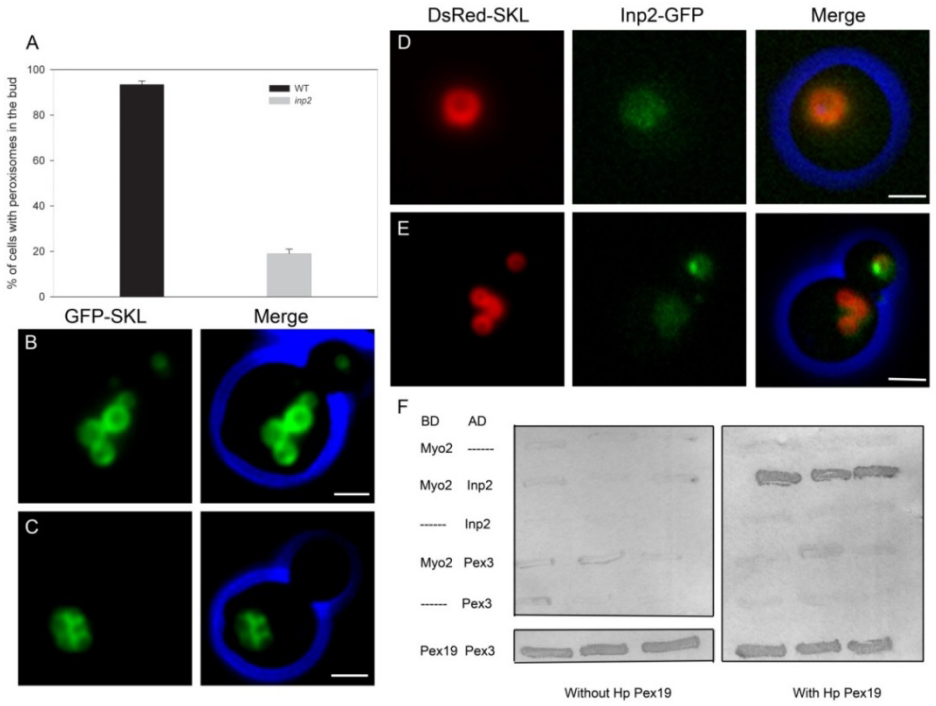

Fig. 2 The role of *H. polymorpha* Inp2 in peroxisome inheritance
Fig. 2 A: quantification of peroxisome numbers in methanol-grown budding WT and *inp2* mutant cells. Organelle numbers were determined by counting from randomly taken CLSM images. For each sample, peroxisomes were counted in 2 x 100 budding cells in 2 independent experiments. The frequency of cells containing the indicated number of peroxisomes is shown. The bar represents the Standard Error of Mean (SEM).
Fig 2 B, C: peroxisomes in budding *H. polymorpha* WT (**B**) and *inp2* mutant (**C**) cells, grown on methanol. In WT cells peroxisomes are mostly located close to the bud neck region, whereas in *inp2* cells peroxisomes are located at the cell cortex and are absent in the bud. Peroxisomes are marked by GFP•SKL. Blue color was applied to the brightfield images using Photoshop. Bars, 1 µm.
Fig. 2 D, E: localization of Inp2•GFP at peroxisomes in non-budding (**D**) and budding (**E**) methanol-grown *H. polymorpha* DsRed•SKL INP2•GFP cells. Peroxisomes are marked by DsRed fluorescence. Blue color was applied to the brightfield images using Photoshop. Bars, 1 µm.
Fig. 2F: 2-hybrid analysis using *H. polymorpha* Inp2 and Myo2. Left panel: *S. cerevisiae* L-40 co-transformants that lack *H. polymorpha* Pex19 (*Hp*Pex19), right panel: *S. cerevisiae* L-40 co-transformants producing *Hp*Pex19. The strong interaction between Inp2 and Myo2 is only observed in cells that produce *Hp*Pex19. Additionally, no interaction is detectable between *Hp*Pex3 and *Hp*Myo2. Empty vectors were used to check for reporter self-activation. The *Hp*Pex3-*Hp*Pex19 interaction was used as positive control.
The top left filter was incubated for 24 hours to detect weak interactions. The bottom left and right filters were incubated for 2-3 hours.

***H. polymorpha* Inp2 interacts with *H. polymorpha* Myo2**

Yeast 2-hybrid analysis was performed to study a possible physical interaction between *H. polymorpha* Inp2 and the globular domain of Myo2. As depicted in **Fig. 2F**, a strong interaction was observed between Inp2 and Myo2. However, this interaction was dependent of the presence of *H. polymorpha* Pex19 in the *S. cerevisiae* host strain, since it was below the limit of detection in co-transformants that lacked *Hp*Pex19. In addition, our 2-hybrid studies failed to resolve a distinct interaction between *H. polymorpha* Pex3 and Myo2, which can not be attributed to Pex3 folding defects, since this protein interacted strongly with *H. polymorpha* Pex19, as expected.

Discussion

In yeast species, peroxisome inheritance requires the function of the actin cytoskeleton and the function of the proteins Inp1, Inp2, Pex3, Pex11 and Pex19 (6, 11, 12, 14, 15, 35) together with the class V myosin motor, Myo2 (13). Of these, the molecular details of the function of Pex11 and Pex19 in this process are still unknown. Inp1 was identified as the peroxisome-specific retention factor, coupling peroxisomes to a yet unknown anchoring moiety in mother cells and developing buds (11). In contrast, Inp2 acts as the peroxisome receptor for Myo2 (12). Recently, Chang and coworkers (20) provided evidence for a function of *Y. lipolytica* Pex3 and, more specifically, its paralog Pex3B in peroxisome inheritance as the peroxisome-specific receptor of Myo2. A similar function was attributed to baker's yeast Pex3. This would imply that *S. cerevisiae* Pex3 has a function in both organelle inheritance and in organelle retention as this peroxin also functions as anchor for Inp1 at the peroxisomal membrane (14). This led us to investigate the presence of a putative Inp2 homolog in *H. polymorpha*. Our data show that *H. polymorpha* contains a weakly conserved Inp2-related protein that indeed functions in organelle movement to developing buds. The strong interaction observed between *H. polymorpha* Inp2 and Myo2 clearly implies a conserved function for Inp2 as the peroxisome receptor for Myo2. Remarkably, this interaction was dependent on

the presence of *H. polymorpha* Pex19, which is consistent with the observed defect in peroxisome inheritance in *Hppex19* mutant cells (6). This may point towards a function for Pex19 as a stabilizing factor in the Inp2-Myo2 interaction. Nevertheless, like in *S. cerevisiae*, peroxisome partitioning is not completely blocked in *H. polymorpha inp2* mutant cells, implying that other proteins may be involved in connecting peroxisomes to the cytoskeleton.

Chang and coworkers (20) have suggested that the presence of an Inp2 counterpart may be confined to yeast species closely related to *S. cerevisiae*. Our *in silico* analyses indicate a possible alternative scenario. Although Inp2 is a very weakly conserved protein, homologous proteins could be identified in all budding yeast species under study using PSI- and PHI-Blast analysis (**Table 2**), and were shown to have a similar structure. Obviously, this similarity does not warrant these proteins to represent functional counterparts of Inp2. However, the fact that one of the proteins with the weakest homology to *S. cerevisiae* Inp2, *H. polymorpha* Hp44g705, indeed acts as an Inp2 counterpart may imply that the other identified proteins might be involved in peroxisome inheritance as well. An exception may be the protein identified in *Y. lipolytica*, YALI0E03124 (accession number CAG79064), that has the same basic structure as Inp2, but rather resembles a conserved protein in filamentous fungi (**Table 2**). Recently, it was demonstrated that YALI0E03124 localizes to the ER rather than to peroxisomes (20). Furthermore, a direct interaction between YALI0E03124 and *Yl*Myo2 could not be observed. These observations were interpreted to indicate that *Y. lipolytica* does not contain an Inp2 counterpart. However, as an alternative explanation, the putative interaction between YALI0E03124 and *Yl*Myo2 may require the presence of *Yl*Pex19 (cf. **Fig. 2F**). Furthermore, the authors did not analyze a YALI0E03124-deficient strain, which would have provided a direct evaluation of a possible role for this protein in peroxisome inheritance. In *Y. lipolyica*, Pex3B appears to have a function analogous to that of *Sc*Inp2 and *Hp*Inp2. Our data (**Table 2**) indicate that this Pex3 paralog is unique for *Y. lipolytica*, and thus does not represent a general inheritance factor. Based on a weak interaction between Pex3 and Myo2, Chang and coworkers (20) have also implied that Pex3 plays a direct role in peroxisome

inheritance. We failed to detect an interaction between *H. polymorpha* Pex3 and Myo2 (**Fig. 2 F**). Thus, the proposed role for Pex3 in peroxisome inheritance may not be generally valid in all budding yeast species.

In conclusion, our data lead us to propose that in budding yeast species, with the possible exception of *Y. lipolytica,* an Inp2-related protein is present that connects peroxisomes to the actin cytoskeleton for their transport to the bud.

Acknowledgements

This project was carried out within the research program of the Kluyver Centre for Genomics of Industrial Fermentation, which is part of the Netherlands Genomics Initiative / Netherlands Organization for Scientific Research.

We would like to thank S. Nagotu and R.J.S. Baerends for plasmid constructions.

References

1. van den Bosch H, Schutgens RB, Wanders RJ, Tager JM. Biochemistry of peroxisomes. Annual review of biochemistry 1992;61:157-197.

2. Mannaerts GP, Van Veldhoven PP. Role of peroxisomes in mammalian metabolism. Cell Biochem Funct 1992;10(3):141-151.

3. Veenhuis M, Van Dijken JP, Harder W. The significance of peroxisomes in the metabolism of one-carbon compounds in yeasts. Adv Microb Physiol 1983;24:1-82.

4. Nagotu S, Saraya R, Otzen M, Veenhuis M, van der Klei IJ. Peroxisome proliferation in *Hansenula polymorpha* requires Dnm1p which mediates fission but not *de novo* formation. Biochim Biophys Acta 2008;1783(5):760-769.

5. Motley AM, Ward GP, Hettema EH. Dnm1p-dependent peroxisome fission requires Caf4p, Mdv1p and Fis1p. J Cell Sci 2008;121(Pt 10):1633-1640.

6. Otzen M, Krikken AM, Ozimek PZ, Kurbatova E, Nagotu S, Veenhuis M, van der Klei IJ. In the yeast *Hansenula polymorpha*, peroxisome formation from the ER is independent of Pex19p, but involves the function of p24 proteins. FEMS Yeast Res 2006;6(8):1157-1166.

7. Titorenko VI, Chan H, Rachubinski RA. Fusion of small peroxisomal vesicles in vitro reconstructs an early step in the in vivo multistep peroxisome assembly pathway of *Yarrowia lipolytica*. J Cell Biol 2000;148(1):29-44.

8. Kim PK, Mullen RT, Schumann U, Lippincott-Schwartz J. The origin and maintenance of mammalian peroxisomes involves a de novo PEX16-dependent pathway from the ER. J Cell Biol 2006;173(4):521-532.

9. Mullen RT, Trelease RN. The ER-peroxisome connection in plants: development of the "ER semi-autonomous peroxisome maturation and replication" model for plant peroxisome biogenesis. Biochim Biophys Acta 2006;1763(12):1655-1668.

10. Veenhuis M, van Dijken JP, Pilon SA, Harder W. Development of crystalline peroxisomes in methanol-grown cells of the yeast *Hansenula polymorpha* and its relation to environmental conditions. Arch Microbiol 1978;117(2):153-163.

11. Fagarasanu M, Fagarasanu A, Tam YY, Aitchison JD, Rachubinski RA. Inp1p is a peroxisomal membrane protein required for peroxisome inheritance in *Saccharomyces cerevisiae*. J Cell Biol 2005;169(5):765-775.

12. Fagarasanu A, Fagarasanu M, Eitzen GA, Aitchison JD, Rachubinski RA. The peroxisomal membrane protein Inp2p is the peroxisome-specific receptor for the myosin V motor Myo2p of *Saccharomyces cerevisiae*. Developmental cell 2006;10(5):587-600.

13. Hoepfner D, van den Berg M, Philippsen P, Tabak HF, Hettema EH. A role for Vps1p, actin, and the Myo2p motor in peroxisome abundance and inheritance in *Saccharomyces cerevisiae*. J Cell Biol 2001;155(6):979-990.

14. Munck JM, Motley AM, Nuttall JM, Hettema EH. A dual function for Pex3p in peroxisome formation and inheritance. J Cell Biol 2009;187(4):463-471.

15. Krikken AM, Veenhuis M, van der Klei IJ. *Hansenula polymorpha pex11* cells are affected in peroxisome retention. The FEBS journal 2009;276(5):1429-1439.

16. Hettema EH, Girzalsky W, van Den Berg M, Erdmann R, Distel B. *Saccharomyces cerevisiae* pex3p and pex19p are required for proper localization and stability of peroxisomal membrane proteins. Embo J 2000;19(2):223-233.

17. Baerends RJ, Rasmussen SW, Hilbrands RE, van der Heide M, Faber KN, Reuvekamp PT, Kiel JA, Cregg JM, van der Klei IJ, Veenhuis M. The *Hansenula polymorpha PER9* gene encodes a peroxisomal membrane protein essential for peroxisome assembly and integrity. J Biol Chem 1996;271(15):8887-8894.

18. Otzen M, Perband U, Wang D, Baerends RJ, Kunau WH, Veenhuis M, Van der Klei IJ. *Hansenula polymorpha* Pex19p is essential for the formation of functional peroxisomal membranes. J Biol Chem 2004;279(18):19181-19190.

19. Baerends RJ, Salomons FA, Kiel JA, van der Klei IJ, Veenhuis M. Deviant Pex3p levels affect normal peroxisome formation in *Hansenula polymorpha*: a sharp increase of the protein level induces the proliferation of numerous, small protein-import competent peroxisomes. Yeast 1997;13(15):1449-1463.

20. Chang J, Mast FD, Fagarasanu A, Rachubinski DA, Eitzen GA, Dacks JB, Rachubinski RA. Pex3 peroxisome biogenesis proteins function in peroxisome inheritance as class V myosin receptors. J Cell Biol 2009;187(2):233-246.

21. Kiel JA, Veenhuis M, van der Klei IJ. *PEX* genes in fungal genomes: common, rare or redundant. Traffic 2006;7(10):1291-1303.

22. van Dijken JP, Otto R, Harder W. Growth of *Hansenula polymorpha* in a methanol-limited chemostat. Physiological responses due to the involvement of methanol oxidase as a key enzyme in methanol metabolism. Arch Microbiol 1976;111(1-2):137-144.

23. J. Sambrook EFFaJS. Molecular cloning : a laboratory manual, : Cold Spring Harbor Laboratory, Cold Spring Harbor, N.Y.,; 1989.

24. Faber KN, Haima P, Harder W, Veenhuis M, Ab G. Highly-efficient electrotransformation of the yeast *Hansenula polymorpha*. Current genetics 1994;25(4):305-310.

25. Sudbery PE, Gleeson MA, Veale RA, Ledeboer AM, Zoetmulder MC. *Hansenula polymorpha* as a novel yeast system for the expression of heterologous genes. Biochemical Society transactions 1988;16(6):1081-1083.

26. van Dijk R, Faber KN, Hammond AT, Glick BS, Veenhuis M, Kiel JA. Tagging *Hansenula polymorpha* genes by random integration of linear DNA fragments (RALF). Mol Genet Genomics 2001;266(4):646-656.

27. Altschul SF, Madden TL, Schaffer AA, Zhang J, Zhang Z, Miller W, Lipman DJ. Gapped BLAST and PSI-BLAST: a new generation of protein database search programs. Nucleic Acids Res 1997;25(17):3389-3402.

28. Ramezani-Rad M, Hollenberg CP, Lauber J, Wedler H, Griess E, Wagner C, Albermann K, Hani J, Piontek M, Dahlems U, Gellissen G. The *Hansenula polymorpha* (strain CBS4732) genome sequencing and analysis. FEMS yeast research 2003;4(2):207-215.

29. Baerends RJ, Smits WK, de Jong A, Hamoen LW, Kok J, Kuipers OP. Genome2D: a visualization tool for the rapid analysis of bacterial transcriptome data. Genome Biol 2004;5(5):R37.

30. Thompson JD, Gibson TJ, Plewniak F, Jeanmougin F, Higgins DG. The CLUSTAL_X windows interface: flexible strategies for multiple sequence alignment aided by quality analysis tools. Nucleic Acids Res 1997;25(24):4876-4882.

31. Huang X MW. A time-efficient, linear-space local similarity algorithm. Adv Appl Math 1991.;12:337-357.

32. Crooks GE, Hon G, Chandonia JM, Brenner SE. WebLogo: a sequence logo generator. Genome Res 2004;14(6):1188-1190.

33. Lupas A, Van Dyke M, Stock J. Predicting coiled coils from protein sequences. Science 1991;252(5010):1162-1164.

34. Lolkema JS, Slotboom DJ. Estimation of structural similarity of membrane proteins by hydropathy profile alignment. Mol Membr Biol 1998;15(1):33-42.

35. Chang J, Fagarasanu A, Rachubinski RA. Peroxisomal peripheral membrane protein YlInp1p is required for peroxisome inheritance and influences the dimorphic transition in the yeast *Yarrowia lipolytica*. Eukaryot Cell 2007;6(9):1528-1537.

Summary

Peroxisomes are single membrane-bound, ubiquitous cell organelles which are involved in a wide variety of metabolic pathways. These organelles are present across all eukaryotic species: from yeast to human, and their function greatly depends on the organism and tissue. Among others, peroxisomes are involved in the beta-oxidation of fatty acids, metabolism of hydrogen peroxide, synthesis of plasmalogens and penicillin, photorespiration and seed germination. These highly versatile organelles can change their number, size and content in order to adapt to changes in environmental conditions.

Peroxisomes are essential for human; mutations in genes responsible for proper peroxisome assembly (*PEX* genes) cause peroxisome biogenesis disorders (PBDs). The most severe PBD is the Zellweger syndrome which is often lethal. However, peroxisomes are dispensable for yeast, making them a suitable host for studying these organelles. In this thesis we used *Hansenula polymorpha*, a methylotrophic yeast, as a model organism to study peroxisome biology. The number, size and protein content of these organelles are strictly regulated. Cells grown on glucose usually contain one small organelle, while on methanol peroxisome formation is induced, leading to the formation of multiple relatively large organelles. Peroxisomes can be formed in two different ways; like mitochondria, peroxisomes can multiply by fission of pre-existing ones. However, these organelles can also be formed *de novo* form the ER. The formation of peroxisomes from ER was observed mainly in cells devoid of these organelles due to mutations in specific *PEX* genes or an inheritance defect. The contribution of both pathways to the actual peroxisome population per cell is debated. The work included in this Thesis aims to further broaden our insight in the principles of peroxisome development and maintenance.

Chapter 1 presents the current knowledge on peroxisome fission, *de novo* formation, inheritance and peroxisome membrane and matrix protein

import. It contains a detailed description of the molecular mechanisms involved in these processes.

In Chapter 2 we analyzed the role of membrane remodeling in the process of peroxisome proliferation. Peroxisome fission is divided in three main steps: membrane elongation, constriction and final fission. We used *H. polymorpha dnm1* cells which are blocked in the final step of the peroxisome fission namely scission. Such cells contain one big organelle in the mother cell which protrudes an extension to the daughter cell. This extension remains intact and is only cut off from the mother organelle via completion of the cross wall between mother cell and bud (during cytokinesis). Using GFP fusions we analyzed the fate of various peroxisome membrane proteins (PMPs) in *dnm1* cells during the organelle fission process. We observed that different PMPs were unevenly distributed over the dividing organelle. Among them were Pex25 – protein involved in formation of peroxisomes from the ER-, Pex14, Pex8 and Pex10 – components of the matrix protein import machinery. Others were concentrated at the base of the extension (Pex11 – a key component in the process of peroxisome fission) in conjunction with others that were distributed evenly over the entire organelle (Pmp47 – an ATP transporter). Interestingly, a similar pattern of protein localizations could be observed in wild type cells. We have noticed that in case of Pex25, Pex14, Pex8 and Pex10 the organelle which had the strongest GFP signal was transported to the daughter cell. This is in line with the view that the smallest organelle, which needs to grow in size, needs the most proteins involved in matrix protein import in order to become a fully functional organelle. Additionally, we found that these differences in protein distribution on the peroxisome membrane are dependent on Pex11. In *dnm1.pex11* cells all proteins studied were evenly distributed over the organelle membrane. Moreover, a further analysis showed that this phenomenon is dependent on the N-terminus of Pex11 which has previously been shown to be involved in the process of membrane bending.

Pex3 plays a key role in peroxisome assembly. Until now it was believed that *pex3* cells do not contain any peroxisome structures. However, our studies

on *pex3* cells in *H. polymorpha*, which are presented in Chapter 3, showed that these cells do contain some Pex14-GFP containing vesicular structures most often found in the proximity of the ER and the nuclear envelope. Given the relatively strong GFP signal in the vacuole, we anticipated that these structures were susceptible to autophagic degradation. To circumvent degradation we constructed a *pex3 atg1* double mutant, which is blocked in degradation due to the absence of Atg1, a key player in autophagy. Subsequent analysis confirmed the peroxisomal nature of these vesicles and showed that these structures contained, apart from Pex14, also Pex8 and Pex13. Other PMPs (Pex10, Pmp47) were unstable and only detectable in the initial time points of the growth in the cytosol. Similarly, Pex11 was present on the ER only in the initial time points. Our aim was to study whether these vesicular structures can form a mature organelle. Therefore, we re-introduced Pex3-GFP into *atg1 pex3* cells. Interestingly, the Pex14-containing structures, but not the ER, were the target for reintroduced Pex3-GFP after which these structures developed into normal functional peroxisomes. Moreover, we also observed that Pex25 and Pex19, two other peroxins proposed to be involved in the *de novo* peroxisome formation, are not involved in the formation of the vesicles in *pex3* cells. This new insight into peroxisome formation fundamentally differs from the generally accepted models.

The peroxisome number and size needs to be tightly regulated. In Chapter 4 we present data on Pex23 family proteins in *H. polymorpha*, which influence peroxisome number and size. Our findings indicate that two proteins of the Pex23 family namely Pex23 and Pex32 co-localize with peroxisomes at peroxisome-inducing (methanol) and non-inducing (glucose) conditions. Additionally, Pex23 was also present at the ER. *pex32* cells grew like wild-type cells on glucose, but failed to grow on methanol as sole carbon source. This phenotype was related to the fact that in these cells peroxisomal matrix proteins mislocalized to the cytosol. *pex23* cells also grew well on glucose, but showed retarded growth on methanol. Electron microscopy analysis showed that Pex23 plays a role in shaping both the ER and peroxisomes. Peroxisomes were enlarged and reduced in number. This phenotype resembles that of *pex11* cells,

thus explaining the growth defect on methanol. The ER however displayed strong network like extensions. Likely, Pex23 has a dual function in peroxisome and ER maintenance. Interestingly, upon deletion of *PEX23* in *pex32* cells we observed the restoration of the peroxisome deficient phenotype of *pex32* cells. Based on data reported on *S. cerevisiae* Pex30, a homologue of Pex23, we speculate that the reappearance of peroxisomes is due to stimulation of peroxisome *de novo* synthesis in *pex32* cells upon deletion of *PEX23*.

In yeast a proper distribution of organelles during budding is crucial. The mother cell needs to ensure that the proper amount of the organelles will be delivered in the daughter cell. Until now, only four proteins involved in peroxisome inheritance have been identified namely Inp1, Inp2, Pex19 and Myo2. Inp1 is responsible for retaining the organelle in the mother cell, Inp2, a protein which connects the peroxisome to Myo2, a motor protein that transports organelles along the actin skeleton. Pex19 is also important for association of Myo2 with Inp2. Until now, it was unknown whether the Inp2 protein was conserved between organisms. Our *in silico* analyses, presented in Chapter 5, identified weak homologues of Inp2 in other yeast species. Therefore, we studied the function of the putative Inp2 in *H. polymorpha*. We observed that Inp2-GFP localizes to peroxisomes. Also, cells lacking *INP2* show an inheritance defect: all peroxisomes were present only in the mother cell while the daughter cells were devoid of these organelles. Additionally, using yeast two-hybrid analysis we showed that Inp2 can interact with Myo2. This interaction was, however, dependent on Pex19. This demonstrates that *H. polymorpha* Inp2 is a bona fide Inp2 homolog.

Samenvatting

Peroxisomen zijn organellen die een belangrijke rol spelen in verschillende stofwisselingsprocessen. Ze komen voor in alle eukaryoten zoals planten, dieren en schimmels. Afhankelijk van het organisme kan de functie van peroxisomen enorm varieren. Belangrijke peroxisomale functies zijn onder anderen de bèta-oxidatie van vetzuren, afbraak van waterstofperoxide, fotorespiratie in planten, de biosynthese van speciale lipiden, de plasmalogenen, en het antibioticum penicilline. De cel reguleert tijdens veranderingen in de levensomgeving de aantallen en grootte van dit veelzijdig organel zorgvuldig.

Peroxisomen zijn essentieel voor mensen. Mutaties in genen die betrokken zijn bij peroxisoom vorming (*PEX* genen) leiden tot ernstige ziektes. Het Zellweger syndroom is daarvan een schrijnend voorbeeld en leidt veelal tot een vroege dood Voor gisten zijn peroxisomen niet perse noodzakelijk om te overleven, waardoor deze organismen ideaal zijn om de vorming en functie van peroxisomen te bestuderen. Voor dit proefschrift hebben we hiertoe de methylotrofe gist *Hansenula polymorpha* gebruikt. In deze gist zijn de aantallen, grootte en eiwitsamenstelling van peroxisomen strikt gereguleerd. Normaliter bevatten de cellen op glucose slechts één peroxisoom, echter wanneer de cellen groeien op methanol als koolstofbron, leidt dit tot meerdere, relatief grote peroxisomen. Peroxisomen worden op twee verschillende manieren gevormd. Net als mitochondriën kunnen ze vermeerderen door te delen. Daarnaast kunnen peroxisomen ook *de novo* gemaakt worden vanaf het endoplasmatisch reticulum (ER). Dit wordt met name waargenomen in cellen waarin deze organellen ontbreken bijvoorbeeld als gevolg van een specifieke mutatie. De daadwerkelijke balans tussen deling en *de novo* vorming van peroxisomen is momenteel nog niet duidelijk. Het werk beschreven in dit proefschrift heeft tot doel ons inzicht in de principes van peroxisoom ontwikkeling en instandhouding te verbreden en te verdiepen.

Hoofdstuk 1 vat onze huidige kennis omtrent peroxisoom deling, *de novo* formatie, overerving en eiwitimport samen. Tevens bevat het een gedetailleerde omschrijving van de moleculaire mechanismen die daarbij betrokken zijn.

In Hoofdstuk 2 worden veranderingen die optreden in de peroxisomale membraan tijdens peroxisoom deling beschreven. De drie voornaamste stadia tijdens peroxisoom deling zijn membraan uitstulping, afknelling en uiteindelijk, splitsing. *H. polymorpha dnm1* cellen zijn geblokkeerd in de laatste stap van deling, de splitsing. Tijdens deling bevat de moedercel een groot peroxisoom met een uitstulping naar de dochter cel. Deze uitstulping blijft intact totdat het wordt afsnoerd als gevolg van de celwand vorming tussen moeder en dochter cel (cytokinese). Door peroxisomale membraan eiwitten (PMPs) te koppelen aan fluorescente eiwitten (bv GFP) hebben we in *dnm1* cellen hun bestemming gedurende de deling van het organel deling bestudeerd. We vonden dat verschillende PMPs ongelijkmatig waren verdeeld over het delende organel. Dit was het geval voor Pex25 - een eiwit betrokken bij de formatie van peroxisomen van het ER, Pex14, Pex8 en Pex10 - componenten van het matrix eiwit import complex- . Andere eiwitten waren geconcentreerd aan de basis van de uitstulping (bv Pex11 - een belangrijke component tijdens peroxisoom deling) of waren gelijkmatig verdeeld over het gehele membraan (Pmp47 - een ATP transporter). Interessant is dat eenzelfde patroon in wild-type cellen optrad. Opvallend was dat steeds het organel met het sterkste signaal van Pex25, Pex14, Pex8 en Pex10 naar de dochter cel gevoerd werd. Dit komt overeen met het idee dat het kleinste organel dat nog moet groeien, de meeste eiwitten die betrokken zijn bij matrixeiwit import, nodig heeft om uit te kunnen groeien tot een volledig functioneel peroxisoom. Bovendien vonden we dat de verschillen in eiwitverdeling over de peroxisomale membraan afhankelijk was van Pex11. In *dnm1 pex11* cellen waren alle eiwitten gelijkmatig verdeeld over het membraan. Daarbij wees verdere analyse uit dat dit fenomeen afhankelijk was van de N-terminus van Pex11 die eerder betrokken bleek te zijn bij membraan vervorming.

Pex3 speelt een belangrijke rol in de vorming van peroxisomen. Voorheen werd gedacht dat *pex3* cellen geen peroxisomale membraan structuren bevatten. Echter, onze studie naar *H. polymorpha pex3* cellen, gepresenteerd in Hoofdstuk 3, laat zien dat ook deze cellen blaasjes-achtige structuren (vesikels) met Pex14-GFP bevatten en dat deze structuren vaak in de nabijheid van het ER en de kern membraan werden gevonden. Omdat relatief veel GFP werd gezien in de vacuole, vermoedden we dat deze structuren onderhevig waren aan afbraak door middel van autofagie. Om dit te voorkomen, maakten we een *pex3.atg1* dubbelmutant die geblokkeerd is in autofagie door afwezigheid van het belangrijke autofagie-eiwit, Atg1. Verdere analyse van deze stam bevestigde de peroxisomale aard van de blaasjes en liet zien dat deze structuren, naast Pex14, ook Pex8 en Pex13 bevatten. Andere PMPs (Pex10, Pmp47) waren niet stabiel en konden alleen tijdens de vroege tijdstippen na peroxisoom-inductie in het cytosol gevonden worden. Ook werd Pex11 slechts op vroege tijdstippen gevonden, echter alleen op het ER. Deletie van *PEX25*, welke voorheen was aangetoond betrokken te zijn bij *de novo* peroxisoom vorming, had geen effect op blaasjes vorming in *atg1 pex3* cellen. Om te onderzoeken of deze blaasjes uit konden groeien tot volwaardige peroxisomen, werd Pex3-GFP geherintroduceerd in *atg1 pex3* cellen. Daarbij waren de structuren met Pex14, en niet het ER, de bestemming voor Pex3-GFP waarna deze structuren uitgroeiden tot normaal functionerende peroxisomen. Verder vonden we dat tevens Pex19, betrokken bij de insertie van PMPs in de membraan, niet essentieel zijn voor de vorming van de blaasjes in *pex3* cellen. Dit nieuwe inzicht in peroxisoom vorming verschilt wezenlijk van de huidige geaccepteerde modellen.

In gist is het aantal peroxisomen en hun grootte strak gereguleerd. In hoofdstuk 4 presenteren we data over twee *H. polymorpha* eiwitten behorende tot de Pex23-family, te weten Pex23 and Pex32, die peroxisoom aantal en grootte beïnvloeden. We hebben vastgesteld dat beide eiwitten lokaliseren op peroxisomen onder zowel peroxisoom-inducerende (methanol) en niet-peroxisoom-inducerende (glucose) condities. Pex23 werd daarnaast ook op het ER gevonden. Op glucose groeiden *pex32* cellen als wild-type, echter ze konden

niet groeien op methanol als enige koolstofbron. Dit fenotype was gerelateerd aan het feit dat deze cellen geen peroxisomen bevatten. *pex23* cellen groeiden ook op glucose, maar vertraagd op methanol. Elektronen microscopie liet zien dat Pex23 een rol belangrijk is voor de morfologie van het ER en peroxisomen. Peroxisomen waren vergroot en stabiel maar verminderd in aantal. Dit fenotype lijk op dat van *pex11* cellen wat hun groei achterstand op methanol kan verklaren. Het ER vertoonde lange netwerkachtige uitstulpingen. Interessant is dat, bij deletie van *PEX23* in *pex32* cellen, het *pex23* fenotype gevonden werd. We speculeren dat door de afwezigheid van Pex23, de novo peroxisoom vorming in pex32 cellen wordt gestimuleerd, waardoor er weer nieuwe peroxisomen ontstaan.

In gisten is de correcte verdeling van organellen gedurende celdeling cruciaal. De moeder cel reguleert het aantal organellen dat naar de dochter cel gaat. Er zijn tot nu toe vier eiwitten bekend die daarbij betrokken zijn namelijk Inp1, Inp2, Pex19 en Myo2. Inp1 is verantwoordelijk voor het vasthouden van organellen in de moeder cel. Inp2 en Pex19 koppellen peroxisomen aan een motoreiwit, Myo2, dat peroxisomen transporteert over het actineskelet naar de knop. Voorheen was het onbekend of de Inp2 sequentie die in bakkersgist was gevonden ook aanwezig is in andere gisten. Daarom hebben we in Hoofdstuk 5 een *in silico* analyse uitgevoerd om the zoeken naar homologen van Inp2 in andere gisten. De gevonden Inp2 homoloog van *H. polymorpha* werd daarna bestudeerd. We vonden dat Inp2-GFP lokaliseert op peroxisomen. Cellen zonder *INP2* hadden een overervingdefect waarbij alle peroxisomen in de moedercel bleven en dochtercellen geen peroxisomen bevatten. Verder genetische analyse liet vervolgens zien dat de interactie tussen Inp2 en Myo2 afhankelijk is van Pex19. Dit bevestigt dat het gevonden gen in *H. polymorpha* daadwerkelijk een *bona fide* Inp2 homoloog is.